UNIVERSITÀ DI PARMA

UNIVERSITA' DEGLI STUDI DI PARMA

DOTTORATO DI RICERCA IN

Scienze del farmaco

CICLO: XXXVI

Microparticulate and nanoparticulate systems as drug delivery vehicles for antimicrobial peptides targeting lung infections

Coordinatore:
Chiar.mo Prof. MARCO MOR

Tutore:
Chiar.ma Prof.ssa ALESSANDRA ROSSI

Dottoranda:
CHIARA OGLIARI

Anni Accademici 2020/2021 – 2022/2023

Table of Contents

Abstract

The increasing misuse and overuse of antibiotics have given rise to the health threat of antimicrobial resistance. To combat this urgent crisis, antimicrobial peptides (AMPs) have emerged as promising candidates due to their unique ability to disrupt bacterial cell membranes, reducing the development of resistance and exhibiting a broad spectrum of activity. This research study focused on the development of vehicles suitable for the delivery, especially through the lung, of three selected peptides, namely WLBU2, LL37 and hLF1-11. Despite the promise of AMPs, their susceptibility to *in vivo* proteolytic enzymes and high manufacturing costs have limited their clinical application. Localized drug administration, particularly via the pulmonary route, offers a targeted and efficient means of treating respiratory infections while minimizing systemic exposure. Dry powder inhalation emerged as the optimal vehicle for delivering AMPs directly to the lungs, enhancing their antimicrobial, anti-biofilm, and mucolytic efficacy. In this study it was demonstrated the potent antibactericidal activity against *P. aeruginosa* of these peptides with over 99% inhibition in just 2 minutes for WLBU2, while LL37 took 8 minutes. hLF1-11 exhibited moderate bactericidal effects in 2 minutes. The initial phase of this research project involved the manufacturing of spray-dried powders containing AMPs. A Design of Experiments approach was used to identify the influence of various process parameters on the spray-dried formulations. These consisted of mannitol and leucine for WLBU2, and trehalose and leucine for LL37 and hLF1-11. *In vitro* studies confirmed the safety and cytocompatibility of these formulations and peptides. Bactericidal activity assessments demonstrated the potency of WLBU2 and LL37, while hLF1-11 exhibited promising inhibition. Similar findings were also observed for the spray-dried formulations.

Biofilm-associated infections, common in cystic fibrosis patients, were also targeted. Preliminary studies showed a reduction in bacterial biomass for WLBU2 and LL37, although further investigations are needed to determine the concentration needed to achieve the same effect once peptides are formulated. Circular dichroism studies revealed a strong interaction between AMPs and bacterial membrane-mimicking molecules, resulting in a conformational change of the peptides from unstructured to alpha helix. Moreover, for WLBU2 microparticles the intensity of this interaction was even more pronounced. Future research will explore these aspects for LL37 and hLF1-11 formulations.

To address specific challenges associated with *P. aeruginosa* infections in cystic fibrosis patients, polymeric nanoparticle systems were explored, and two manufacturing processes were applied and compared. LL37, WLBU2 and hLF1-11 were encapsulated in nanoparticles of PLGA either by nanoprecipitation or nanoprecipitation assisted by microfluidics. The microfluidic technique led to particles in size of 200 nm, with AMPs encapsulation efficiency of about 30 % compared to the 10 % obtained with nanoprecipitation where particles were also > 250 nm. This was due to the inherent characteristics of this production method that allow the mixing processes to be controlled accurately and reproducibly. However, *in vitro* cell studies raised cytotoxicity concerns, requiring further investigation and optimization.

This research has provided valuable insights into the potential of spray-dried and nanoparticle-based AMPs formulations. Further studies, especially from a biological point of view regarding the antibacterial activity of the proposed systems, are essential to gain a comprehensive understanding of how effectively they can be utilized in the fight against bacterial infections and to make a meaningful contribution to the global battle against antimicrobial resistance. Additionally, addressing the specific challenges associated with cystic fibrosis-related infections remains a critical aspect of this research.

List of acronyms

AMR	Antimicrobial Resistance
CF	Cystic Fibrosis
AMPs	Antimicrobial Peptides
LPS	Lipopolysaccharide
MPO	Myeloperoxidase
IL-10	Interleukin-10
COPD	Chronic Obstructive Pulmonary Disease
MIC	Minimum Inhibitory Concentration
MBC	Minimum Bactericidal Concentration
API	Active Pharmaceutical Ingredient
MDI	Metered Dose Inhaler
DPI	Dry Powder Inhaler
PLGA	Poly(lactic-co-glycolic)acid
CFTR	Cystic Fibrosis Transmembrane Conductance Regulator
FDA	Food Drug Administration
DoE	Design of Experiments
TFA	Trifluoroacetic acid
CQAs	Critical Quality Attributes
EF	Emitted Fraction
RF	Respirable Fraction
LOD	Limit of Detection
LOQ	Limit of Quantification
HPLC	High Performance Liquid Chromatography
UHPLC	Ultra High Performance Liquid Chromatography
WLBU2 SD	WLBU2 spray-dried
LL37 SD	LL37 spray-dried

hLF1-11 SD	hLF1-11 spray-dried
DSC	Differential Scanning Calorimetry
SEM	Scanning Electron Microscopy
FSI	Fast Screening Impactor
CFC	Coarse Fraction Collector
FPC	Fine Particle Collector
IP	Induction Port
FPD	Fine Particle Dose
NGI	Next Generation Impactor
DD	Delivered Dose
FPF	Fine Particle Fraction
MMAD	Mass Median Aerodynamic Diameter
GSD	Geometric Standard Deivation
CD	Circualar Dichroism
CV	Crystal Violet
LPS	Lipopolysaccharide
LPSd	Detoxified Lipopolysaccharide
SDS	Sodium Dodecyl Sulfate
CFU	Colony Forming Unit
EC_{50}	Half Maximal Effective Concentration
MHA	Mueller Hinton Agar
TSB	Tryptic Soy Broth
TSBG	Glucose Tryptic Soy Broth
QbD	Quality by Design
Dv	Volumetric diameter
d_{ae}	Aerodynamic diameter
EE	Encapsulation Efficiency
DL	Drug Loading

rcf	Relative Centrifugal Force
d_H	Hydrodynamic diameter
PDI	Polidispersity index
FRR	Flow Rate Ratio
TFR	Total Flow Rate
DLS	Dynamic Light Scattering
TEM	Trasmission Electron Microscopy
MTT	3-(4,5-dimethylthiazol-2-yl)-2,5-diphenyltetrazolium bromide
CCK-8	Cell Counting Kit 8

Chapter I

Introduction to the antimicrobial peptide's delivery and therapy

1 The global threat of antimicrobial resistance

Antibiotic resistance is one of the most significant medical concerns. The rise in mortality attributed to infectious diseases resulting from drug-resistant bacteria represents a substantial issue, with over 23,000 annual fatalities in the United States, over 33,000 in Europe, and a projected global toll exceeding 10 million by 2050 [1–3]. Antimicrobial resistance (AMR) is a biological phenomenon, but its severity is exacerbated by the misuse and overuse of antibiotics, which involves treating bacterial infections with drugs to which bacteria have developed resistance [4,5]. The most significant drawback of AMR primarily impacts individuals with chronic diseases, which are susceptible to infections and for which only a limited number of pharmaceuticals currently exhibit efficacy. As an example, respiratory conditions such as cystic fibrosis (CF), tuberculosis, and pneumonia can be worsened by pathogens belonging to the ESKAPE family *(Enterococcus faecium, Staphylococcus aureus, Klebsiella pneumoniae, Acinetobacter baumannii, Pseudomonas aeruginosa, and Enterobacter species*) which are considered among the most difficult species to treat due to the absence of adequate therapy [6]. Indeed, these conditions necessitate prolonged treatment with conventional antimicrobial agents, simultaneously augmenting the potential of bacteria to evolve resistance mechanisms [5,7].

Antibiotic resistance occurs when microorganisms become resistant to the effects of antimicrobial drugs, rendering these medications less effective or completely ineffective in treating infections [2]. From an evolutionary point of view, bacteria utilize two genetic strategies to respond to antibiotic pressures: (i) mutations that take place in genes associated with the mode of action of the antimicrobial agent, and (ii) the uptake of external DNA containing resistance elements via horizontal gene transfer [8,9]. Apart from these genetic path processes, bacteria can develop alternative

methods to elude the effects of antibiotics. These approaches can be classified according to the underlying biochemical mechanisms connected to resistance, as delineated below: (i) adjustments to the antimicrobial molecule itself, (ii) obstruction of the compound's ability to reach the antibiotic target by reducing penetration or actively ejecting the antimicrobial substance via the activation of efflux pumps, and (iii) changes to target sites [9,10]. An overview of the resistance mechanisms is shown in Figure 1.

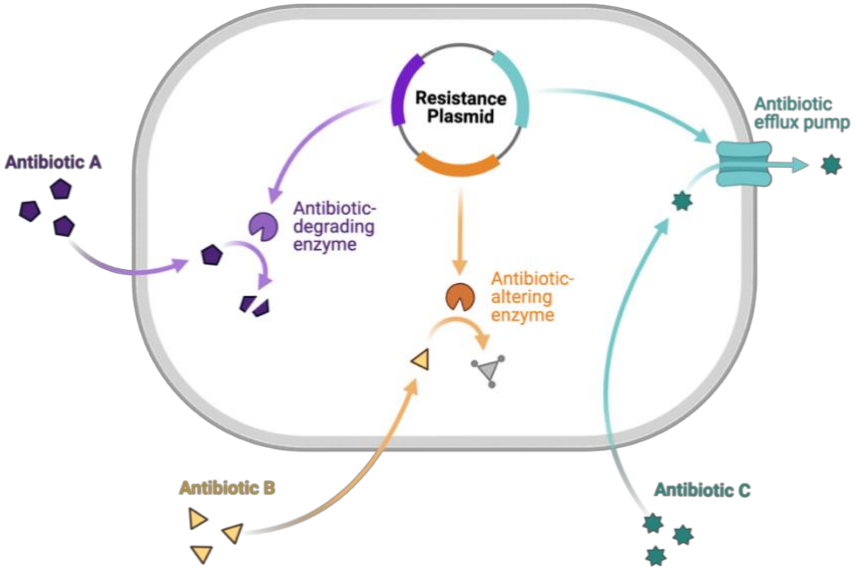

Figure 1. Antimicrobial resistance mechanisms involving the expression of degradation enzymes, altering enzymes or efflux pumps that make antimicrobial drugs no longer effective (created with BioRender.com).

Within this context, new candidates like antimicrobial peptides are emerging. Indeed, the first report of antimicrobial peptide activity dates to 1939, when gramicidin was extracted from *Bacillus brevis* and its efficacy against both gram-positive and gram-negative bacteria was showcased. Subsequently, cecropins and magainins were introduced [11]. The primary contrast with conventional antibiotics lies in their interaction and perturbation of bacterial membrane cells, resulting in cell death and reduced likelihood of resistance development [11,12].

Hence, the simplicity of peptide chemical synthesis, coupled with the evolving principles of engineering and their robust broad-spectrum effectiveness, have triggered substantial scientific interest in these substances over the past decade. This

interest has yielded significant progress in the comprehension of the molecular-scale antimicrobial activity of peptides [5].

2 Antimicrobial peptides

The issue of antibiotic resistance has become challenging to tackle and therefore, pharmaceutical companies are looking for new alternatives to conventional therapies. In this direction, the area of antimicrobial peptides presents promising therapeutic possibilities. During the 1940s, antimicrobial peptides (AMPs) or Host Defense Molecules were initially discovered, and at present, several of them are undergoing clinical trials for potential utilization as novel drugs across various therapeutic applications [13,14]. AMPs were discovered to play an important role both in the innate immune response of living organisms and in the evolution process of many microorganisms [11]. They act as a primary defense against the attack of pathogens exhibiting a wide-ranging spectrum of activity, with efficacy against both gram-positive and gram-negative bacteria, mycobacteria, and fungi, while also participating in the regulation of the immune system's response [15,16]. They are adaptable molecules, offering a multitude of opportunities for chemical alterations. These modifications yield new agents with enhanced therapeutic properties and safety profiles [17].
The effectiveness of AMPs relies on their physical and chemical properties. Altering any one of these characteristics results in the modification of others, subsequently affecting the biological activity [11,16]. These features and the AMPs classification are presented in the following sections.

2.1 Surface charge

From a structural point of view, it is difficult to identify properties that completely unite the antimicrobial activity of these peptides. Some structural features, such as the positive charge that ensures electrostatic interaction with the negative charges expressed along bacterial membranes, are recurrent [3,16]. The positive charge is often attributed to the prevalence of cationic amino acids such as lysine, histidine, and arginine within these peptides [18,19]. This leads the AMPs to be capable of

electrostatic interactions with the negatively charged membrane of bacteria, precisely with phospholipids and teichoic acid of the peptidoglycan in gram-positive and lipopolysaccharides (LPS) in gram-negative [19]. This is also responsible for most AMPs exhibiting cell-specific selectivity because bacterial cell membranes consist of a high portion of negatively charged phospholipids, whereas mammalian cells predominantly exhibit zwitterionic phospholipids [20,21]. Indeed, the average charge described for most peptides is +6, and this value is particularly important as it has been shown by Dathe et al. that by increasing the charge by even one unit, a cytotoxic effect or a reduction in antibacterial activity can be observed [11,22,23].

In the context of antimicrobial peptides, the evaluation of their haemolytic effect against human erythrocytes serves as a rapid method for the first assessment of their toxicity towards higher eukaryotic cells [24,25]. Specifically, the haemolytic effect in eukaryotic cells needs peptides to insert perpendicularly within the hydrophobic core of the cell membrane. This process is based upon interactions between the non-polar face of the amphipathic α-helix within the peptide and the hydrophobic core of the cell lipid bilayer, resulting in the creation of transmembrane channels via the "barrel-stave mechanism". Conversely, when targeting prokaryotic cells such as bacteria, a distinct approach becomes a requisite. Peptides must orient themselves parallel to the cell membrane's surface, with the non-polar side of their amphipathic α-helix interacting with the hydrophobic region of the cell membrane [25,26]. Furthermore, the positively charged components of the peptide bind the negatively charged phospholipid head groups, in a detergent-like process, ultimately resulting in the formation of transmembrane channels or pores [24,25]. Islam et al. reported that, on average, peptides are particularly active on bacteria when the surface charge is between +4 and +5, while there is zero haemolytic effect in the presence of a +5 /+6 charge. Contrary to this, they also noted that by increasing the charge of certain peptides, such as VF13K, by even one unit, the haemolytic activity varies considerably [27].

2.2 Amphipathicity

Amphipathicity represents another crucial feature worth considering. It relies on the arrangement of peptides in two dimensions (2D) or three dimensions (3D), governing their adaptability in structure. This factor holds considerable significance in both the

effectiveness of therapeutic applications and the potential for toxicity [28,29]. The amphipathic structure can be obtained in various conformations, but the most common is the alpha-helix. This allows the peptide to form two faces, the polar and the non-polar, relative to the position of the hydrophobic and hydrophilic chain in the helix [19,30]. Previously published data demonstrated that approximately 50-60 % of AMPs sequences comprise hydrophobic components, which play pivotal roles in determining how well the peptide integrates into the bacterial membrane [15,29]. The hydrophobic nature of these peptides arises from the indole ring of tryptophan and the guanidine nature of arginine residues. Tryptophan facilitates the interface interaction between AMPs and the lipid bilayer of the membrane, initiating its disruption, while arginine ensures a strong electrostatic interaction with the cell membrane [20,31]. Nonetheless, an insufficient presence of hydrophobic residues leads to feeble interactions and decreased permeability, whereas an excessive amount can result in hemolysis [11].

2.3 Secondary structure

The third important feature concerns the secondary structure of AMPs (Figure 2). Two main classes of AMPs are described according to their secondary structure, while two others are a combination of the formers. The most described are β-sheet peptides and α-helical peptides. The former include cyclic peptides such as defensins and protegrins which contain cysteine residues that tend to form disulphide bonds responsible for structural stability and increased resistance to protease activity [30,32,33]. The latter, on the other hand, are usually linear molecules that are unstructured in aqueous solution, *i.e.* random coils, but which undergo a conformational change, assuming an amphipathic helix structure, upon contact with hydrophobic membranes [30]. This structuring is typical of linear peptides that exhibit periodicity in the succession of polar and apolar groups along their chain [13,34]. Examples in this class include cecropins, magainins, and some cathelicidins such as LL37 [22,23].

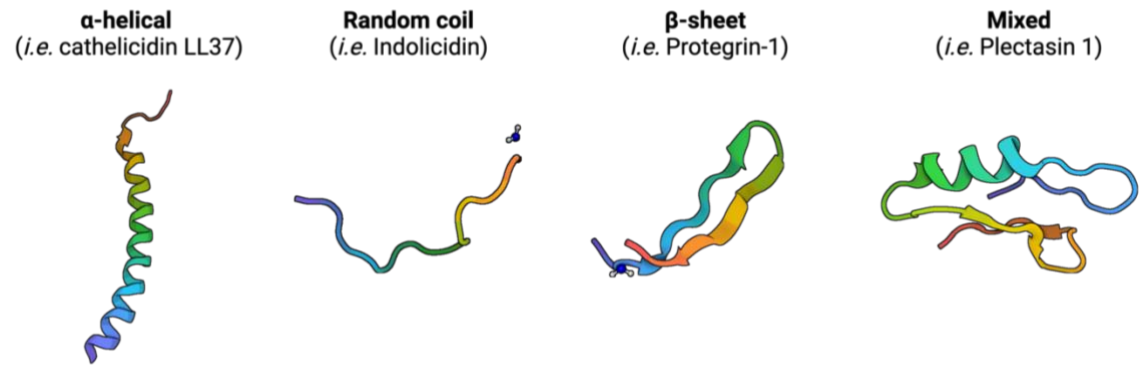

Figure 2. Antimicrobial peptide's secondary structure (created with BioRender.com).

2.4 Classification

Antimicrobial peptides are also distinguished according to their origin: they can be naturally produced or chemically synthesized [30]. Among the natural ones, ribosomally and non-ribosomally peptides can be identified. The former have more recently been discovered for their role in the innate immune response and their therapeutic potential. They are genetically encoded by all living species and their synthesis occurs through mRNA translation with the help of ribosomes [35]. In mammals, they are mainly found in the granules of neutrophils and in the secretions of epithelial cells of the skin and mucous surfaces [19]. Most of them require proteolytic cleavage to be activated, as they are produced as pro-peptides. Cathelicidins and defensins are among the most studied families, whose expression changes at each stage of human growth [19,35].

Non-ribosomal peptides are expressed almost exclusively by bacteria; indeed, they are also called bacteriocins. Their purpose is to protect the bacterium from other microorganisms competing to colonize the same environment [30]. Non-ribosomal peptides experience post-translational alterations that give rise to distinctive configurations. They are recognized as cyclic or branched peptides containing a significant proportion of proteogenic amino acids, which can undergo changes such as acetylation, glycosylation, lipidation, or the incorporation of functional groups through N-methylation or N-formylation [36,37].

Regarding chemically synthesized AMPs, they represent an emerging category of pharmaceutical agents. Various synthetic approaches have been employed, with the most prevalent methods including i) solid-phase synthesis, ii) solution-phase synthesis, iii) development of organometallic complexes, iv) creation of peptide-polymer hybrids, v) usage of recombinant DNA technology [38]. As the dynamic and/or intrinsic conformations play a pivotal role in influencing their mechanism and selective cytotoxicity, diverse strategies for enhancing AMPs, including modifications, innovative designs, and hybrid approaches, can enhance the biological attributes of the examined AMPs [39]. For instance, Haisma and colleagues modified LL-37 by removing and substituting amino acids at either the N- or C-terminal, resulting in the synthesis AMPs with an extended antimicrobial range, effective against both Gram-negative and Gram-positive bacteria [39,40].

Because not all AMPs possess all the necessary attributes, such as potency, selectivity, stability, and ease of production, additional engineering is typically necessary to enhance their effectiveness to match that of their natural counterparts, as well as to improve their activity and stability in biological environments [41].

3 Mechanism of action of antimicrobial peptides

Different mechanisms of action by which AMPs interfere with bacterial cell growth have been described. A first group of AMPs permeates the membrane and destroys it causing cell death, while a second group interacts with intracellular targets, often in synergy with the membrane permeabilization activity [11,42].

Three models have been proposed to elucidate how antimicrobial peptides disrupt membranes: the 'carpet model' or ‘detergent-like model’, 'barrel-stave model,' and 'toroidal pore model' [14]. As shown in Figure 3, key factors are the electrostatic interactions between cationic peptides and the negative charge of the membrane as they allow the peptide to penetrate the inner part of the cell membrane [19]. Certain interactions may take place with anionic phospholipids or LPS in the case of Gram-negative bacteria, or with lipoteichoic acids in the case of Gram-positive bacteria [43]. When the bacterium is Gram-negative, the cationic AMPs can replace bivalent cations such as Mg^{2+} and Ca^{2+}, bound to the LPS, and being bulky, they create a cavity on

the outer membrane of the bacterium allowing the peptide to cross it. Thus, in contact with the bacterial membranes, the AMPs form an amphipathic secondary structure essential for their action [14,19,44].

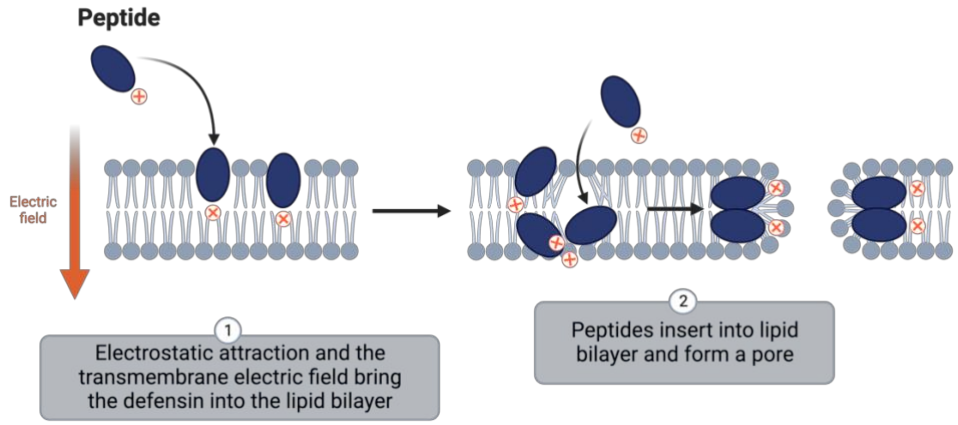

Figure 3. Peptide interactions with hydrophobic membranes of bacteria (created with BioRender.com).

Deepening the models above proposed to explain this activity, in the 'barrel-stave model' (Figure 4A), when a threshold concentration is reached, peptides are arranged perpendicularly in the lipid bilayer, creating barrel-like clusters or staves [4,44]. Typically, the barrel-stave model results in the formation of a transmembrane pore with a unilateral size where hydrophilic regions of the peptide face the lumen, creating the pore's interior, while Van der Waal's attractions occur between the hydrophobic regions of the peptides and the lipid core [3,45].

The 'carpet model' (Figure 4B) suggests that peptides accumulate parallel to the membrane, with the hydrophobic regions of the peptide associated with the anionic phospholipid head groups present on the membrane surface and with the hydrophilic regions being attracted to the polar solvent [46,47]. When a threshold concentration is reached, the formation of micelles occurs, leading to a detergent-like activity with pore formation along the membrane, osmotic imbalance, and membrane destabilization [3,5].

In the 'toroidal-pore model' (Figure 4C), as the concentration reaches a critical threshold, peptides insert vertically into the lipid bilayer, causing the lipid monolayer to flex, without peptide-peptide interaction [45]. Subsequently, lipids bend, resulting in the creation of a pore that is lined by both peptides and lipid heads from the membrane,

forming distinctive, highly curved peptide-lipid toroids [5,44]. This process leads to an inward bending of the membrane so that both the bilayer and the peptide line the channel. The resulting structure is a toroidal pore, characterized by positive curvature, facilitating the entry of additional antimicrobial-peptide molecules [3,48].

Peptides that act at the intracellular level interact with and cross the cytoplasmic membrane following the permeabilization of the outer membrane, reaching intracellular targets. This usually results in the disruption of vital processes such as inhibition of both protein synthesis and enzyme activity [45].

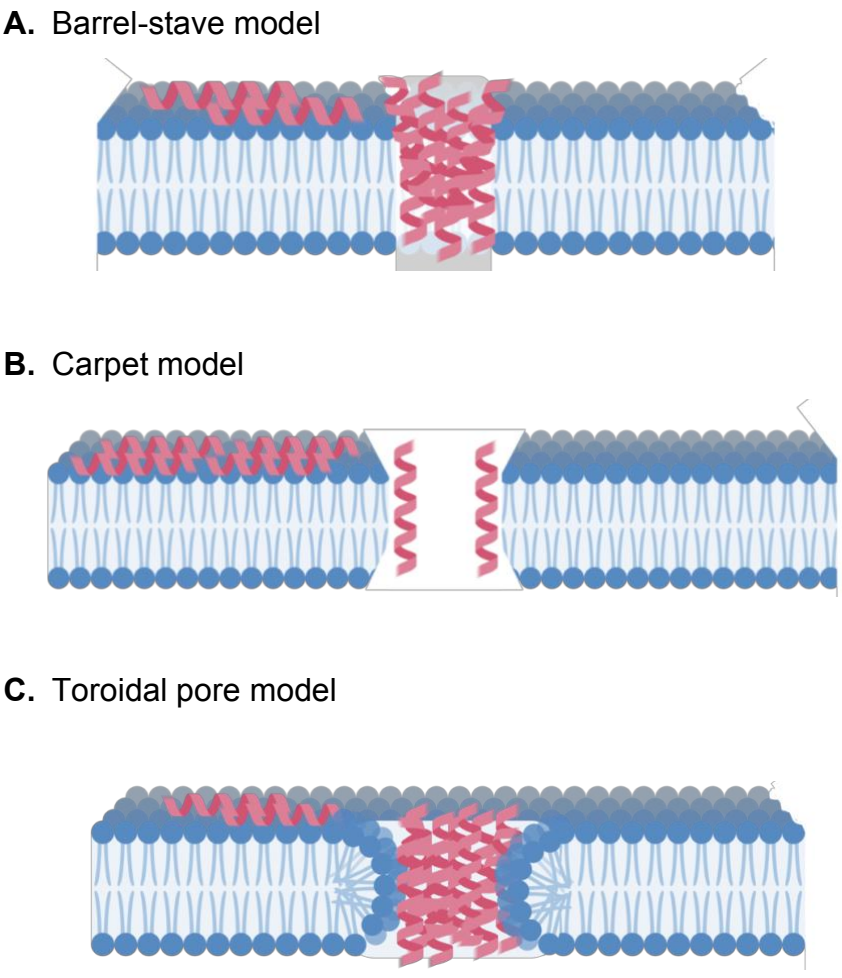

Figure 4. Mechanism of membrane permeabilization and destabilization underlying the antimicrobial activity of AMPs (created with BioRender.com).

It is worth noting that AMPs are recognized also for their immunoregulatory capabilities. The expression of the AMPs can either be continuous or induced by infectious or inflammatory triggers, which, in turn, enhance innate immunity by

attracting and activating immune cells, ultimately leading to intensified bactericidal activity and inflammation control [19]. They serve as potent modulators of inflammation, promoting chemotaxis and angiogenesis, influencing immune cell differentiation, and initiating adaptive immune responses [44]. The immunomodulatory mechanisms have been elucidated through various models. According to the 'alternate ligand model', AMPs directly bind to specific cell surface receptors, thereby enhancing receptor activity and initiating intracellular signaling pathways [45]. In the 'membrane disruption model,' AMPs induce local modifications in the membrane, which impacts the portion containing the receptor and indirectly affects its activation state and function. Lastly, in the 'trans-activation model', peptides trigger the release of a membrane-bound growth factor, which subsequently interacts with its high-affinity receptor, activating it [19,45].

4 Antimicrobial peptides selected for this research project

4.1 LL37

Three main classes of antimicrobial peptides have been described in humans: defensins, histatins and cathelicidins. All cathelicidins, identified in numerous mammalian species, share common structural features. They have a highly conserved N-terminal domain consisting of a signal sequence and a region called 'cathepsin L inhibitor' [49]. They are polypeptides produced by macrophages, leucocytes and epithelial cells that play a crucial role in mammalian immune defense. Most have a linear structure with 27-37 amino acids and fold in amphipathic helices in contact with hydrophobic surfaces [11]. Among these, cathelicidin LL37, the only one identified in humans is the active form of a pro-peptide, encoded by the CAMP gene, that by proteolytic cleavage releases the C-terminal region and thus the LL37 fragment [50]. This name is derived from its composition, consisting of 37 amino acids, with the initial two being leucine residues (Figure 5) [51]. The cleavage process takes place just before the release by neutrophil granules, likely facilitated by proteinase-3, an endogenous serine protease [52].

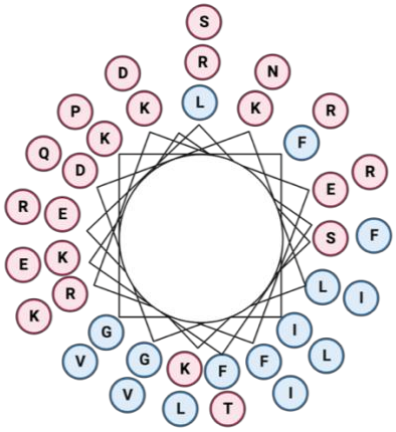

Figure 5. Amino acid sequence of LL37 peptide. D: aspartic acid, E: glutamic acid, F: phenylalanine, G: glycine, I: isoleucine, K: lysine, L: leucine, N: asparginine, P: proline, Q: glutamine, R: arginine S: serine, T: threonine, V: valine. The hydrophobic amino acids are represented in blue, while the polar ones are in red (created with BioRender.com).

As an antimicrobial, LL-37 is largely effective against Gram-positive and Gram-negative bacteria. The typical α-helix structure, which is assumed upon encountering hydrophobic surfaces, allows the peptide to kill the bacterium by compromising its membrane integrity through two types of mechanisms: the carpet model and the toroidal model [53]. The hydrophobicity and positive charge (+6), inherent in the amino acid sequence, determine LL-37's ability to interact with and cross anionic bacterial membranes [54].

Its synthesis is induced by LPS derived from gram-negative bacteria, such as *P. aeruginosa* and pro-inflammatory cytokines, thereby accounting for its abundant presence at infection sites and in the context of inflammatory responses. As a result, LL-37 serves as a chemotactic agent for phagocytic cells, contributing to the activation of the innate immune response [55]. Notably, in cases of infection, as exemplified in a study involving CF patients, LL-37 was quantified within airway secretions at substantial bactericidal levels, reaching concentrations of up to 30 μg/ml [41]. The significance of LL-37 in the host's defense against common opportunistic pathogens in CF was substantiated in a murine model by Felgentreff K. et al [56]. In their study, mice treated with an adenovirus vector harboring the cDNA for LL-37/hCAP-18 exhibited a reduced bacterial burden and diminished inflammatory response compared to untreated mice infected with *P. aeruginosa* PAO1. Elevated LL-37

expression in the airways corresponded with a decrease in *P. aeruginosa* bacterial load and the subsequent attenuation of the pro-inflammatory response following bacterial exposure [56]. However, its bactericidal activity is significantly diminished by the acidic environment, proteolytic activity, and elevated salt concentration within airway surface fluid [57].

4.2 WLBU2

WLBU2 is an engineered cationic amphipathic peptide composed of 13 arginine, eight valine, and three tryptophan residues for a total of 24 amino acids [58,59]. Its sequence was designed from the cationic structure of the intracellular motif observed in the HIV-1 transmembrane protein gp41 [60]. This motif is also present in other antimicrobial peptides, such as the cathelicidin LL37 [61,62]. The particularity of WLBU2 derives from the arrangement of the amino acids, shown in Figure 6: the valine (V) and tryptophan (W) residues form the hydrophobic face, while the positively charged arginine (R) residues form the polar face [63,64]. The result is a peptide characterized by an ideal amphipathic helical conformation, which is hypothetically associated with increased antimicrobial activity and minimal cytotoxicity to host epithelial cells [41,63]. Regarding the amino acid composition, Deslouches et al. investigated the role of tryptophan (W) in the structure and the importance of preserving the hydrophobic aspect for antimicrobial activity. To this end, they conducted a comparative analysis of the effects between LBU series peptides, composed exclusively of arginine and valine sequences, and their WLBU-series derivatives [65]. These derivatives were engineered by substitution of tryptophan residues in the hydrophobic domains. For instance, the substitution of tryptophan in the WLBU2 derivative resulted in an increase in activity against *P. aeruginosa* compared to LBU2 [59]. Furthermore, optimisation of WLBU2's structure has proved to be crucial for its resistance in high salt concentration environments due to the presence of sodium chloride or bivalent cations [58]. This is a problem prevalently highlighted for peptides of natural origin, such as LL37 and certain beta-defensins. The crucial difference between LL37 and WLBU2 relates to the structure, in that LL37 has 14 different amino acids imperfectly distributed within the amphipathic structure,

whereas WLBU2 and other engineered peptides only have two or three different amino acids modeled to form ideal amphipathic helices [6,31,59]. These characteristics led to WLBU2 being the first antimicrobial synthetic peptide capable of inhibiting *in vivo P. aeruginosa* in a systemically treated mouse model [64].

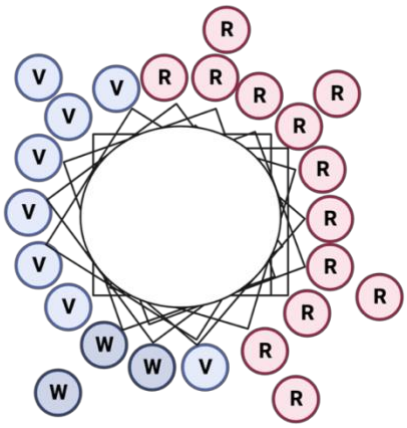

Figure 6. Amino acid sequence of WLBU2 peptide. R: arginine; V: valine; W: tryptophan. The hydrophobic amino acids, in blue, are positioned on the south face of the peptide to form the apolar face, while the polar ones, in red, are positioned on the opposite face. This allows amphipathic alpha-helix structuring on contact with hydrophobic surfaces (created with BioRender.com).

4.3 hLF1-11

Lactoferrin (LF) is a multifunctional, iron-binding glycoprotein, synthesized by mucosa and neutrophils in response to inflammatory stimuli. It is present in human and mammalian milk, blood plasma, neutrophil-specific granules, and it is a major component of all mammalians exocrine secretions, such as saliva, bile, tears, and pancreatic juice [66]. Its functions include regulation of innate immunity, transfer of iron to cells, control of free iron levels in the blood, interaction with nucleic acids and polysaccharides, and antimicrobial and antiviral activity. Some of these properties and functions are also maintained by derivatives of this molecule. Indeed, by means of acid pepsinolysis, the N-terminal fragment can be cleaved resulting in the antimicrobial peptide hLF1-11, shown in Figure 7, which has garnered significant attention due to its antimicrobial and immunomodulatory properties [66,67]. From a structural point of

view, the amino acid sequence has a predominantly hydrophilic balance with two cysteines, essential for its structuring. Indeed, the presence of cysteines in peptides has been documented to favor the formation of disulfide bonds between several peptide molecules [68]. The hydrophilic balance and the formation of disulfide bonds between cysteines influence how this peptide interacts with hydrophobic membranes [68,69].

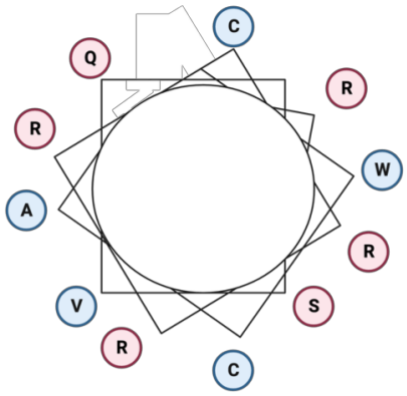

Figure 7. Amino acid sequence of hLF1-11 peptide. The hydrophobic amino acids are represented in blue, while the polar ones are in red (created with BioRender.com). A: alanine, C: cysteine, Q: glutamine, R: arginine, S: serine, V: valine, W: tryptophan.

Similarly to other groups of antimicrobial peptides, hLF1-11 possesses modulatory effects on immune cells, and it can stimulate the activity of macrophages and dendritic cells, thus helping to counteract the infectious activity of pathogens [70]. var der Does et al. investigated possible intracellular targets mediating the immunomodulatory effects of this peptide by observing how hLF1-11 can penetrate monocytes and inhibit myeloperoxidase (MPO) enzyme activities [71]. MPO is a negative regulator of IL-10 production by LPS-stimulated monocytes. Indeed, neutrophils from MPO-deficient mice express higher levels of IL-10 in response to LPS than cells isolated from wild-type mice. This is demonstrated by the fact that MPO has been reported to negatively affect one or more signal transduction pathways that regulate IL-10 production, as ABAH, an MPO inhibitor, behaves similarly to hLF1-11 [71]. Using molecular modeling technique, it was confirmed that the peptide binds to the enzyme's active site and that the cysteine at position 10 is crucial for its activity [71]. Furthermore, a clinical study conducted by Velden et al. showed that its antimicrobial activity is maintained even in

an immunodeficiency context and that no toxicity was observed following intravenous administration in healthy volunteers at decreasing doses [72].

5 Pulmonary delivery of AMPs for *P. aeruginosa* infections

5.1 Requirements and advantages of the pulmonary route

The respiratory system is recognized as a highly favorable route of administration, suitable both for systemic purposes and for local treatment of respiratory diseases such as asthma, chronic obstructive pulmonary disease (COPD), and CF [73,74]. When used for systemic administration, several advantages over other routes must be considered. These include the large absorption surface area, reduced metabolic activity, high vascularity, and the thin barrier between air and blood [75]. In addition, inhalation is less invasive than injections [76]. When used as a local treatment, advantages include the possibility of administering a relatively small dose, minimal systemic side effects, and high efficacy for specific drugs [73,77].

In terms of anatomical composition, the airways can be segmented into three distinct regions: the upper airways, the middle airways, and the lower airways. Starting at the highest point, the nasopharyngeal and oropharyngeal areas constitute the upper airways. Descending further down, the tracheobronchial tract, also known as the middle airways, concludes with the small bronchioles, alveolar ducts, and alveoli, collectively known as the lower airways or deep lung region [74,78]. The lungs are the main elements of the respiratory system and are enveloped by a lubricating fluid known as the pleura. This fluid plays a dual role: to safeguard the lungs from injury during the breathing process and to position the lungs against the chest wall [75]. An overview of the anatomical composition and division of the respiratory tract is presented in Figure 8.

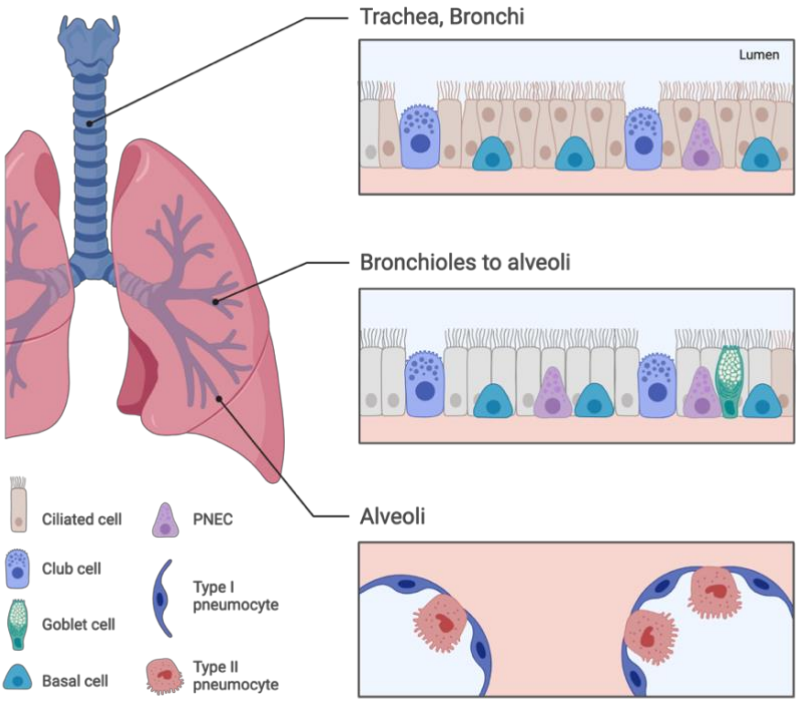

Figure 8. Representation of the respiratory tract regions from the upper airway to the deep lung (created with BioRender.com).

Despite the considerable number of benefits that can be obtained from the pulmonary administration of peptides, several challenges must be overcome for high efficacy to be guaranteed [78]. Indeed, when inhaling particles, the size of them is crucial. The aerodynamic diameter (d_{ae}), defined as 'the size of a sphere with a density of one unit, moving through the air at the same speed as a non-spherical particle with any density', plays a crucial role in determining how particles settle in the respiratory system [79]. The aerodynamic diameter (d_{ae}) depends on the airflow (particle's Reynolds number, R_e) and particle properties (geometric size, shape, and density) and can be calculated as follows:

$$d_{ae} = d_V \sqrt{\frac{\rho}{\chi \rho_0}}$$

where d_V stands for the volume-equivalent diameter, ρ_o is the unit density (of spherical calibration spheres), ρ is the particle density and χ is the dynamic shape factor, defined as the ratio of the drag force on a particle to the drag force on the particle volume-

equivalent sphere at the same velocity [80]. Particles are transported to the respiratory system through a combination of sedimentation, impaction, and diffusion mechanisms. Particles in the size range of 0.1 μm to 1 μm are deposited mainly through diffusive and gravitational mechanisms, while particles in the size range of 1 μm to 5 μm are deposited by impaction and sedimentation [74]. Specifically, impaction predominantly occurs in the upper bronchial airways, while sedimentation governs the deposition process in the lower bronchial airways. Larger particles, exceeding 5 μm, are typically filtered out in the nose or oropharynx and subsequently eliminated through coughing or sneezing [81].

It should also be mentioned that the pulmonary route has distinct natural clearance mechanisms that must be considered during drug development and administration [76,81]. Larger particles are mainly cleared through the mucociliary clearance system, which serves as the primary defense mechanism in the upper airways. In contrast, clearance in the peripheral region is mainly facilitated by alveolar macrophages, which are motile phagocytic cells responsible for monitoring the inner surface of the alveoli, engulfing and crushing pathogens and finer particles [75].

However, it is worth noting that while micro-sized particles are processed by lung macrophages, nanoparticles (NPs) with a diameter smaller than about 260 nm can evade macrophage clearance [82].

Furthermore, one of the main limitations of peptide administration is the risk of triggering immunogenic reactions causing local or systemic immune responses. Despite that, most peptides and proteins have been found to be safe after pulmonary administration [44]. An example is the approval of Pulmozyme®, based on dornase alpha, or inhaled insulin which have been proven safe for a period of two years, or glucacone-like peptides for the treatment of diabetes and other examples [77,78]. Even before Pulmozyme®, the U.S. Food and Drug Administration (FDA) approved the medicines Afrezza® and Exubera®, composed of insulin dry powder formulations. For Afrezza®, efficiency in controlling blood glucose levels was demonstrated, while for Exubera® reduced bioavailability due to the development of insulin antibodies was observed and thus it was withdrawn from the market [77]. Nonetheless, recent advances in biotechnology and pharmaceutical delivery allow the development of formulations suitable for pulmonary delivery of peptides and proteins, which together

with the physiology of the respiratory system means that inhalation can be considered an extremely promising route [77,78].

5.2 Antimicrobial peptides for lung infections

As stated by the World Health Organization, lower respiratory infections, including bronchitis and pneumonia, along with other respiratory diseases like asthma and COPD represent a substantial clinical concern [83]. Given the continuous exposure of the upper airways to pathogenic agents, the integrity of the respiratory system relies on a variety of host defense mechanisms, as described by Elkasabgy et al. [75]. In addition to mucociliary clearance and the secretion of chemokines and cytokines, AMPs play a crucial role in the defense system of the respiratory tract [19]. Myeloid cells, macrophages, neutrophils, and airway epithelial cells serve as the chief contributors of AMPs throughout the respiratory tract.

Examples of these peptides include cathelicidins (*e.g.* LL-37), defensins, lactoferricin, and mucins, representing only a subset of the many significant peptides produced in this region [83]. An illustration of AMPs with potential applications in lung disease is the human LL-37. It displays a moderate level of activity, with a minimum inhibitory concentration (MIC) falling within the range of 2 to 10 μM, effectively targeting both *Mycobacterium tuberculosis* H37Rv strains and multidrug-resistant *Mycobacterium tuberculosis* strains. Rivas-Santiago and colleagues investigated the antimycobacterial properties of several synthetic peptides. Notably, the D-LAK peptides demonstrated compelling efficacy against *M. tuberculosis*, exhibiting a lower MIC value of approximately 1.1 μM [17,84].

Among the conditions that favor the onset of lung infections is CF, an autosomal recessive disease caused by a deficiency in the gene coding for the CFTR channel that regulates the flow of chlorine ions at the membrane of mucus-producing epithelial cells. Alteration of this channel is associated with a change in mucus production with altered pH, abnormal thickness, and high stickiness [85]. In addition, this also causes a reduction in the efficiency of the clearance mechanisms by the ciliated cells with an accumulation of external agents in the mucus (Figure 9) that can favor the onset of local bacterial infections that are difficult to eradicate [86,87].

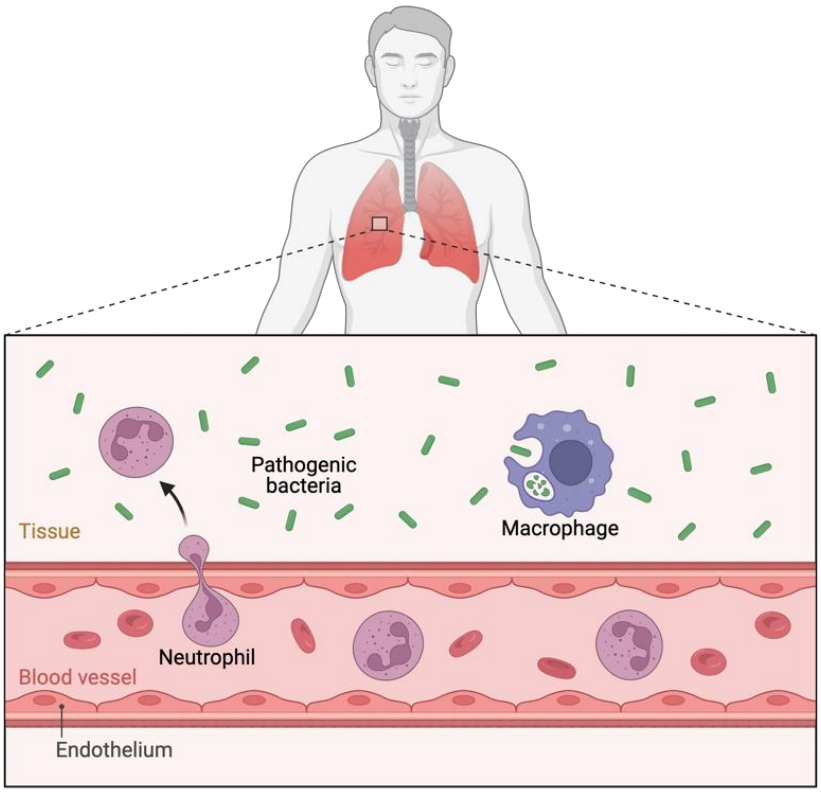

Figure 9. Representation of bacterial infection occurring in the lung (created with biorender.com).

The most common pathogen isolated from the sputum of patients with CF is *P. aeruginosa* [87]. The presence of this Gram-negative opportunistic bacterium in the lungs and airways is associated with poor respiratory function, motility, and mortality. Indeed, once it has colonized the lung area in a patient with CF is difficult to eradicate due to its plasticity, rapidity in adhering to forming biofilm and especially its ability to develop resistance to conventional antibiotics [88,89]. The antimicrobial activity of various peptides against *P. aeruginosa* is reported in the literature. Sajjan et al. studied the activity of a histatin derivative, produced in human salivary glands, as an agent for the treatment of chronic CF infections. They demonstrated the potent killing activity of the P-113 derivative, with 90% inhibition of bacterial growth at 2.5 μg/ml on the reference strain *P. aeruginosa* ATCC27853 and 6.3 μg/ml on the clinical isolate strain, demonstrating its potency in an inhalation therapy [89]. Similarly, Ridyard et al. studied the antimicrobial effect of cathelicidin LL37 in synergy with polymyxin B, demonstrating how the combination was able to induce greater membrane permeabilization resulting in reduced MIC and minimum bactericidal concentration (MBC) compared to the two

peptides used individually on *P. aeruginosa* [90]. Chen et al. also studied the activity of LL37 by comparing it with the WLBU2-engineered peptide and demonstrated that both peptides showed activity against *P. aeruginosa* PAO1 with MICs of 2 μM and 4 μM, respectively [41]. Despite this, the only peptide used today in the therapy of patients with CF is colistin, whose low bioavailability, requiring a double dose of 160 mg twice a day by nebulization, makes clear the need to combine the potent activity of AMPs with a correct formulation capable of increasing bioavailability and preserving AMPs activity [91].

6 Microparticulate drug delivery systems for antimicrobial peptides

6.1 Dry powders inhalers

In the context of pulmonary drug delivery to the lungs, the drug needs to be formulated in a stable solid particulate dispersion or a suspension of solid particles or liquid in a gaseous medium, commonly referred to as an aerosol [92]. Three frequently employed pharmaceutical aerosol systems are nebulizers, metered dose inhalers (MDIs), and dry powder inhalers (DPIs). Among these systems, dry powder aerosols containing respirable drug particles exhibit enhanced stability in their solid state, making them a more favorable option for delivering protein and peptide drugs to the lungs [93]. DPIs consist of an active pharmaceutical ingredient (API) and excipients, with sugar-based carriers like mannitol or lactose being the most used [92]. These carriers serve the purpose of improving drug particle flowability, thereby enhancing dosing precision, targeting, and deposition [94]. It is important to emphasize, however, that special care must be taken in choosing the correct excipient not only because of performance efficiency but also from the perspective of ensuring product safety. To the end of this, regulatory authorities defined the class of excipients Generally Recognized as Safe (GRAS) [92]. Among these, lactose, mannitol, lecithin, polysorbate 80, polyethylene glycol (PEG), sodium chloride and glycine are the most common because they are associated with a long history of use and safety in various applications both pharmaceutical and food or because of their role in helping to maintain the pH of formulations and influencing the tonicity of solutions making them compatible with the

respiratory tract [94]. Therefore, the GRAS designation assures that these excipients are safe for use in pharmaceutical products when used following established guidelines. It reflects a combination of historical use, scientific evidence, and expert consensus on their safety profiles. Manufacturers adhere to these standards to ensure patient safety and regulatory compliance in the development of pulmonary drug delivery systems [73].

DPIs offer several advantages, including chemical and physical stability, they can accommodate hydrophobic drug molecules for long-acting formulations, do not require propellants, and are portable devices that allow patients to administer the formulation relatively easily [95]. Effective powders for inhalation need to exhibit high dispersibility, maintain drug stability, have a narrow size distribution, and offer sustained release and/or specific targeting mechanisms. Therefore, the performance of DPI systems is influenced by various factors, including powder formulation and device characteristics [77]. Deposition is highly dependent on inhalation parameters, especially inhaled flow rate, inhaled volume, and breath-hold pause when using DPIs. "Quick" inhalation is generally recommended as it generates shear forces that aid in dispersing the drug powder, ensuring a sufficiently high respirable dose [73].

As mentioned before, particle size is a critical factor in determining the effectiveness of therapy. Particles within an aerodynamic size range of 1–5 μm are considered respirable and can effectively deposit in small airways and alveoli regions [96]. Particle size, along with shape, density, and porosity, significantly influences drug deposition in the lungs [92,95]. However, due to their small size, microparticles tend to be highly adhesive and cohesive. Therefore, it is imperative to employ techniques that allow for control over particle size, morphology, and structure. This controlled production of drug products is commonly referred to as "particle engineering" [96]. Among the various properties that can be engineered are particle size distribution, shape, and porosity/density, all of which directly impact aerosolization performance, *in vitro* and *in vivo* deposition profiles, and bioavailability [97].

6.2 Microparticle's engineering by spray-drying

During particle engineering by spray-drying, the transformation of a liquid into a powder takes place by atomization in a flow of hot gas [98]. The process consists of 4 steps (Figure 10): 1) atomisation; 2) drying; 3) formation of dry particles; 4) separation and collection of the dried product. The process involves the introduction of a solution or suspension into the drying chamber employing a peristaltic pump passing through the atomizer, which in the presence of a needle with various diameters allows the generation of small droplets in the micrometer range [94]. These droplets are subsequently subjected to solvent evaporation with the formation of dry particles that are separated by a flow of air through a cyclone that ends with a glass particle collector [94,99]. The technique is widely applied because it is rapid, continuous, reproducible, single-step, and therefore scalable.

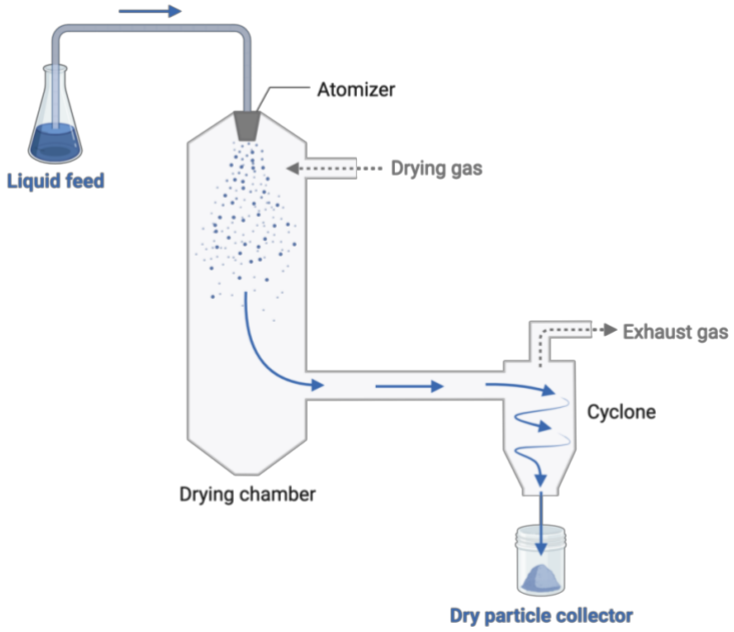

Figure 10. Spray-drying process (created with BioRender.com from Sosnik et al. [100]).

It offers the possibility of drying different types of compounds, including heat-sensitive ones [101]. In fact, although the product is exposed to high temperatures during drying, the exposure time is relatively low, in the order of milliseconds, and the actual temperature of the spray droplets is considerably lower due to evaporation cooling [80,101]. This means that the thermal stress on biologics may not be as high as it

appears based on the drying gas temperature [80]. The issue of thermal stress to which biological molecules may be exposed has also been addressed using stabilizing excipients. Excipients, such as carbohydrates, which are water-soluble, can protect the biological molecule, but also maximize deposition and lung retention. They are non-toxic, biodegradable and FDA-approved [100]. These excipients create matrices that reduce molecular mobility, slowing down the degradation processes in the powders as specific interactions between the matrix and the biologics, often involving hydrogen bonding, are beneficial for enhancing stability [80]. Furthermore, in spray-dried formulations, it is noted that peptides tend to accumulate on the particle surface due to their surface activity and slower diffusion. To counteract this phenomenon, surface-active excipients such as amino acids and surfactants are employed [96]. The incorporation of hydrophobic amino acids like L-leucine and phenylalanine is explored to enhance aerosol performance and reduce moisture-induced degradation [97].
However, scaling up this process to produce inhaled biologics necessitates careful consideration of several factors, including nozzle design, cyclone collection efficiency, wall loss, and air temperature, as they impact the powder yield and the biochemical stability of the biologics [80]. One notable success of this process is the production of Exubera® inhaled insulin, which is the first marketed protein designed for administration via inhalation to achieve a systemic therapeutic effect [100,102].

7 Nanoparticulate drug delivery systems for antimicrobial peptides

Nanotechnologies have demonstrated significant potential as promising drug delivery systems in various aspects of managing microbial infections. These nanomaterials possess unique physicochemical characteristics, making them sensitive and selective in detecting bacterial signaling and even exhibiting intrinsic antimicrobial properties [103]. They are defined as all systems between 1 nm and 1000 nm in size consisting of various materials including metals, polymers, and lipids. These vehicles can be used to protect antimicrobial agents from proteolytic degradation *in vivo* and to control their release [104]. In this direction, nanomaterials, especially of a polymeric nature, offer promising advantages in reducing collateral effects and dose, and maintaining constant drug levels in the blood. Furthermore, nanomaterials facilitate intracellular

drug delivery, mitigating the development of drug-resistant bacteria [105]. The primary purposes of using nanoparticle systems include:

- Enhancement of therapeutic efficacy through targeted delivery of drugs;
- Ability to improve the pharmaceutical and pharmacological properties of drugs, without altering their functionality;
- High stability and prolongation of circulation time following administration and release of the drug;
- Reduction of toxic and off-target effects.

Numerous types of nanomaterials, such as liposomes, polymeric nanoparticles, inorganic nanoparticles, and micelles, have undergone extensive research for encapsulating AMPs. Some examples are presented in Figure 11.

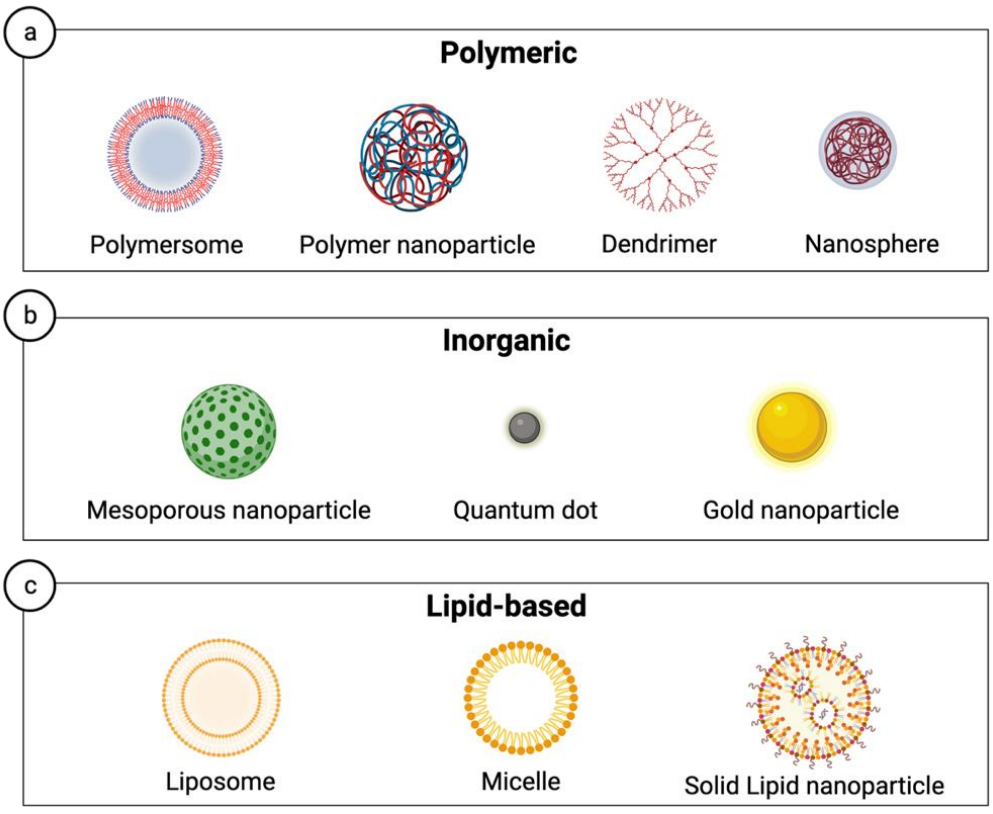

Figure 11. Nanosystems used in drug delivery (created with BioRender.com).

7.1 The use of polymers in nanotechnology

Polymeric nanomaterials have significantly impacted the field of medicine, generating substantial therapeutic interest due to their adaptable chemical and physical properties, which can be easily adjusted to match specific usage requirements [106]. They can be prepared by simple synthesis methods and have the potential to be functionalized, thus further expanding the opportunities for use in new therapies [107]. Initially, the polymers used were mainly non-biodegradable, such as polymethacrylates, polyacrylamide, or polystyrene [108]. Since these polymers are not biodegradable, they need to be quickly and effectively eliminated from the body or physically removed. Indeed, in response to the identification of chronic toxicity and severe inflammatory reactions triggered by these polymers, the scientific community has progressively shifted to the adoption of biodegradable and biocompatible polymers that can be readily accepted by the host organism [108]. The use of non-biodegradable polymers can only be accepted if they have a molecular weight below the renal excretion threshold, as in the case of Burman's patented polymer which, despite not being biodegradable, is considered safe for humans due to its rapid and efficient removal through urine [109].

Biodegradable polymers encompass both synthetic options, including polylactic acid (PLA), poly-lactic-co-glycolic acid (PLGA), and polycaprolactone (PLC), as well as natural alternatives such as albumin, chitosan, alginate, and gelatin. These polymers undergo physiologically driven hydrolysis processes, yielding biocompatible and metabolizable byproducts [110].

This PhD research project primarily focused on using PLGA nanoparticles to encapsulate AMPs due to their broad utility and the potential to modify the polymer matrix composition [103]. PLGA is a biodegradable and biocompatible polymer identified in 1960. It is easily hydrolyzed into lactic acid and glycolic acid, which become part of the citric acid cycle and are therefore subsequently removed from the body. Depending on the ratio of the two monomers, the degradation rate is also controllable, which constitutes an additional [111].

PLGA has been approved by FDA for various pharmaceutical applications. Among the first systems to be mentioned, leuprolide was encapsulated in PLGA microspheres for

the treatment of prostate cancer by exploiting the controlled drug release allowed by the polymer [112].

The potential of PLGA can also be exploited for the delivery of antimicrobial peptides. Casciaro et al., successfully developed PLGA nanoparticles for delivering AMPs derived from the esculentin-1a peptide, enhancing its transport through synthetic cystic fibrosis mucus, and simulated bacterial extracellular matrix *in vitro* [113]. Chereddy et al. proposed LL37 encapsulated PLGA nanoparticles (PLGA_LL37 NPs) as a treatment for wound closure by providing a sustained release of both LL37 and lactate [114]. In full-thickness excisional wounds, treatment with PLGA_LL37 NPs significantly speeded up the healing process when compared to the administration of PLGA or LL37 alone. Wounds treated with PLGA_LL37 NPs exhibited advanced granulation tissue formation, characterized by significantly higher collagen deposition, re-epithelialization, and enhanced neovascularization [114].

7.2 PLGA nanoparticles' synthesis

The preparation of PLGA nanoparticles involves various methods, each tailored to specific applications and particle characteristics. Two notable methods are bulk nanoprecipitation and nanoprecipitation assisted by microfluidics. These approaches offer diversity in manufacturing and advantages. Bulk nanoprecipitation, a traditional method, is known for its simplicity and scalability. In contrast, microfluidics-assisted nanoprecipitation provides precise control over particle size and distribution. In this discussion, we explore the distinctions and benefits of these methods for PLGA nanoparticle synthesis, highlighting their crucial roles in pharmaceutical advancements.

7.2.1 Bulk Nanoprecipitation

Nanoprecipitation, also known as solvent displacement, is a simple method for preparing PLGA nanoparticles. The basic requirement is the presence of two mixable phases: an organic phase in which the polymer and the drug to be encapsulated are solubilized, and an aqueous phase in which a nanoparticle stabilizer is dissolved [115].

Nanoprecipitation starts through three phases, namely nucleation, growth, and aggregation, guided by supersaturation, *i.e.* the ratio between the polymer concentration and its solubility in the organic phase [116]. Nucleation depends on this supersaturation and so does the rate of nanoparticles formation. The supersaturation phenomenon, in turn, depends on the mixing of the two phases, whereby a poor mixture produces larger particles as the nucleation phase is prolonged [115,116].

However, this is not the only mechanism by which nanoprecipitation has been described. It is also reported to be the result of a difference in surface tension between the two phases [115,117]. Briefly, the polymer and the drug are solubilized in an organic solvent of medium-high polarity and this solution is added drop by drop to an aqueous (non-solvent) solution and kept in continuous agitation. Due to the spontaneous diffusion of the polymer solution into the aqueous phase, the hydrophobic polymer and drug precipitate and form nanoparticles to avoid water molecules [117]. What happens is a purely kinetic phenomenon [118]. A liquid characterized by high surface tension, such as the aqueous phase, exerts a more pronounced attractive force on the neighboring liquid in comparison to a liquid with lower surface tension, as is typical of the organic phase solvent [119]. This disparity in surface tension between the aqueous and organic phases serves as the catalyst for interfacial turbulence and thermal non-uniformities within the system. Consequently, this dynamic gives rise to the continuous generation of solvent vortices at the interface of these two liquids. As a result, the organic solvent diffuses from regions with lower surface tension, prompting the gradual precipitation of the polymer on the surface of the organic phase and culminating in the formation of nanoparticles, as shown in Figure 12 [116,120]. The organic solvent generally used is acetone due to its medium-high polarity of 5.1 and a dielectric constant of 20.7, which allow the formation of small nanoparticles due to its rapid diffusion in the aqueous phase. Surfactants may be included in the composition of the formulation to ensure the stability of the colloidal suspension, although their presence is not necessary for the formation of nanoparticles. After the assembly, the organic solvent is evaporated by means of rotavapor or simply by stirring at atmospheric pressure, if the solvent is sufficiently volatile as in the case of acetone [116].

Overall, smaller nanoparticles can be obtained with this method than with other methods, *e.g.* emulsification/solvent diffusion. In contrast, some drawbacks of

nanoprecipitation are the poor encapsulation of hydrophilic drugs, which remain confined in the aqueous phase, the lower encapsulation efficiency, and the difficulty in completely removing the solvent after the assembly [117,120].

7.2.2 Nanoprecipitation microfluidics-assisted

The nanoprecipitation assisted by microfluidics for PLGA nanoparticle synthesis combines the precision of microfluidics with the versatility of PLGA, resulting in controlled and efficient drug delivery systems that offer improved reproducibility and customization [121].

Microfluidic nanoprecipitation is a quite novel approach that leverages the power of microscale fluid dynamics to engineer PLGA nanoparticles overcoming some limitations, in terms of particle size distribution and encapsulation, of traditional methods [122]. Microfluidic-based nanoprecipitation addresses these challenges by offering a controlled and reproducible process for nanoparticle synthesis. The principle of this technique relies on its precise control of fluid flow within microscale channels. These tiny channels provide an ideal environment for rapidly mixing PLGA with a non-solvent and therapeutic agent of interest [122]. This controlled mixing initiates the precipitation of PLGA nanoparticles, resulting in particles with a remarkably narrow size distribution. The instantaneous nature of this process distinguishes it from conventional methods, where a broader size range and less uniform distribution are common issues [123].

One of the significant advantages of microfluidic nanoprecipitation is its potential for enhancing reproducibility. Batch-to-batch variations can be a significant concern in traditional nanoparticle synthesis methods. Microfluidics eliminates much of this variability, allowing for consistent and reliable production [120].

Furthermore, it allows for precise control over various parameters, including flow rates, concentrations, and mixing ratios, enabling the tailoring of particle size and drug encapsulation efficiency. This adaptability proves indispensable in drug delivery applications, given the varying requirements for particle size and drug release kinetics based on the specific therapeutic objective [124].

The applications of microfluidic-assisted nanoprecipitation span a broad spectrum of therapeutic compounds. It is suitable for encapsulating a variety of drugs, ranging from small molecules to biomacromolecules such as proteins and nucleic acids. This versatility makes it an attractive option for a wide array of pharmaceutical and biomedical applications [125].

Chapter II

Aims and objectives of the PhD project

Antimicrobial resistance poses an urgent concern, and antimicrobial peptides have gained substantial interest as a potential alternative for addressing resistant bacterial strains. They offer broad-spectrum activity, reduced resistance risk, rapid microbial action, and versatility in various applications. However, they may have limited stability, high production costs, and potential toxicity concerns. Consequently, the optimum formulation is required to efficiently deliver the AMPs to the target site, while maintaining the physical integrity and stability of the peptides.

Three antimicrobial peptides were selected, named LL37, WLBU2 and hLF1-11 as potential agents for the treatment of pulmonary infections caused by resistant bacteria such as *P. aeruginosa*. Indeed, these peptides demonstrated effectiveness against both *P. aeruginosa* planktonic bacteria and bacterial biofilms. Nevertheless, for their development into therapeutic products, it becomes necessary to formulate them into a suitable pharmaceutical form that mitigates potential toxicity while maintaining their stability. Therefore, the overall aim of this PhD thesis was to investigate two different formulative approaches based on microsized and nanosized formulations, specifically sugar-based dry powders, and polymeric nanoparticles. The former systems aimed to produce a respirable powder for potential peptide inhalation, since the pulmonary route could facilitate the management of *P. aeruginosa* predominantly isolated in the lungs. In contrast, the latter systems addressed concerns related to the instability of the peptide and its ability to diffuse through the mucus in the inflamed airways, as seen in the case of the airways of cystic fibrosis patients, who are highly susceptible to *P. aeruginosa* infections.

The initial focus of the research project was directed toward the design and manufacturing of spray-dried powders intended for inhalation delivery of these peptides. The dry powder manufacturing process was executed via spray drying technology, identified as an efficient and readily industrialized method. The microparticles, composed of a matrix of mannitol or trehalose combined with leucine,

underwent assessment regarding drug content and physical-chemical characterization. Additionally, their aerodynamic performance for lung administration was analysed *in vitro*, employing abbreviated impactors like the Fast-Screening Impactor and the Next Generation Impactor, as outlined in the European Pharmacopoeia. An experimental design approach was utilized to optimize the entire production process. Concurrently with formulation development, investigating the biological activity against *P. aeruginosa* represented another primary objective. Specifically, the antimicrobial effect was assessed both before and after formulation, aiming to discern if the formulations could maintain or potentially enhance peptide antimicrobial properties. The final goal of this work package was to assess the *in vitro* cytocompatibility of both the peptides and their corresponding powder formulations. Given the intended pulmonary administration, human bronchial cells (BEAS2B) and alveolar cells (A549) were chosen as models.

The second objective concerned the formulation of peptides in nanoparticle systems. As mentioned before, this necessity emerged not only to overcome the limitations presented by these molecules, *i.e.* potential toxicity, reduced half-life, *in vivo* instability, but also to tackle the difficulties in targeting *P. aeruginosa* in patients with cystic fibrosis. This disease is a hereditary condition impacting pulmonary epithelial cells responsible for mucin secretion. A mutation in the CTFR gene leads to increased mucus viscosity, obstructing airways, and facilitating bacterial colonization, notably by *P. aeruginosa*. This dense mucus poses challenges for effective treatment. Scientific reports indicate that polymeric systems with a maximum dimension of 300 nm demonstrate efficient mucus penetration, enabling targeted delivery to the pulmonary site [91]. Therefore, in this part of the study carried out at the Lüdwig Maximilians Universität, Munich, Germany we aimed to encapsulate LL37 and WLBU2 peptides within PLGA nanoparticles. This biodegradable and biocompatible polymer offers versatility for protecting biomolecules facilitating mucus penetration. Two distinct manufacturing techniques were investigated: bulk nanoprecipitation and nanoprecipitation assisted with the microfluidics technology. The latter provides simplicity but inefficient loading properties, while microfluidics ensures precision and scalability. Particles underwent characterization to assess their physical properties, including size, polydispersity index, surface charge, and drug loading properties.

Furthermore, a cytotoxicity screening was crucial to identify the critical aspects of the formulation in different lung cell models*, i.e.* human bronchial cells (16HBE14o-) and murine alveolar macrophage cells (MHS).

Chapter III

Microparticulate systems for Pulmonary delivery of Antimicrobial Peptides

1 Introduction

The pulmonary delivery of AMPs could represent a favorable approach to treat respiratory infections. Indeed, the lung provides direct access to the site of action, resulting in a rapid onset of therapeutic effect. This circumvents the need for systemic administration and reduces the risk of side effects and drug-drug interactions. Furthermore, the lung's vast surface area and extensive capillary network facilitate efficient drug absorption, potentially allowing for lower therapeutic doses. Additionally pulmonary delivery can improve patient compliance and comfort as it is a non-invasive route of administration. This is particularly important in the treatment of chronic respiratory conditions such as CF where long-term therapy may be required.

Dry powder formulations have gained prominence as a preferred method for the pulmonary delivery of AMPs as they ensure the long-term integrity of the API, exhibit improved aerosolization and drug deposition characteristics into the lungs. To produce dry powder formulations, the spray-drying technique is widely used as a method to engineer microparticles that deliver drugs to the lungs.

The engineering allows for a vehicle to be manufactured with characteristics potentially suited for the purpose, such as a particle size in terms of aerodynamic diameter between 1- 5 μm, low density, and spherical morphology, occasionally wrinkled depending on the formulation composition and manufacturing parameters. The formulation often requires the incorporation of excipients to optimize the DPI performance, enhance flowability, and reduce aggregation. Within the study, we examined the role of mannitol, trehalose and leucine when employed as excipients in the manufacturing of spray drying powders, deepening this technique by means of a Design of Experiments (DoE). This systematic approach enables to fine-tuning

microparticulate formulations by methodically varying key factors during the drying step to achieve desired quality attributes and performance while conserving resources and time. The application of DoE in combination with particle engineering techniques could enhance the ability to design and develop systems for pulmonary AMPs delivery that are effective, robust, and reproducible.

In this part of the project, the purpose was focused on the formulation development of the antimicrobial peptides LL37, WLBU2, and hLF1-11 to promote their pulmonary delivery. To this end, the spray-drying technique was used for the development of respirable powders that were characterized from a chemical-physical point of view, for their aerodynamic performance *in vitro* and for their biological activity of pulmonary cells and bacterial culture.

2 Materials

WLBU2 (RRWVRRVRRWVRRVVRVVRRWVRR, 3400.12 Da), LL37 (LLGDFFRKSKEKIGKEFKRIVQRIKDFLRNLVPRTES, 4493.29 Da), and hLF1-11 (GRRRRSVQWCA, 1374.58 Da) were purchased from GenScript Biotech (Rijswijk, Netherlands) as white lyophilized powder (TFA salt) with a purity of ≥ 90% and stored at -20 °C. Mannitol (C*PharmMannidex 16700, Lot number 0521520), trehalose dihydrate (Ph. Eur., Lot number DR015) and L-leucine (USP, Lot number 70960004) were purchased from A.C.E.F. S.p.A (Piacenza, Italy). Hard hydroxy-propyl methylcellulose (HPMC) capsules (size 3) were donated as gift from Capsugel (Colmar, France). RS01 Dry Powder Inhaler DPI device was provided without charge by Plastiape S.p.a (Osnago, LC, Italy). All the solvents used were of analytical grade. Glass Fiber Filters 1µm, 76 mm (Pall Corporation, Sartorius, Lot number 25827086) and glass microfiber filters 934-AH 82,6 mm (GE Healthcare Life Science, Whathman, UK, Lot number 9829490) were employed.

3 Methods

3.1 Designing Dry Powder Delivery Systems for Antimicrobial Peptide

3.1.1 Formulation study of WLBU2 microparticles: DoE approach

A regular three-factors two-level full factorial (2^3) DoE with three center points (Design-Expert Software Version 13®, Stat-Ease, Inc., USA) for a total of 11 experimental runs, was carried out to investigate the effect of spray-drying process parameters on selected Critical Quality Attributes (CQAs) of WLBU2 dry powders. The process parameters chosen as input variables were: (A) feed concentration (mg/ml), (B) feed rate (ml/min), and (C) inlet temperature (°C). Each factor was investigated on two levels (-1,1) plus a middle level (0) to check for a possible curvature. Specifically, feed concentration values were 1, 3, and 5 mg/ml; feed rates 3, 4, and 5 ml/min, and inlet temperatures 90, 105, and 120°C. The effect of these factors was assessed on the drying process yield (%), the particle size (µm), the aerodynamic performance represented by the Emitted Fraction (EF %) and the Respirable Fraction (RF %), and finally the residual moisture content. The experimental design matrix is summarized in Table 1. Each response was analyzed by ANOVA test with a confidential interval of 95% ($p < 0.05$) to define the significance of the mathematical model.

Table 1. Matrix of the experimental design applied for spray-dried microparticle preparation.

Runs	Factor A Feed Concentration [mg/ml]	Factor B Feed rate [ml/min]	Factor C Inlet Temperature [°C]
#1	3	4	105
#2	5	3	120
#3	5	5	90
#4	1	5	90
#5	3	4	105
#6	3	4	105
#7	1	3	90
#8	5	5	120
#9	1	3	120
#10	1	5	120
#11	5	3	90

Formulations containing 20 % w/w of WLBU2, 20 % w/w of leucine and 60 % w/w mannitol were spray-dried using a Mini Spray Dryer B-290 (Buchi Labortechnik, Flawill, Swizterland) equipped with B-295 dehumidifier operating in closed loop mode using nitrogen as drying gas. A two-fluid nozzle with an orifice diameter of 0.7 mm as well as a co-current spraying mode, where the airflow from one channel and the feed solution from the other moved in the same direction until they reached the nozzle, were employed. Spray-dried particles were separated from the drying gas by high-performance. The atomizing air flow rate and the aspirator rates were kept constant at their maximum capacity of 742 L/h and 35 m^3/h, respectively, the feed rate and the inlet temperature were varied from 3 to 5 ml/min and 90°C to 120°C, respectively. The third variable factor of the DoE was the feedstock concentration from 1 to 5 mg/ml. Considering that the peptides can undergo degradation in the presence of high oxygen concentration, the selected amount of WLBU2 was weighed in a glove box under a nitrogen atmosphere within a relative humidity percentage lower than 6 %. WLBU2 was dissolved, under a magnetic stirring at 400 rpm, in an ultrapure water (MilliQ grade, Millipore), in which the excipients were previously added. In trials of the DoE where an inlet temperature was set at 90 °C (*i.e.* run #3, #4, #7, #11) to improve the water evaporation 10 % v/v was added. However, this variable was not considered in the statistical analysis performed during the DoE. The final dry powder product was collected, weighed on an analytical balance, and stored at 4°C inside amber glass vials sealed with plastic caps. The yield of the process was calculated as a percentage, using the following formula:

$$yield\ (\%) = \frac{mass\ of\ collected\ spray\ dried\ powder\ (mg)}{mass\ of\ initial\ solid\ components\ before\ spray\ drying\ \ (mg)} * 100$$

Blank microparticles composed of mannitol and leucine in a 3:1 % w/w ratio, as in the formulations manufactured during the DoE, were prepared by applying the process conditions of Run #10 and with the aim of testing the cellular cytocompatibility of the excipients.

3.1.2 LL37 and hLF1-11 dry powder formulations

For LL37 peptide, taking into consideration the information obtained from WLBU2 DoE, spray-dried powders were produced by dissolving mannitol or trehalose together with LL37 in ultrapure water to achieve a final concentration of 1 % w/v. The solutions were spray-dried using the Mini Spray Dryer B-290 (Buchi Labortechnik, Flawil, Switzerland). The following parameters were applied: inlet temperature 120 °C, nitrogen air flow rate 742 L/h, air aspirator 35 m^3/h, and flow rate varied from 3 to 5 mL/min. A two-fluid spray nozzle with an internal diameter of 0.7 mm was used. Trehalose/leucine and mannitol/leucine were chosen applying a mass ratio of 95:5 and 85:15 (excipient:API) to increase LL37 amount within the powders. The microparticle system consisting of a matrix of trehalose and leucine was also used for the encapsulation of the hLF1-11 peptide, applying the same process parameters as those that led to the powder F of LL37.
As for WLBU2, for further *in vitro* cytocompatibility investigation blank spray-dried microparticles were prepared with a mannitol to leucine ratio of 7.5:1 as in formulation #F.

Table 2. Preliminary screening and formulation study for LL37 spray-dried powders.

	Formulation Design		
	Excipient	**Drug/excipient ratio**	**Feed rate [ml/min]**
A	Mannitol	95:5	5
B	Mannitol	95:5	3
C	Trehalose	95:5	5
D	Trehalose	95:5	3
E	Trehalose	85:15	5
F	Trehalose	85:15	3

3.1.3 WLBU2 content assay

The quantitative determination of WLBU2 within the spray-dried powders was carried out by means of High-Performance Liquid Chromatography (HPLC). A LC-10 AT VP system coupled to an UV detector SPD-10 A VP, a SIL-20 HT autosampler and a

column heating oven CTO-10AS VP (Shimadzu, USA, Manufacturing INC) was used. The analysis was carried out in reverse phase chromatography with an INERTSIL 5 ODS-3 150 x 3 mm column (GL Science, Torrance, CA, USA) coupled with a guard column. The elution was performed in a gradient mode with 100 % ultrapure water + 0.05 % v/v trifluoroacetic acid (TFA) as mobile phase A and acetonitrile:H_2O + 0.05 % TFA 95:5 v/v as mobile phase B (from 5 % v/v to 95 % v/v phase B). Flow rate was set to 0.4 ml/min, injection volume of 50 µL, run time 35 minutes, and temperature 35°C. The detection wavelength was set at 210 nm. WLBU2 calibration curve was obtained by plotting the peak's area referred to 6 solutions from 5 to 300 µg/ml assessing the linearity in this range with R^2 = 0.99 (Figure 12). The limit of detection (LOD) and the limit of quantification (LOQ) were found to be 0.03 µg/ml and 0.09 µg/ml, respectively.

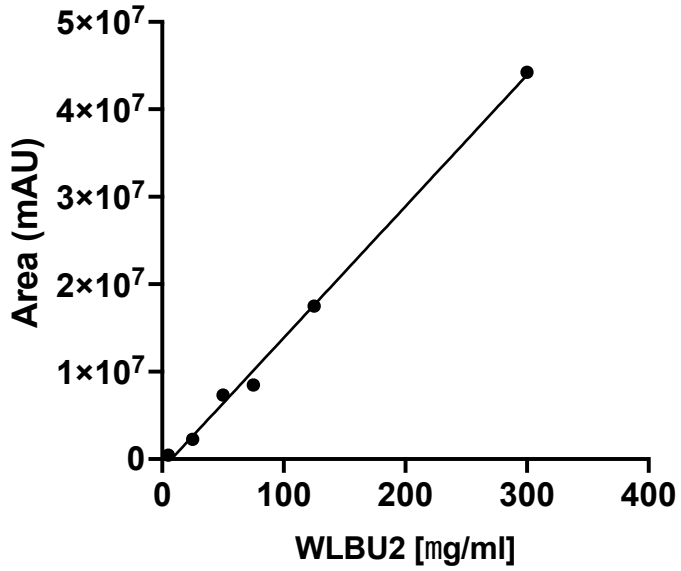

Figure 12. WLBU2 calibration curve showing linearity in the range of concentration tested (mean value ± standard deviation, n = 3).

3.1.4 LL37 and hLF1-11 content assay

A method to detect LL37 was developed using an Ultra High Performance Liquid Chromatography system (UHPLC). A Shimadzu Nexera series LC-40D XS system (Shimadzu Manufacturing INC, USA), coupled with an UV SPD-M40 detector, autosampler SIL-40C XS and column oven CTO-40C, was employed. The separation

was carried out in reverse phase chromatography with a Poreshell 120 EC-C18 2.7 μm, 2.1 x 75 mm column (Agilent, Santa Clara, CA, USA) and the elution was performed in a gradient mode from 5 % v/v to 95 % v/v of mobile phase B. Mobile phase A was composed by 100 % ultrapure water + 0.05 % v/v TFA, while mobile phase B was a mixture of acetonitrile and mobile phase A in a 95:5 v/v ratio. Flow rate was set at 0.4 ml/min, injection volume of 20 μl, run time of 10 minutes under an oven temperature of 30 °C. LL37 was detected with a wavelength of 210 nm with a retention time of 6.8 minutes. A calibration line, shown in Figure 13, was obtained by plotting the peak's area referred to solutions from 10 μg/ml to 100 μg/ml. Linearity was determined in this range with R^2 = 0.99. For LL37 LOD and LOQ were found to be 0.18 μg/ml and 0.54 μg/ml, respectively

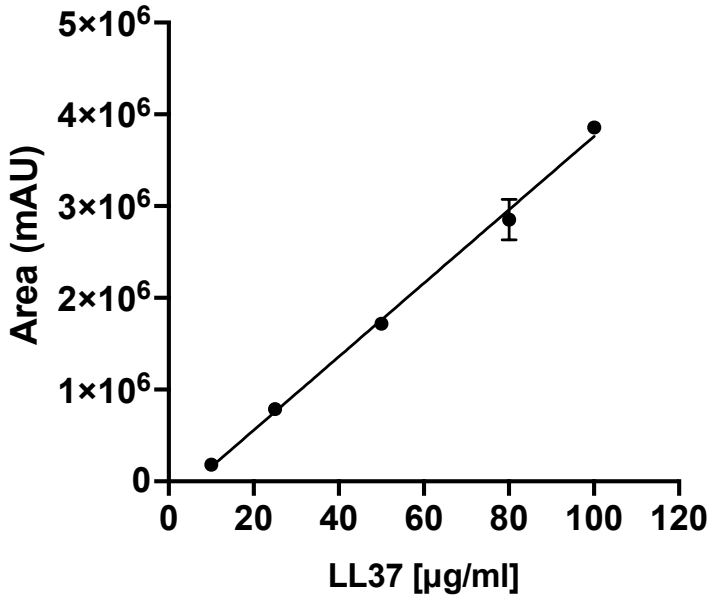

Figure 13. LL37 calibration curve showing linearity in the range of concentration tested (mean value ± standard deviation, n = 3).

The same method described above was applied for hLF1-11 detection and quantification in the spray-dried powders. hLF1-11 retention time was 3.9 minutes. Calibration line was obtained by plotting the peak's area referred to solutions from 5 μg/ml to 100 μg/ml (Figure 14). Linearity was determined in this range with R^2 = 0.99, with a LOD and LOQ of 0.14 μg/ml and 0.42 μg/ml.

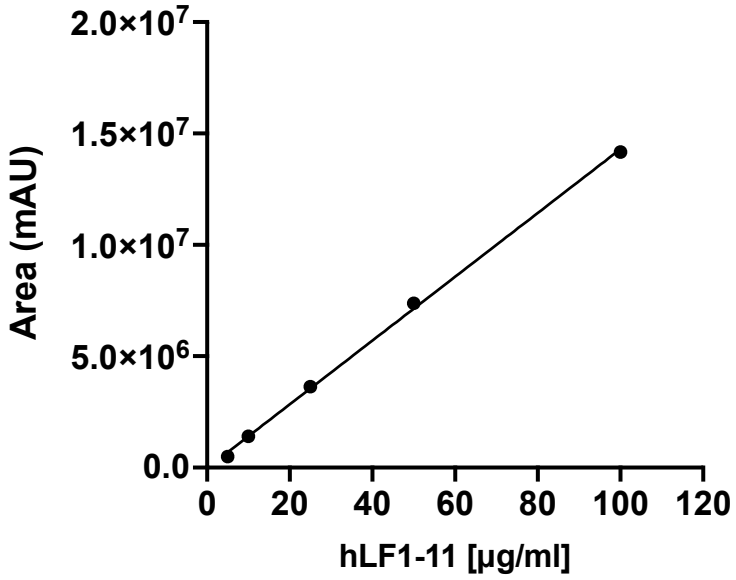

Figure 14. hLF1-11 calibration curve showing linearity in the range of concentration tested (mean value ± standard deviation, n = 3).

3.1.5 Particle size distribution

The particle size distribution of the spray-dried microparticles (WLBU2 SD, LL37 SD, hLF1-11 SD) was determined by laser diffraction using a Spraytec® (Malvern Instruments Ltd., Worcestershire, UK) equipped with a 300 mm focal lens which allowed the measure of particles ranging from 0.1 to 900 µm. Briefly, 5.00 ± 0.15 mg of each spray-dried powder was weighed on an analytical balance and suspended in 10 ml of cyclohexane solution containing 1 % w/v Span 85. Each suspension was sonicated for 1 minute in an ultrasonic bath (Ultrasound bath, USC 300 T VWR International, Fontenay-sous-Bois, France) to avoid aggregate formation. Measurements were performed in triplicate. The particle size was expressed as the mean volume diameter (µm) and the distribution was graphically obtained by plotting the percentage of particle volume versus the logarithmic scale of the size (µm). Results were represented by Dv_{10}, Dv_{50}, Dv_{90} indicating respectively the 10%, 50%, and 90% volume diameters of the particle population [126]. The Span value [$(Dv_{90}-Dv_{10})/Dv_{50}$)], *i.e.* the width of the particle-size distribution from the median particle range, was also

calculated. All the analyses were performed at an obscuration level of approximately 7-8 %.

3.1.6 Thermal analysis

The thermal behavior of unprocessed peptides and spray-dried microparticles was investigated by differential scanning calorimetry (DSC). Analysis was carried out by means of an Indium-calibrated Mettler DSC 821, driven by STARe software (Mettler Toledo, Switzerland). DSC is a method for measuring the heat flow generated in a sample as it is gradually heated to a specific temperature. During this heating process, the sample can undergo one or more phase changes, with melting being the most extensively studied. Throughout the experiment, the DSC apparatus measures the heat flow from the furnace to the sample, comparing it to the heat flow of a reference material. Approximately 5 mg of each powder was accurately weighed in a 40 µL aluminum pan (Me-27331 with pin, Mettler Toledo), sealed and pierced. The aluminum pans were then positioned in the furnace for the thermal analysis. The samples were subjected to a thermal scanning in the temperature range 25 -350 °C at a heating rate of 10 K/min under a nitrogen flow (100 ml/min).

3.1.7 Scanning Electron Microscopy

The morphological properties of raw material peptides and the spray-dried microparticles were observed using scanning electron microscopy (SEM, Auriga Compact, Zeiss, Oberkochen, DE) operating under high vacuum conditions with an acceleration voltage (EHT) kept constant at 1kV, a working distance (WD) between the sample and the column for the emission of the electrons beam of 5-6 mm and with a secondary electron's detector SE2. The images were collected at different magnifications. Samples were prepared by depositing 1-2 mg of raw material peptides or spray-dried particles on a double-sided adhesive tape pre-mounted on an aluminum stab and analyzed after a 30-minutes depressurization into the high vacuum chamber.

3.1.8 *In vitro* aerodynamic assessment of the spray-dried powders

3.1.8.1 Fast Screening Impactor

During the formulation screening, carried out according with the DoE, the *in vitro* aerodynamic performance of the manufactured formulations was carried out by means of the Fast Screening Impactor (FSI, Figure 15 A). The FSI segregates particles based on their size into two collectors: the Coarse Fraction Collector (CFC) and the Fine Particle Collector (FPC), representing the two stages of the impactor. The former captures large non-inhalable particles using an interchangeable insert, setting a cutoff at 5 µm, while the latter, equipped with an A/E glass filter (76 mm, Pall Corporation, USA), collects particles not captured by the CFC but entrained in the airstream. The FSI consists of three additional components: the induction port (IP), resembling the human throat with a right-angle steel tube, a mouthpiece adapter for airtight DPI-IP connection, and a vacuum pump that simulates inspiratory flow by creating airflow through the impactor. The analyses were conducted at a flow rate of 60 L/min, generating approximately 4 kPa of pressure. The actual flow was verified using a mass flow meter (DFM 2000, Copley Scientific Ltd., Nottingham, UK) before each actuation to ensure the desired flow rate.

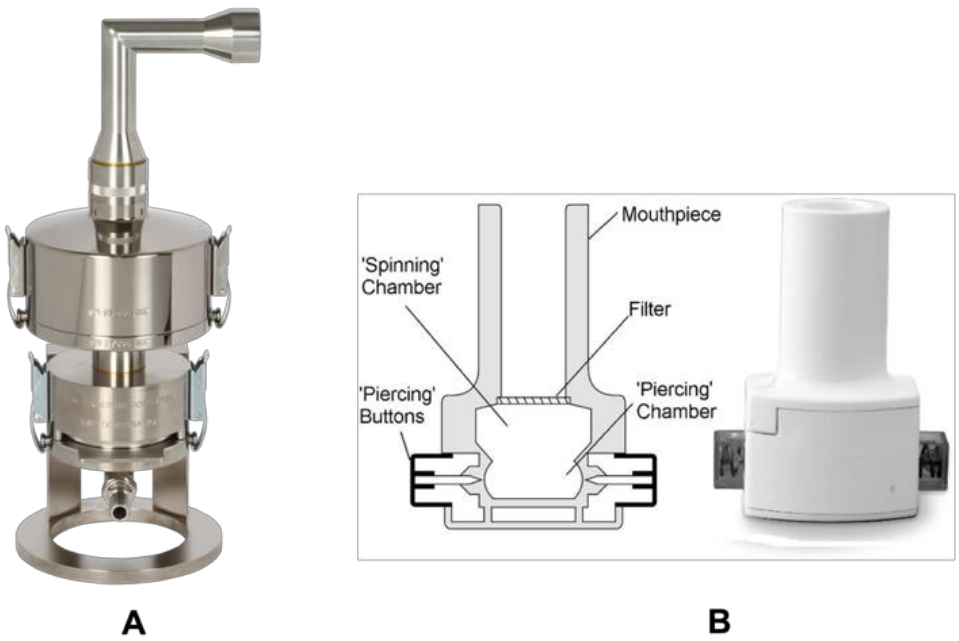

Figure 15. A) FSI (Copley Scientific Limited, Nottingham, United Kingdom) and B) RS01 DPI and its internal section (Berry Global Inc., Italy).

Approximately 20 mg ± 0.05 mg of each spray-dried powder were loaded into two hard HPMC capsules size 3. Subsequently, one capsule at a time was inserted into the holder chamber of an RS01 DPI device (Figure 15 B, Plastiape S.p.a, Osnago, LC, Italy) pierced by pressing the two buttons located on the side of the device base, and aerosolized with the test lasting for 4 seconds. Ultrapure water served as a solvent for sampling the powder in the CFC, filter located in the FPC, IP, mouthpiece adapter, device and capsule. Briefly, the mouthpiece adapter and the induction port were collectively washed with of ultrapure water in a 25 ml volumetric flask. Likewise, the CFC and the device were separately washed in a 10 ml volumetric flask. The filter was subjected to a 5-minute sonication in an ultrasonic bath, the solution was transferred in a 10 ml volumetric flask and then filtered using 0.45 µm cellulose acetate syringe filters. Finally, the two capsules were extracted from the device, dissolved with ultrapure water in a 10 ml volumetric flask, sonicated for 20 minutes, and filtered with 0.45 µm cellulose acetate syringe filters. The quantification of WLBU2 was carried out by HPLC, according to the method described in Chapter III, section 3.1.3. Key parameters considered were the EF % represented by the percentage of WLBU2 released from the inhaler compared to the loaded dose; the amount of powder deposited on the A/E glass filter, termed as Fine Particle Dose (FPD), and the RF % expressed as the ratio of FPD to the emitted dose.

3.1.8.2 Next Generation Impactor

The *in vitro* aerodynamic performance of selected formulation of WLBU2 SD and LL37 SD was further investigated with the Next Generation Impactor (NGI) (Copley Scientific, Nottingham, UK). Formulations tested are listed in Table 3.

The NGI has become one of the impactors of choice for the *in vitro* aerodynamic evaluation of inhalation products, as it allows the size distribution of drug particles to be determined in terms of aerodynamic diameter. Thus, by calculating the fraction of particles reaching the lowest stages, considered the first respirable fraction (< 5 μm), it allows regional deposition in the lung to be hypothesized [127].

Table 3. Peptides formulations selected for NGI testing. For WLBU2 peptide the best performer in terms of size and aerosolization properties from the DoE was chosen, *i.e* Run 10, while for LL37 the selection was primary based on the drug content findings.

Formulation	Mannitol %	Trehalose %	Leucine %	Feed concentration [mg/ml]	Feed rate [ml/min]	Inlet T [°C]
WLBU2 SD #10	60	-	20	1	5	120
LL37 SD #F	-	75	10	1	3	120

There are different parameters that can be calculated considering the amount of drug deposited on the NGI stages: Delivered Dose (DD mg), Fine Particle Fraction (FPF), Median Mass Aerodynamic Diameter (MMAD) and Geometric Standard Deviation (GSD). DD corresponds to the amount of drug that after the aerosolization reaches the impactor, while FPF is referred to the percentage of particles that has a size equal or lower 5 μm. MMAD is the average particle size corresponding to the value at which 50% of the particles are greater and 50% of the particles are smaller than the MMAD itself [128,129]. MMAD was determined by plotting the cumulative percentage of mass less than stated aerodynamic diameter (probability scale) versus the natural logarithm of the effective cut-off diameter of each stages using GraphPad Prism, Version 9 (Graphpad Software Inc., La Jolla, CA, USA) The geometric standard deviation (GSD) represents the spread of the distributions within the different stages of the NGI, it is calculated from the cumulative plot applying the following formula:

$$GSD = (X/Y)^{0.5}$$

where X and Y represented the 84 % and 16 %, respectively, of the drug mass recovered from the NGI from stages 1 to 7. As reported by Ceschan et al., the distribution appears to be narrow when GSD is lower than 3 [130].

2 hard HPMC capsules size 3 were loaded with 40 mg ± 0.05 mg each of WLBU2 SD and 45 ± 1.38 mg each of LL37 SD, then inserted one at time within the holder chamber of an RS01 DPI (Plastiape, Osnago, Italy) device and pierced. The NGI was composed of seven pierced stages and a micro-orifice collector (MOC), where a filter (glass microfiber filter, 82.6 mm, GE Healthcare Whatman, UK) was placed to collect the finest particles. The impactor was also equipped with a mouthpiece adapter and a

steel induction port (IP), that imitates the human throat. The cut-off diameters of the NGI stages were: d_{st1} 8.06 µm, d_{st2} 4.46 µm, d_{st3} 2.82 µm, d_{st4} 1.66 µm, d_{st5} 0.94 µm, d_{st6} 0.55 µm, d_{st7} 0.34 µm. Each stage was previously coated with a Tween 20 EtOH 2% w/v solution to enable powder deposition. The analysis was carried out with a flow of 65 L/min adjusted prior to each analysis by means of a mass flow meter (DFM 2000, Copley Scientific Ltd., Nottingham, UK). For the analytical quantification, the mouthpiece adapter and the IP were washed with ultrapure water in a 25 ml volumetric flask. The same procedure was employed for the device. The two capsules were removed from the device, dissolved together with ultrapure water in a 25 ml volumetric flask, sonicated for 20 minutes and filtered with 0.45 µm cellulose acetate syringe filters. The filter was washed and sonicated for 5 minutes in an ultrasonic bath; thus, the solution was transferred in a 10 ml volumetric flask and filtered with 0.45 µm cellulose acetate syringe filters. WLBU2 and LL37 quantification was carried out with HPLC and UHPLC as described in Chapter III, sections 3.1.3 and 3.1.4.

3.2 Circular Dichroism spectroscopy

Far-UV Circular Dichroism (CD) experiments were performed using a J-1500 Circular Dichroism Spectrophotometer (Jasco, Easton, MD, USA), equipped with a Peltier thermal controller set at 20°C. CD spectra were recorded from 250 to 195 nm, as an average of 4 determinations, with wavelength steps of 0.5 nm, scanning speed of 50 nm/min and bandwidth of 1.0 nm, using 1 mm quartz cuvettes (Hellma, type 100-QS, match 284). Aqueous solution of the selected peptides (100 µM) and WLBU2 SD (50 µM) were prepared from an initial solution at 0.6 mM stored at 4 °C. The spectra were recorded in the presence or absence of lipopolysaccharide (LPS) 0.03 %, detoxified lipopolysaccharide (LPSd) 0.083 %, sodium dodecyl sulphate SDS 50 mM. Each solution was prepared in a final volume of 200 µl. CD spectra of excipients were acquired in the same conditions. Following baseline correction, the observed ellipticity θ (millidegrees) was converted to molar mean residue ellipticity [θ] (deg cm^2 $dmol^{-1}$), according to the following formula:

$$[\theta] = \frac{\theta}{(10 \text{ x } C \text{ x } l \text{ x } n)}$$

where 'C' represents the concentration expressed in molarity, 'l' the optical path expressed in 'cm', and 'n' the number of residues of the peptide.

3.3 *In vitro* cytotoxicity studies on peptides-loaded microparticles

The *in vitro* cytotoxicity study of the raw material peptides and spray-dried formulations was performed on the human lung adenocarcinoma cell line A549 and the immortalized human bronchial cell line BEAS-2B. The two cell lines were cultured with RPMI-1640 medium supplemented with 2 mM glutamine, 10 % fetal bovine serum (FBS Gibco, Life Technologies) and antibiotics such as penicillin 100 U/ml and streptomycin 100 mg/ml. The cell lines were maintained at 37°C in a water-saturated atmosphere of 5 % CO_2 humidified incubator. Cells were detached using trypsin-EDTA 0.25 % v/v which was then deactivated by adding fresh complete medium, and cells were centrifuged at 1740 rpm for 3 minutes. The supernatant was removed, and the pellet was resuspended in RPMI medium. A549 and BEAS-2B (density of 3 x 10^3 cells/dish) were seeded into a 96-well plate and incubated overnight for attachment. Cell viability was evaluated by crystal violet (CV) staining. Both raw material peptides and spray-dried microparticles were dissolved in RPMI, stored at 4°C and then diluted in fresh medium before treating the cells. After 24 h, A549 and BEAS-2B cells were seeded and exposed to increasing concentrations of WLBU2, LL37, and hLF1-11 peptides and their respective formulations. 72 h after treatment, the medium was removed, and cells were fixed with 100 μl of ice-cold methanol for 15 minutes at 4°C. Then, methanol was removed and 100 μl of a crystal violet solution at 0.5 % w/v was added to each well. After 15 minutes, crystal violet was removed, and a solution of PBS Triton 0.5 % v/v was applied to solubilize the crystals obtained. The plate was left to shake for 30 minutes and the absorbance at 570 nm was measured using a microplate reader (TECAN Infinity® 200 PRO, Männedorf, Switzerland). As a control, the cytocompatibility of blank microparticles was also assessed with the same procedure.

3.4 *In vitro* antimicrobial studies

3.4.1 Antimicrobial activity against planktonic cells

WLBU2, LL37, and hLF1-11 were solubilized in water at a concentration of 2 mg/ml. The *in vitro* antimicrobial activity was evaluated against planktonic bacterial cells of *P. aeruginosa* ATCC 27853 and *P. aeruginosa* PECHA 4 by colony forming unit assays (CFU). Bacterial suspension representative of nearly 500 CFUs were incubated in absence (control) or presence of serial concentrations of either the peptides or their formulation at 37 °C for 5 hours, then spread on Mueller-Hinton Agar plates (MHA). After 24 hours of incubation CFUs were enumerated and peptide bactericidal activity was determined as a percentage of CFU inhibition. Each assay was carried out in triplicate, and at least two independent experiments were performed for each condition. This assay was carried out also for WLBU2 SD, while for LL37 SD and hLF1-11 SD only a preliminary evaluation was performed on *P. aeruginosa* PECHA 4 investigating the effect at 5 and 2 μg/ml. Results were expressed by the half-maximal effective concentration (EC_{50}) obtained by nonlinear regression analysis using GraphPad Prism 10 (San Diego, CA, USA).

3.4.2 Time killing kinetics

Afterwards, the bactericidal activity of peptides and/or formulations was also evaluated over time performing a time-killing assay. Each peptide, was added to the bacterial suspension at the concentration of 5 μg/ml, corresponding to the minimal bactericidal concentrations at 5 hours. The kinetics of the killing activity were determined by CFU assays where samples were collected for CFU determination after 2, 5, 8, 10, 20, 30, and 60 minutes of incubation. As regards the formulation tested, the assay was performed on WLBU2 SD.

3.4.3 Biofilm assays

Bacteria such as *P. aeruginosa* are prone to growth in microbial communities forming biofilms at the site of infection. This environment makes bacteria more resistant to antibiotic treatment so that the ability of new antimicrobial molecules to treat biofilms

is an important factor that needs to be considered [131]. This research evaluated the effect of WLBU2/WLBU2 SD and, preliminarily, of LL37/LL37 SD on mature biofilm. For the assay, bacteria were cultured on MHA at 37°C overnight and then standardized in tryptic soy broth (TSB) with 0.5 % glucose (TSBG) at an optical density OD_{530} = 0.3 for both standard and clinical *P. aeruginosa* strains. The suspension was added (100 μL/well) into 96-well polystyrene flat-bottomed microtiter plates and incubated at 37 °C.

3.4.3.1 Treatment on mature biofilm

To investigate the effect of WLBU2/WLBU2 SD and LL37/LL37 SD on mature monomicrobial biofilm, bacterial suspensions were incubated at 37 °C for 24 hours in a wet chamber, then after washing, the biofilms were treated with 100 μL of water (control) of peptides w/o formulation at a final concentration of 5 μg/ml for 5 hours and 24 hours at 37 °C. Each assay was performed in triplicate, and at least two independent experiments were performed for each condition.

3.4.3.2 Biofilm biomass quantification

The biofilm biomass of the treated and control samples was quantified by a CV assay. Briefly, after treatments, the wells were washed with water, fixed by air drying, stained with 100 μL of 0.25% CV for 15 min in the dark, washed three times with water, and eluted with 85% ethanol. The biofilm biomasses were quantified by measuring the absorbance at 540 nm with a Multiskan Ascent Plate Reader (Thermo Labsystems). The results were expressed as the percentage of biofilm inhibition in the treated samples vs. the controls.

3.5 Statistical analysis

Differences between groups were assessed with one-way analysis of variance (ANOVA), p values ≤ 0.05 were considered statistically significant. During the *in vitro*

biological evaluation, each assay was performed at least in duplicate. Data were shown as the mean ± standard deviation.

4 Results and Discussion

4.1 Formulation study of WLBU2 microparticles: a DoE approach

The spray drying process is widely used to obtain powder products as it is practical, versatile, and highly applicable on an industrial level. Nevertheless, during the drying process, materials can be exposed to stress, especially thermal one, which can adversely affect the quality of the product. To optimize the process conditions to reduce the stress applied to the materials and in particular the peptides used, WLBU2 was formulated following an experimental design, as described in Chapter III, section 3.1.1. This made it possible not only to identify a prototype that could be defined as promising in terms of aerodynamic behavior *in vitro,* but also to identify the critical parameters that influence the quality attributes of the final product [132]. The experimental design aimed to study a combination of spray-drying process parameters to obtain a powder capable of being deposited in the lung, while at the same time being composed of excipients capable of ensuring adequate peptide delivery following their dissolution [133]. Considering this, the composition of the microparticle system was kept constant and included 20 % w/w WLBU2, 60 % w/w mannitol, and 20 % w/w leucine. Mannitol was the sugar of choice for the formation of the microparticle matrix by its many properties including that of bulking agent, stabilizer, and moisture protector. In the case of peptides, which are considered small biopharmaceutical molecules, the stabilization induced by a non-reducing sugar such as mannitol can be explained by the water replacement theory. Specifically, during the drying process, the non-reducing excipient can establish hydrogen bonds with the biomolecule by positioning itself as a substitute for the water molecules present in the hydrated state. This allows the biomolecule to maintain its integrity and native conformation [102,134]. In addition, mannitol exhibits low hygroscopicity with a hyperosmotic effect that improves mucociliary clearance and thus lung function in patients with respiratory diseases. Consequently, it is especially used to produce DPI formulations of

biopharmaceutical molecules. Moreover, the addition of mannitol usually results in the formation of crystalline particles because of the extremely low glass transition of this excipient leading to tensely smooth surfaces that reduce the cohesion forces between the dried particles and improve their aerodynamic properties [102,134–136]. The second excipient constituting the microparticle matrix was L-leucine, a neutral hydrophobic amino acid. The use was technological since it enables the production of flowable powders by reducing inter-particle cohesion, thus positively affecting the emitted dose, one of the key parameters defining the efficacy of a product intended for pulmonary administration [102]. The mechanism of this is related to the movement of leucine at the air-liquid interface during the drying process, creating crystals along the surface of the particles being formed, making them rough and improving their flowability. Once the critical concentration of leucine is reached, it forms nuclei that grow into crystals around the evaporating solvent droplets, forming a crystalline structure that tends to appear wrinkly on the surface [97]. Leucine is thus a modifier of the surface of the microparticles. L. Li et al. described a sigmoidal relationship between the initial mass of leucine and the molar ratio found along the surface of the dried particles, showing that a leucine content between 5 and 20 % resulted in partial coverage of the particles surface (~20%, molar percentage) [137]. This phenomenon has a morphological consequence: the presence of 5 to 20 % leucine results in a slightly wrinkled surface, while when the concentration increases to 40 %, particles appear significantly corrugated and up to 80 % this morphology is heavily observed [134,137,138]. To define the factors of the experimental design, it was necessary to clarify what happens during the spray-drying process. Briefly, a solution or suspension is atomized through a flow of hot air or other gas with the formation of droplets. Subsequently, the droplets undergo an evaporation process, better termed rapid dehydration within the drying chamber, producing dried particles. During this step, sugars change to a solid state either by crystallization or precipitation into amorphous products depending on the type of sugar and thus on its hygroscopic characteristics and water content. During this process, factors such as feed rate, feed concentration, airflow rate, and drying temperature can induce both mechanical and thermal stress on the peptide, leading to a loss of stability and eventual degradation. To reduce this, the Quality by Design (QbD) approach made it possible to identify combinations of factors that lead to a reduction in the stress to which the materials were exposed

[95,139]. Consequently, a two-level full Factorial Design with three factors was employed to investigate the production of the spray-dried powders. Table 4 summarizes the matrix of the DoE.

Table 4. Matrix of the DoE with factors values and responses.

Run	Factor A Feed concentration (mg/ml)	Factor B Feed rate (ml/min)	Factor C Inlet temperature (°C)	Yield (%)	D_{v50} (μm)	EF (%)	RF (%)	Moisture content (%)
#1	3	4	105	59.70	4.54±0.00	89.9	48.83	1.39 ± 0.12
#2	5	3	120	67.36	5.15±0.34	88.75	50.66	1.32 ± 0.05
#3	5	5	90	63.31	5.27±0.07	98.97	65.09	1.43 ± 0.02
#4	1	5	90	50.52	3.76±0.09	97.38	83.82	1.28 ± 0.07
#5	3	4	105	55.66	4.96±0.17	87.39	59.35	1.56 ± 0.16
#6	3	4	105	60.86	4.35±0.16	91.07	55.62	1.40 ± 0.07
#7	1	3	90	43.05	5.23±0.01	90.41	75.56	2.34 ± 0.77
#8	5	5	120	61.67	6.01±0.03	94.08	44.43	0.69 ± 0.12
#9	1	3	120	59.90	3.37±0.38	91.53	70.37	2.22 ± 0.47
#10	1	5	120	48.89	3.84±0.08	86.12	75.28	0.54 ± 0.26
#11	5	3	90	51.01	5.78±0.02	90.75	54.10	0.70 ± 0.07

According to the design, eight runs plus three center points for a total number of eleven experiments were generated in a randomized way to prevent bias. The three factors, and the corresponding low, middle, and high levels were the following: A, feed concentration (1, 3, and 5 mg/ml); B, feed rate (3, 4, and 5 mg/min); C, inlet temperature (90, 105 and 120 °C).

From the process point of view, the choice of feed concentration and feed rate as factors was justified by the fact that the former influences the structure of the solid obtained because of the evaporation, while the latter influences the size of the particles formed. Both are important parameters as they indirectly influence the aerodynamic performance of the spray-dried powder [126].

The inlet temperature was selected because the outlet temperature, *i.e*. the temperature to which the particles are exposed, depends on it. This factor is relevant to the residual water present in the powder, which can affect its dispersion characteristics [135].

The DoE responses*, i.e.* the CQAs of the final product, were identified on the basis of a careful review of the literature with reference to the fundamental characteristics of a powder product for inhalation administration. CQAs are defined as properties that must have a value within a limit to ensure good product quality. According to ICH Q8, it is necessary to define those quality parameters in such a way that these can be controlled at any time during the process [140]. Based on that, the CQAs evaluated were the yield of the process (%); the particle size distribution (μm); the EF, %; the RF %, and the moisture content (%) [141,142].

4.2 WLBU2 content in the spray-dried powders

The amount of WLBU2 within the spray-dried powders is shown in Table 5. WLBU2 recovery, *i.e.* the ratio of experimental to theoretical WLBU2 content expressed as a percentage, was optimal for almost all the spray-dried powders since it was never below the 85 %. This result agreed with that reported by Eedara et al., who pointed out that since drying occurs by exposure to a hot gas, molecules such as peptides and proteins may undergo thermal degradation. However, it was reported the rarity of this phenomenon as the temperature of denaturation is also dependent on the water content and the type of molecules, not just on the exposure temperature. Furthermore, the drug content obtained highlighted the crucial role of the chosen excipients in protecting the molecules from the mechanical stress produced during drying [95].

Table 5. WLBU2 content assay by HPLC analysis.

Run	Theoretical WLBU2 content (mg)	Experimental WLBU2 content (mg)	WLBU2 recovery (%)
#1	1.06	1.05 ± 0.05	99.24 ± 5.24
#2	1.04	0.90 ± 0.06	85.88 ± 5.85
#3	1.00	0.99 ± 0.01	99.75 ± 0.49
#4	1.02	0.99 ± 0.01	97.24 ± 0.58
#5	1.06	1.14 ± 0.06	108.38 ± 6.25
#6	1.04	1.00 ± 0.02	97.02 ± 1.74
#7	1.10	0.99 ± 0.01	89.89 ± 0.53
#8	1.02	0.94 ± 0.01	91.27 ± 0.42
#9	1.18	1.19 ± 0.01	101.30 ± 0.63
#10	1.08	1.08 ± 0.08	99.81 ± 7.90
#11	1.10	1.08 ± 0.05	98.36 ± 5.18

4.3 Characterization of WLBU2 spray-dried microparticles

4.3.1 Yield of drying

The solutions composed by WLBU2, mannitol and leucine were spray-dried according to the DoE as reported in Chapter III, section 3.1.1. The process yield was variable in the range of 45-65 % with some differences depending on the process parameters selected. The higher yield was evident for prototype 2 obtained from a solution at a concentration of 5 mg/ml, with feed rate of 3 ml/min and at inlet temperature of 120 °C. A detailed overview of the results is shown in Table 6.

Table 6. Spray drying process parameters and yields.

Run	Feed concentration (mg/ml)	Feed rate (ml/min)	Inlet temperature (°C)	Outlet temperature (°C)	Yield (%)
#1	3	4	105	58	59.70
#2	5	3	120	71	67.36
#3	5	5	90	47	63.31
#4	1	5	90	46	50.52
#5	3	4	105	58	55.66
#6	3	4	105	58	60.86
#7	1	3	90	52	43.05
#8	5	5	120	69	61.67
#9	1	3	120	52	59.90
#10	1	5	120	66	48.89
#11	5	3	90	54	51.01

The ANOVA analysis is shown in Table 7. Considering the low p value ($p < 0.05$), factor A as well as factor C had a significant effect on the process yield. However, factor B-Feed rate was found to be not significant (p 0.69), but model reduction by its removal could not be performed since it supported the hierarchy of the model and because its interaction with the inlet temperature was found to be significant. For this model, the Predicted R^2 of 0.8066 is in reasonable agreement with the Adjusted R^2 of 0.8699: *i.e*., the difference is less than 0.2, meaning that no transformation is needed during the DoE analysis. Adequate Precision measures the signal to noise ratio. A ratio greater than 4 is desirable. The ratio of 12.451 indicates an adequate signal. This model can be used to navigate the design space.

Table 7. Statistical evaluation of the relation between the yield and DoE factors. Results are from ANOVA analysis.

Source	Sum of Squares	df	Mean Square	F-value	p-value	
Model	502.31	5	100.46	14.37	0.0055	significant
A-Feed concentration	210.02	1	210.02	30.05	0.0028	significant
B-Feed rate	1.18	1	1.18	0.1686	0.6984	
C-Inlet temperature	111.98	1	111.98	16.02	0.0103	significant
AB	12.88	1	12.88	1.84	0.2327	
BC	166.26	1	166.26	23.79	0.0046	significant
Residual	34.95	5	6.99			
Lack of Fit	20.04	3	6.68	0.8967	0.5656	not significant
Pure Error	14.90	2	7.45			
Cor Total	537.26	10				

The magnitude of the chosen effects is explained by the Pareto chart (Figure 16 A). In detail, effects above the Bonferroni limits are considered the most important, while values above the t-value limit are only likely to be important. Based on this, the Pareto chart confirmed that both factor A and B as well as the interaction between factor B and C were important. This interaction means that the positive effect of the individual C-factor can not be considered as such but must be related to the change in the effect of the feed rate.

As it can be observed from the interaction graph in Figure 16 B, at the lowest level of C (90 °C) the yield appears to increase by 10 % as the feed rate increases (3 to 5 ml/min) while the yield decreases by the same percentage at the highest level of C (120 °C) as the feed rate increases. This implies that adequate evaporation of the solvent, resulting in the formation of dry particles with less tendency to impact the chamber walls, can be achieved by keeping the temperature constant at 120°C and the feed rate at its lowest level. This combination (120 °C, 3 ml/min) allows the droplets to be exposed to the high temperature for a longer time guaranteeing the removal of the solvent, resulting in a less sticky powder that settles more easily in the collector instead of sticking to the walls of the drying chamber or cyclone [133,143,144].

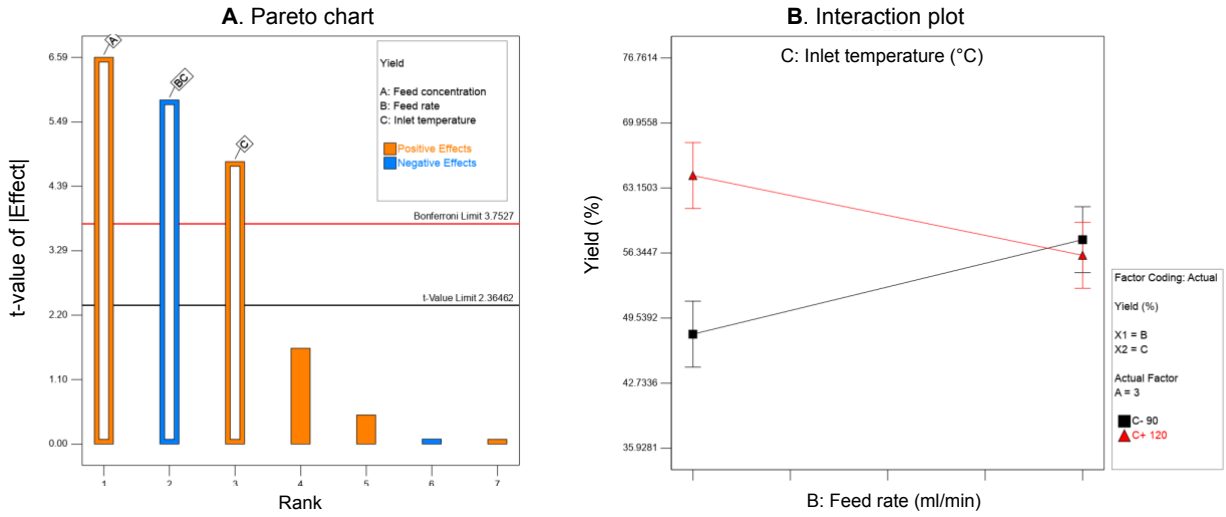

Figure 16. A. Pareto chart from Design Expert Software referred to the yield as response. Orange bars mean positive effect, blue bars stand for negative effect. B. Interaction plot for B-feed rate vs C-inlet temperature.

Furthermore, in the DoE the inlet temperature was studied at a level -1 corresponding to 90 °C and to speed up the evaporation process 20 % v/v ethanol was added to the feed solution. Contrary to previous studies, such as those presented by Seville et al., the organic solvent had no significant effect on the process yield obtained. Rabbani et al. showed that a reduction in process yield associated with the organic solvent can be explained in terms of an increase in the viscosity of the feed solution, which therefore requires more energy to be atomized [145]. On the contrary, the presence of ethanol in this study seemed not to affect the final yield of the drying.

The process yield is also strongly dependent on the outlet temperature to which the particles are exposed and the residual water present in the final product. When the outlet temperature is high, as in the case of run 2 (71 °C), the residual water content is lower (1.3 %) and the yield increases because the product is dried and less prone to adhere to the walls of the spray-dryer chamber [133,143].

The feed concentration positively affected the yield of the drying. Indeed, the highest yields were obtained at high feed solution concentrations. This was because when the feed solution is highly concentrated, the droplets have lower amounts of solvent, which leads to shorter drying times, lower residual moisture content, and higher yields. In any case, in most of the DoE trials yields exceeded 50 % (average 56.6%). Overall, yields obtained in this study were relatively homogeneous and acceptable with regard to lab-scale spray-drying equipment [142].

4.3.2 Particle size distribution

The particle's size distribution was assessed following the procedure described in Chapter III, section 3.1.5, by laser diffraction. Together with the aerodynamic behavior, particle density and shape, the size is a key factor influencing powder flow properties, especially when intended for inhalation [126]. Results are presented in Table 8. Data are expressed considering the volumetric diameter that divides the volume or mass of the sample into two equal halves (Dv_{50}) and particle size distribution is defined by the span values [126,145].

Table 8. Particles size distribution of spray-dried powders. Data are expressed as the mean ± standard deviation of three measurements (n=3).

Run	Feed concentration (mg/ml)	Feed rate (ml/min)	Inlet T (°C)	Dv_{10} (μm)	Dv_{50} (μm)	Dv_{90} (μm)	Span
#1	3	4	105	2.77 ± 0.09	4.54 ± 0.00	7.54 ± 0.19	1.05 ± 0.06
#2	5	3	120	3.01 ± 0.25	5.15 ± 0.34	9.37 ± 1.00	1.22 ± 0.06
#3	5	5	90	3.29 ± 0.00	5.27 ± 0.07	8.64 ± 0.22	1.01 ± 0.02
#4	1	5	90	2.12 ± 0.00	3.76 ± 0.09	6.54 ± 0.31	1.16 ± 0.05
#5	3	4	105	3.14 ± 0.05	4.96 ± 0.17	8.59 ± 1.22	1.09 ± 0.19
#6	3	4	105	2.63 ± 0.07	4.35 ± 0.16	8.26 ± 1.65	1.28 ± 0.31
#7	1	3	90	2.85 ± 0.05	5.23 ± 0.01	9.54 ± 0.08	1.27 ± 0.03
#8	5	5	120	3.73 ± 0.00	6.01 ± 0.03	9.83 ± 0.12	1.01 ± 0.16
#9	1	3	120	2.12 ± 0.16	3.37 ± 0.38	5.06 ± 0.63	0.86 ± 0.03
#10	1	5	120	2.35 ± 0.03	3.84 ± 0.08	6.36 ± 0.19	1.04 ± 0.01
#11	5	3	90	3.57 ± 0.01	5.78 ± 0.02	9.62 ± 0.11	1.04 ± 0.01

As shown in Table 8, the prepared dry powders showed a Dv_{50} between 3.3 μm and 6.0 μm, a range partially acceptable for pulmonary delivery. Indeed, although the true indicator of lung deposition as a function of size is the d_{ae}, the size distribution

represents crucial prior information. Indeed, the $d_{ae,}$ defined as the diameter of a sphere having unit density, is directly proportional to the volumetric diameter: as D_{v50} decreases, d_{ae} diminishes as well thus improving the aerosolization properties [146,147]. Generally, a size range between 1 - 5 μm is reported as a reference for lung deposition associated with a narrow and homogeneous distribution, indicated by span values not exceeding 1.5 [140,148].

Analysis of the response by ANOVA test was performed using Design Expert® and showed that the model was significant as stated by the Model F-value of 9.58 (Table 9). Regards the significant model terms, only the feed concentration was considered as single significant factor ($p<0.0019$) while the others were recommended to be removed from the model. Even the interaction between factor B-Feed rate and C-Inlet temperature had a marginal but significant effect on the Dv_{50}. Both the significance model terms, resulted in a positive effect as shown in the Pareto Chart (Figures 17 and 18).

Table 9. ANOVA results for the selected factorial model for the yield of the spray drying process.

Source	Sum of Squares	df	Mean Square	F-value	p-value	
Model	6.29	4	1.57	9.58	0.0089	significant
A-Feed concentration	4.52	1	4.52	27.53	0.0019	significant
B-Feed rate	0.0528	1	0.0528	0.3220	0.5910	
C-Inlet temperature	0.3486	1	0.3486	2.13	0.1951	
BC	1.37	1	1.37	8.35	0.0277	significant
Residual	0.9841	6	0.1640			
Lack of Fit	0.7893	4	0.1973	2.03	0.3568	not significant
Pure Error	0.1949	2	0.0974			
Cor Total	7.27	10				

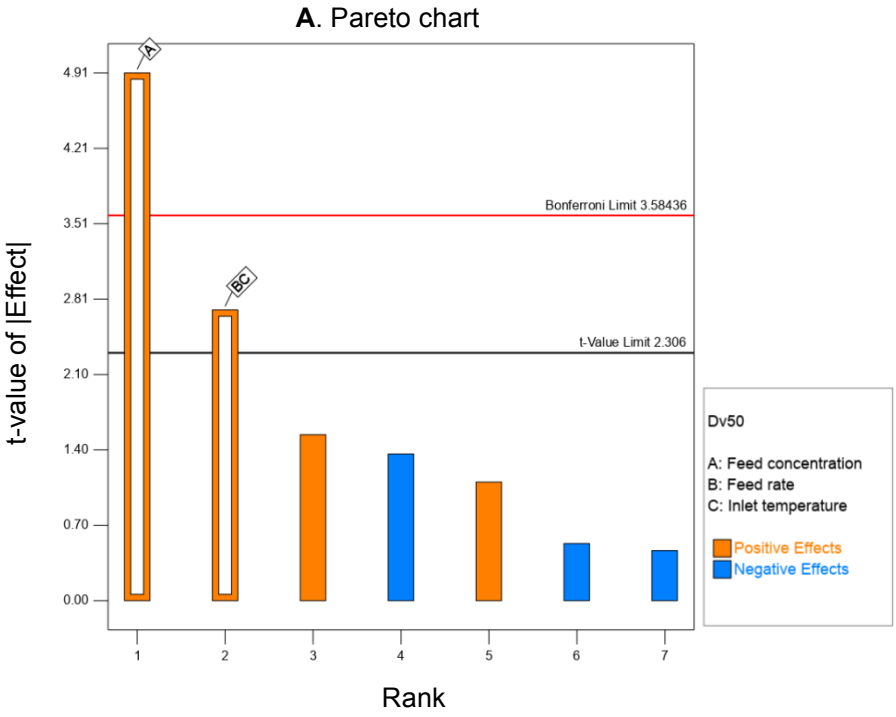

Figure 17. Pareto chart from Design Expert Software referred to the volumetric diameter (Dv_{50}) as response. Orange bars mean positive effect, blue bars stand for negative effect.

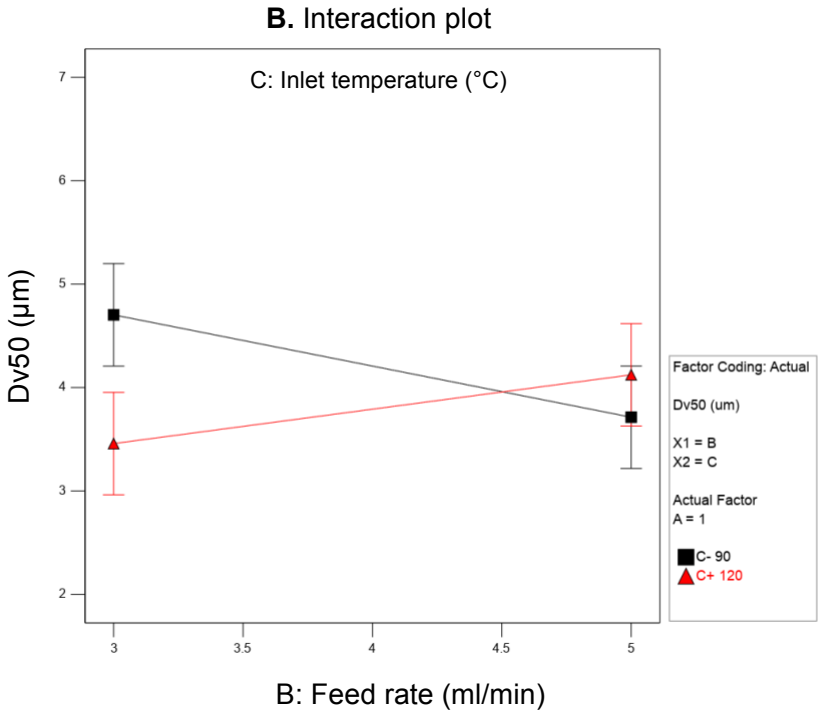

Figure 18. Interaction plot for BC: feed rate is represented on X1 axis while inlet temperature on X2 axis where black line stands for -1 level and red line for +1 level.

Factor A had a positive effect on the size distribution of the particle population, so as its level increases, the size increases. This relationship was previously highlighted by Pinto et al. and expressed in the mass balance defining the geometric diameter of spray-dried particles (d_g), by the following equation:

$$dg = \sqrt[3]{\frac{FC}{\rho p}} d_D$$

where FC stands for feed concentration, ρp for particle density and d_D for droplet diameter. The direct proportionality between feed concentration and geometric diameter is evident from the DoE, whereby the highest Dv_{50} was obtained at a concentration of 5 mg/ml. From a physical point of view, this is because the higher the concentration of the solution, the more energy is required for atomisation as the viscosity also tends to be higher [149,150]. Viscosity also depends on the composition of the spray solution. Pinto et al. pointed out that the properties of this liquid in terms of interfacial tension, viscosity, and density can play a key role in controlling droplet size [102]. Considering this, it is remarkable to note that for runs #3, #4, #7 and #11, powders were manufactured at an inlet temperature of 90°C by adding 10 %ethanol to the feed solution. Ethanol is more volatile and has a lower boiling point (78.37°C) than water (100°C), which means it dries more quickly at the same temperature [149,151]. Therefore, less heat energy is required to vaporize ethanol and a lower temperature can be used to dry the droplets. For this reason, an inlet temperature of less than 100°C could be used, ensuring almost complete evaporation of the solvent. However, the use of ethanol to aid the evaporation process introduced a new effect to consider, namely the influence that the organic solvent could have on the size and morphology of the particles obtained. For WLBU2 SD, excluding run 4 and 9, the largest particles were obtained in the presence of ethanol. This result agrees with Belotti et al., who analyzed the influence of ethanol on the morphology and size of spray-dried particles of amikacin sulphate and showed by means of a Central Composite Design how the organic solvent together with a rapid feed rate are responsible for an increase in volumetric diameter and span [151,152]. Two other factors to be considered in defining the influence on particle size are temperature and feed rate, which are significant through their interaction. As previous studies have

shown, the higher the inlet temperature, the larger the particles obtained. This could be justified by the fact that as the temperature increases, the time required for the droplets to dry into particles decreases and this could lead to larger particles with a higher moisture content and sometimes the formation of agglomerates [133].
The feed rate exerts an influence on particle size. According to existing literature, an increase in the feed rate, and consequently in the volume of fluid delivered, leads to a reduced amount of energy per droplet and results in larger particle sizes [150,153]. However, it is important to note that the feed rate itself does not appear to have a direct impact on particle size, as evidenced by the fine particles produced in runs #4 and #10. Surprisingly, despite being produced at the highest feed rate of 5 ml/min, two out of three of the smallest Dv_{90} values were achieved in these runs.

4.3.3 Residual water content

Residual water content in all spray-dried powders was determined following the procedure described in Chapter III, section 3.1.6. by analyzing the mass loss occurring in the temperature range of 25 - 130 °C. The water content was considered as a CQA for DPIs since it can detrimentally affect powder flow properties and hinder their ability to effectively reach the lungs [126,137]. While defining the spray-drying parameters, it is imperative to minimize the moisture content in the final product [142]. Furthermore, also Maltesen et al. have identified moisture content as a CQA in the context of spray-drying insulin powders [154]. Maintaining a moisture content of less than 6% within the dried powders is crucial to mitigate the risk of chemical degradation through hydrolysis and to reduce capillary forces between particles [155].
An overview of the residual moisture contents for each spray-dried powder is presented in Table 10. Values varied from 0.5 to 2%, underscoring the efficiency of the solvent evaporation process.

Table 10. Matrix of the results associated with moisture content. Data are expressed as mean ± standard deviation of three measurements (n=3).

Run	Feed concentration (mg/ml)	Feed rate (ml/min)	Inlet T (°C)	Moisture content (%)
1	3	4	105	1.39 ± 0.12
2	5	3	120	1.32 ± 0.05
3	5	5	90	1.43 ± 0.02
4	1	5	90	1.28 ± 0.07
5	3	4	105	1.56 ± 0.16
6	3	4	105	1.40 ± 0.07
7	1	3	90	2.34 ± 0.77
8	5	5	120	0.69 ± 0.12
9	1	3	120	2.22 ± 0.47
10	1	5	120	0.54 ± 0.26
11	5	3	90	0.70 ± 0.07

The model obtained for residual water proved to be significant, showing the preponderant influence of feed rate and feed concentration, both as individual factors and in their interactions. The experimental space in this case becomes extremely complicated. As can be seen in the Pareto chart (Figure 19), the negative effect of B becomes secondary to the effect of its interaction with A (Figure 20). As the feed concentration increases (1 to 5 mg/ml), the residual water content decreases when the feed rate is at its minimum level (3 ml/min), whereas it remains approximately constant at the maximum feed rate (5 ml/min). This agrees with what Lechanteur et al. reported: for the same reason that a high feed rate would lead to a larger particle's size, increasing this factor results in higher residual water content in the final product [150,156]. As shown in the interaction plot (Figure 21), with regard to the effect of the interaction between feed rate and inlet temperature, it is emphasized that as the feed rate changes (from 3 to 5 ml/min), the residual water content decreases when the inlet temperature is at its highest level (120 °C), while it remains constant when at its lowest level (90 °C). This agrees with Focaroli et al., who noted a correlation between feed

rate and temperature such that high temperatures together with a fast feed rate are associated with a dried product [133,145,157].

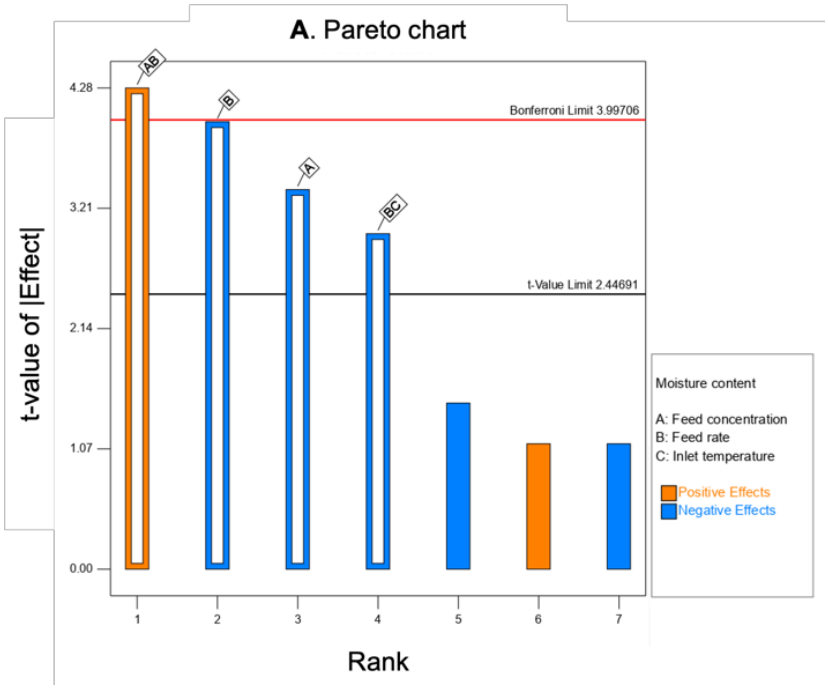

Figure 19. Pareto chart from Design Expert Software referred to the residual moisture content as response. Orange bars mean positive effect, blue bars stand for negative effect.

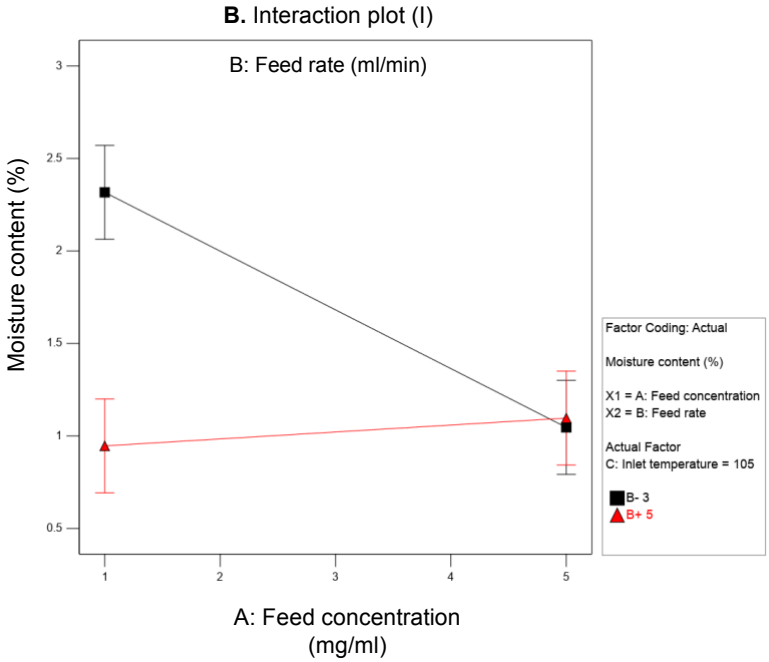

Figure 20. Interaction plot for AB – feed concentration and feed rate. Reduced moisture content can be achieved with the highest level of feed rate (red line) and low level of feed concentration or by increasing at the high the feed concentration while keeping at the low the feed rate.

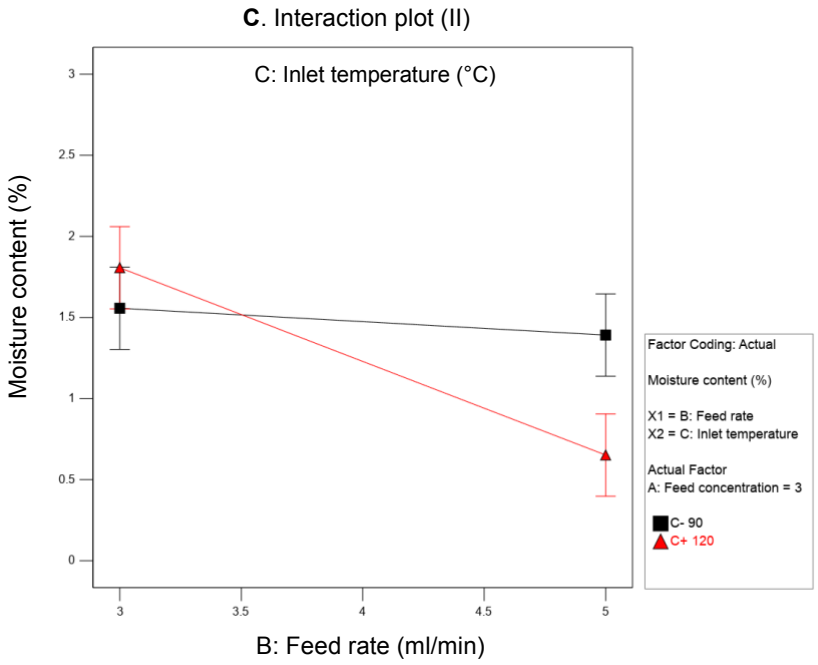

Figure 21. Interaction plot for BC – feed rate and inlet temperature. Low residual water content can be obtained with high feed rate and high inlet temperature.

4.3.4 Thermal behavior of WLBU2 spray-dried particles

The thermograms of selected WLBU2 SD formulation (Run #10), WLBU2 raw material, mannitol, and leucine are presented in Figure 22. Formulation #10, obtained with 1 mg/ml feed concentration, 5 ml/min feed rate and at 120 °C, was selected because it presented CQAs in favorable ranges, with a size < 4 μm, EF % > 85 %, and a RF % of 75 % with a peptide content over 99 %.

The thermogram of WLBU2 raw material indicated a characteristic endothermic sharp peak at 220 °C, corresponding to the melting point with ΔH_f of -163 J/g. When mannitol and leucine were analyzed, a sharp endothermic peak for both was observed at 165 °C (ΔH_f = - 297.43 J/g) and 310 °C (ΔH_f = - 1115.83 J/g), respectively.

The spray-dried formulation exhibited a pronounced endothermic peak at about 165 °C, a minor endothermic peak at 220 °C, and a second sharp endothermic peak at 310-315 °C. A comparative analysis with thermograms of WLBU2 and its excipients confirmed these events as the sequential melting of mannitol, followed by WLBU2, and ultimately leucine, as reported also by Vinjamuri [138,158]. The distinctive peak representative of WLBU2 was also present in the formulation thermogram, with a ΔH_f

of -148.83 J/g, suggesting that the spray-drying process has not induced amorphization of the peptide, which retained its crystalline state [141,147]. Similarly, mannitol was present in the formulation in either its α or α/β crystalline forms. However, an examination of the enthalpies associated with these phase transitions indicates that while the degree of crystallinity in WLBU2 remained almost unchanged due to a 10 % reduced crystallinity, mannitol underwent a reduction in ΔH_f from - 297 J/g to - 140 J/g. Since the enthalpy associated with the transition serves as a metric for crystallinity, it is clear that the mannitol in the spray-dried microparticles did not exhibit the same degree of crystallinity as the mannitol control, with a reduced crystallinity compared to the mannitol raw material [159,160]. As pointed out by Patil et al., it is assumed that the presence of the peptide can alter the polymorphic forms of mannitol, which therefore presents alterations in its characteristic peak [138]. However, as documented in the literature, the crystalline nature of WLBU2 SD can have a favorable impact on the aerosolization of the powder. Indeed, particles present a reduced area-to-volume ratio and thus have less tendency to aggregate and are more easily dispersed than their amorphous counterparts. Nevertheless, the presence of API in its crystalline form could also lead to a reduction in its bioavailability [84,161].

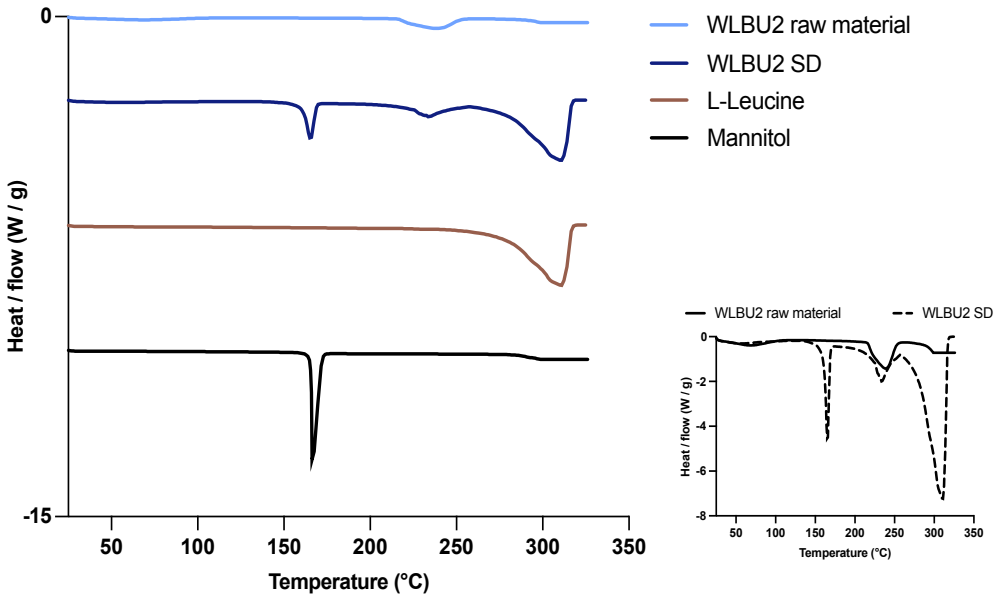

Figure 22. Thermograms for WLBU2 rm, WLBU2 formulated within the spray dryer powders (WLBU2 SD), L-Leucine and mannitol. The insert on the right shows the superimposed thermograms of WLBU2 raw material and WLBU2 SD (^exo).

4.3.5 Morphology of WLBU2 spray-dried microparticles

Particles' morphology plays a key role in defining powder flow properties, the aerodynamic particle size and the dispersibility of the powder [162]. It is considered such an important parameter that in 2012 Paluch et al. introduced a system for classifying particles in terms of morphology by dividing them according to shape, irregular or spherical, and according to surface, smooth or wrinkled. Based on these characteristics, it is possible to predict the aerodynamic behavior of spray-dried particles for inhalation [102,163]. Overall, the absence of aggregated particles, the presence of uniform size, slightly rough surface and spherical shape provide favorable aerosolization [141]. Figure 23 and Figure 24 report the SEM images depicting both the DoE runs and the unprocessed WLBU2 peptide. Images were taken at 10.000 X of magnification with exception made for unprocessed WLBU2 (rm) whose images were taken at 5.000 X magnification as the material underwent ablation by the beam and tended to structure itself in flakes. WLBU2 SD exhibited a notably heterogeneous morphology. Upon microscopic examination, it becomes evident that most of the spray-dried particles exhibited a round shape, with only a minor number of exceptions. The first explanation for this morphology lies in the composition of the sprayed solution. Mannitol is a sugar alcohol, has a crystalline structure and dissolves easily in water. When mannitol is dissolved and atomized in the spray-drying process, it forms tiny droplets that tend to round into spheres during drying. This inherent spherical tendency contributes to the spherical shape of the spray-dried particles. On the other hand, leucine is an amino acid that can act as a flow enhancer in pharmaceutical formulations. When leucine is combined with mannitol during the spray-drying process, it can further promote the formation of spherical and smoothness particles [164]. In this regard, Ferrari et al. aimed to demonstrate that enhancing the smoothness of particles results in improved flowability. They achieved this by altering the surface roughness of lactose particles through a process involving wetting the surface with an ethanol/water mixture in a high shear mixer [165]. This perspective was also supported by other researchers who investigated the impact of particle morphology on drug delivery. Their studies revealed that augmenting surface smoothness leads to an increase in the fraction of fine particles and contributes to the prevention of aggregation among the finest particles [97,165]. Furthermore, previous

research showed how the use of amino acids-based excipients such as L-leucine could influence particles' surface behavior [119]. Boraey et al. observed that an increase in the mass fraction of this amino acid could lead to the formation of more porous particles. This change in the particle property may be explained by L-leucine precipitation on the surface of drying droplets, forming a hydrophobic shell layer with a slightly wrinkled texture [166]. Considering the factors that were varied during the experimental design, one of the most influential was the solute concentration. More concentrated solutions exhibit a medium to high viscosity and therefore less solvent in the droplets being formed during atomization. As a result of this, there is an increase in the Peclet number, a reduction in evaporation time, and the formation of particles that tend to be porous. This is also related to the influence of the spray temperature, as high spray temperatures accelerate the evaporation process, creating a pressure gradient inside and outside the droplet with consequent effects on the particle morphology [135,150].

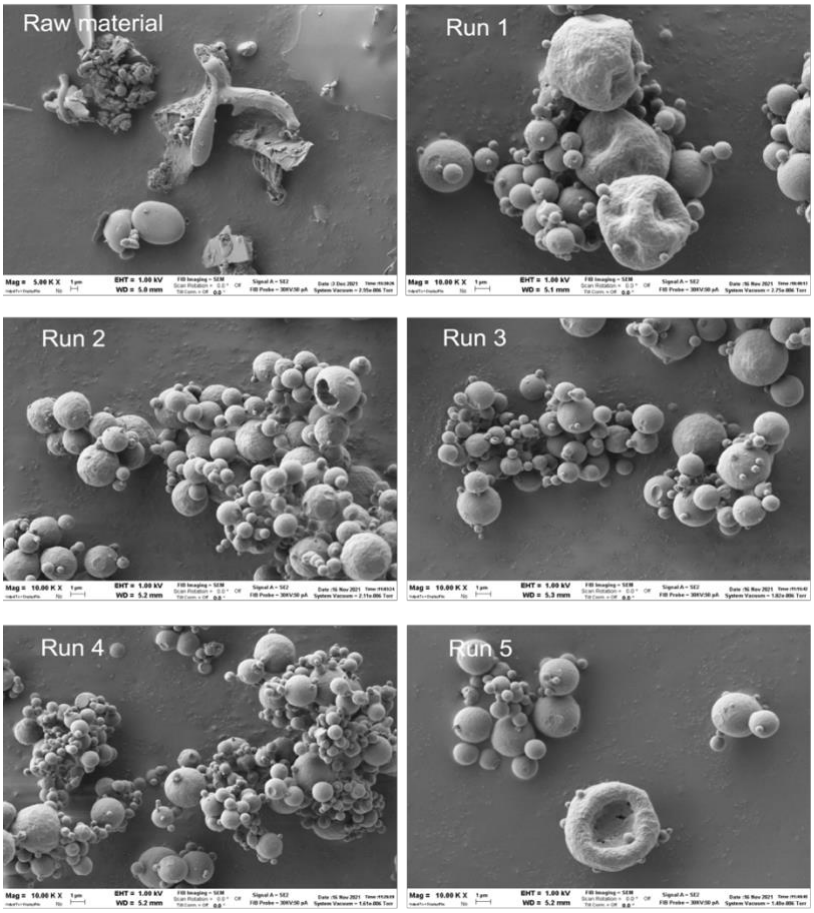

Figure 23. SEM images of WLBU2 raw material taken at 5.000 X of magnification and run from #1 to #5 taken at 10.000 X of magnification.

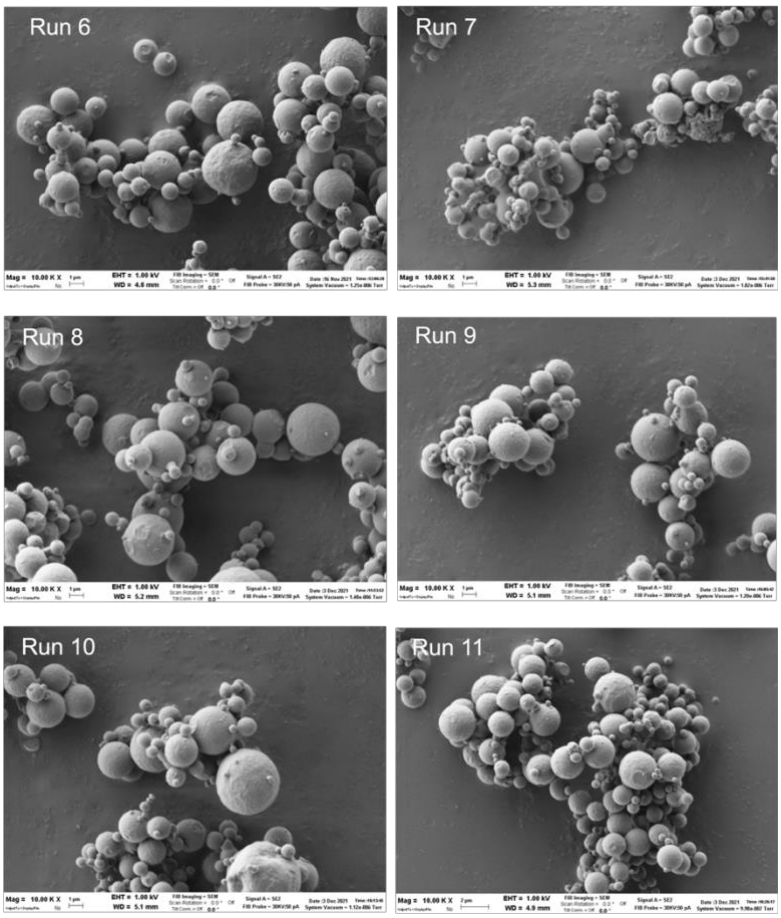

Figure 24. SEM images of WLBU2 SD from run #6 to #11 at 10.000 X of magnification.

4.3.6 *In vitro* aerodynamic assessment

4.3.6.1 Fast Screening impactor

The *in vitro* aerodynamic assessment was conducted using the FSI. Within the array of parameters collected during the DoE, EF % and the RF % associated with the ED (mg) were selected as CQAs for evaluating the aerodynamic performance of WLBU2 spray-dried microparticles. RF % serves as a lung deposition indicator, representing the proportion of the API with an aerodynamic diameter smaller than 5 μm. It is worth noting that particles with aerodynamic diameters falling between 1 and 5 micrometers are recognized as capable of achieving lung deposition, as mentioned earlier [146,155,167]. The comparison of the emitted fraction and the respirable fraction from the spray-dried powders, prepared according to the DoE, is shown in Figure 25.

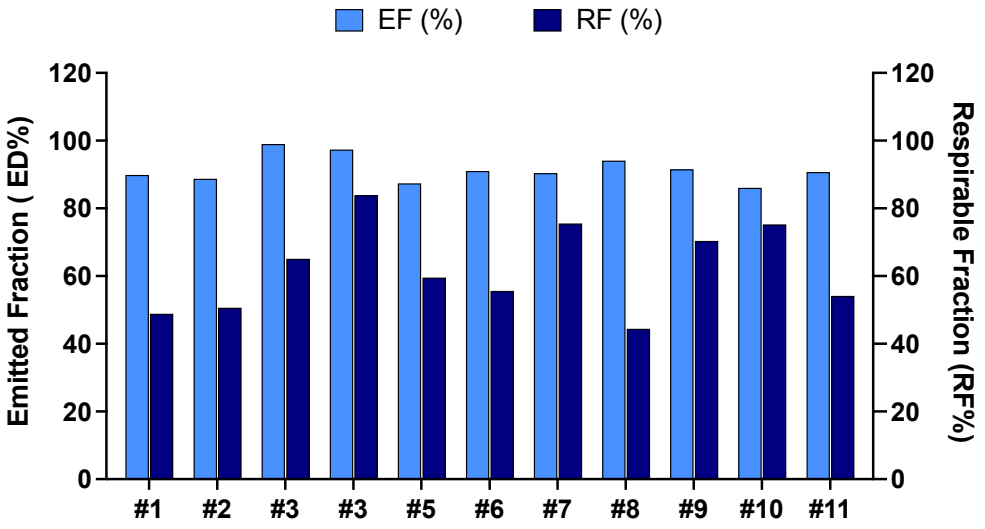

Figure 25. Emitted fraction and respirable fraction after the aerosolization of WLBU2 SD form RS01 DPI Inhaler according to the DoE.

As it can be noted in Figure 26, the EF % of WLBU2 was between 85 and 98 % with no significant differences between formulations. The lowest value was achieved during the run #5, where powder production occurred with all three factors set to medium levels, including a feed concentration of 3 mg/ml, a feed rate of 4 ml/min, and an inlet temperature of 105°C. In contrast, the highest value corresponded to a single run, specifically run #3, which was manufactured with the highest feed rate (5 ml/min) and feed concentration (5 mg/ml), along with the lowest inlet temperature (90°C). Upon examining the values summarized in Figure 25, it becomes evident that as the feed concentration increases (as seen for runs #3 and #8), the emitted dose is pushed towards higher values. According to the DoE, the main important effects were the factor A-feed concentration and its interaction with factor B-Feed rate. The magnitude of these effects is reported in the Pareto Chart (Figure 26).

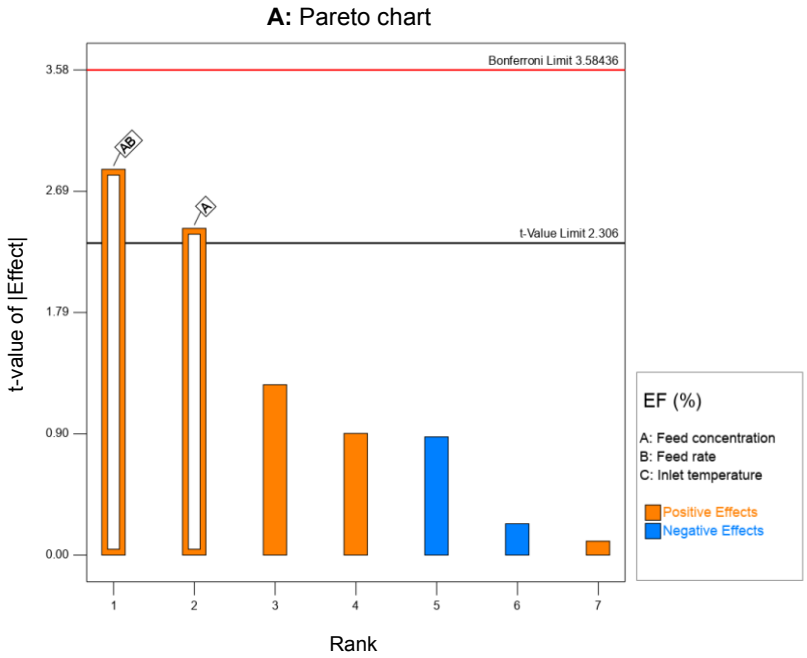

Figure 26. Pareto chart from Design Expert Software referred to the emitted fraction as response. Orange bars mean positive effect, blue bars stand for negative effect.

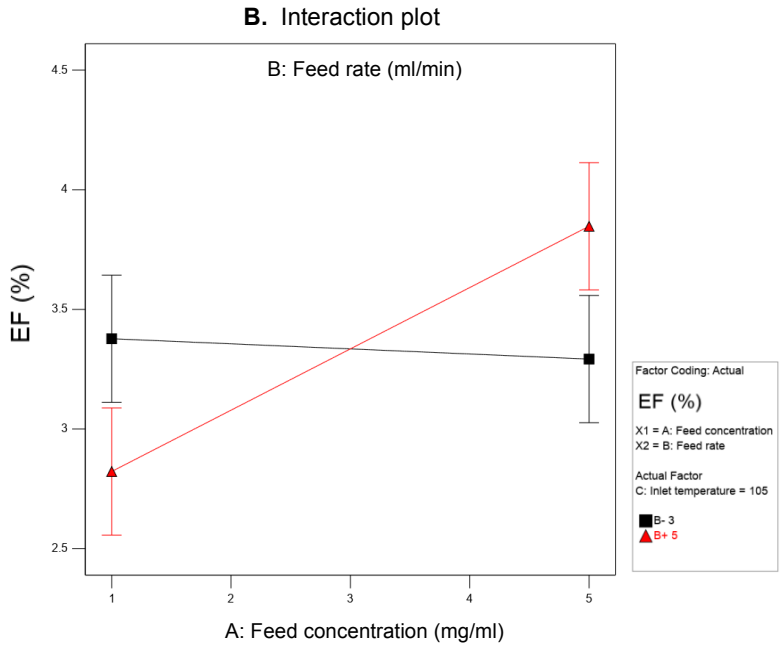

Figure 27. Interaction plot for AB: feed concentration is represented on X1 axis while feed rate on X2 axis where black line stands for -1 level and red line for +1 level.

It can be observed from the AB-interaction graph (Figure 27) that by increasing the feed rate with a high concentrated solution results in a highly flowable powder with a high emitted fraction, while keeping the feed concentration at the minimum level does not significantly vary the emitted fraction as the feed rate increases. However, the EF% response exhibited a non-significant effect for all the selected factors; therefore, EF% was not further considered. The ANOVA indicated the significance of the curvature term, highlighting the necessity to expand the design to a Response Surface model. (Table 11).

Table 11. ANOVA for the selected factorial model when the Emitted Fraction is considered as the response.

Source	Sum of Squares	df	Mean Square	F-value	p-value	
Model	1.06	2	0.5289	6.98	0.0216	significant
A-Feed concentration	0.4418	1	0.4418	5.83	0.0465	
AB	0.6160	1	0.6160	8.12	0.0247	
Curvature	0.4386	1	0.4386	5.78	0.0471	
Residual	0.5308	7	0.0758			
Lack of Fit	0.2440	5	0.0488	0.3402	0.8568	not significant
Pure Error	0.2869	2	0.1434			
Cor Total	2.03	10				

As previously mentioned, the second quality attribute considered for evaluating the aerodynamics of the spray-dried powders was the RF %. The highest RF % values were obtained for runs #4, #7, #9 and #10, falling within the range of approximately 70-85%. All powders in these runs were manufactured using the lowest feed concentration (1 mg/ml). According to the ANOVA analysis, only factor A was seemed statistically significant. While Factor C was not deemed significant in the model, it demonstrated a slight effect on the response, as shown in the Pareto Chart in Figure 28 A. The Pareto Chart shows the strong negative effect of factor A-Feed concentration, also confirmed by the perturbation plot (Figure 28 B), and the slight influence of factor C-Inlet temperature since its bar is only a little above the t value limit. In particular, an increase in the level of Factor A was associated with a decrease in RF%.

A

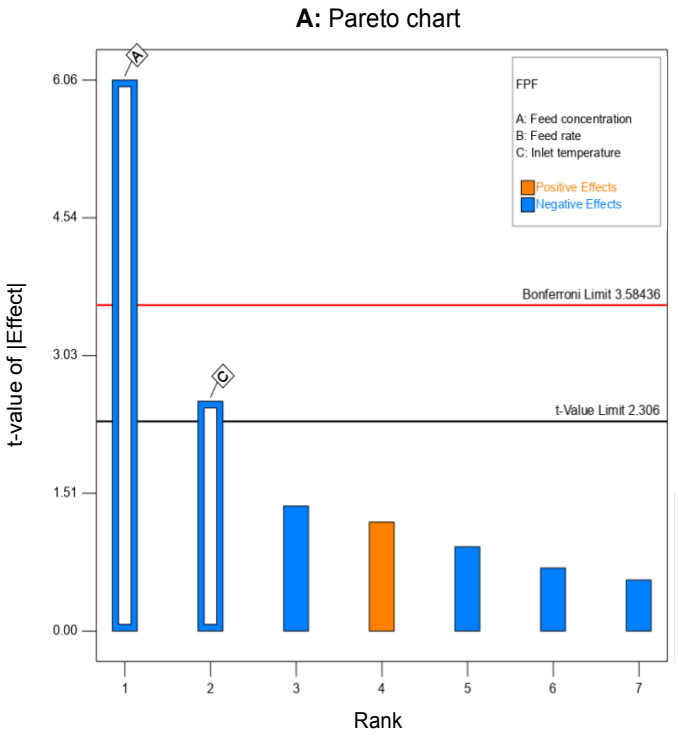

B

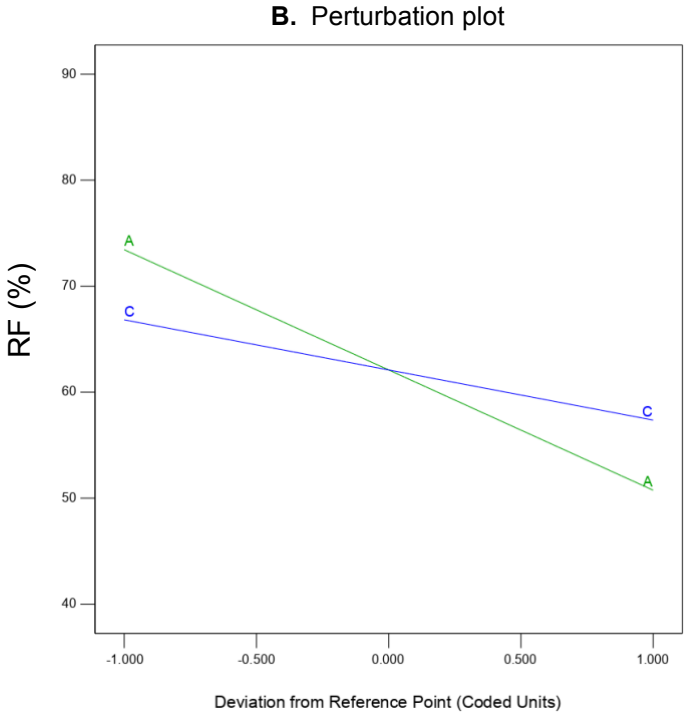

Figure 28. A. Pareto chart for RF % as response. Orange bars mean positive effect, blue bars stand for negative effect. B. Perturbation plot for feed concentration and inlet temperature vs respirable fraction.

4.3.6.2 Next Generation Impactor

A deeper investigation of the aerodynamic characteristics of the spray-dried powders showing better performance after the DoE, *i.e.* runs #4 and #10, was carried out by means of NGI. In each analytical instance, a pair of HPMC capsules, size 3, each loaded with 40 mg of spray dried powder, underwent activation within an airflow system operating at a rate of 60 L/min for a duration of 4 seconds.

Table 12. Summary of the data obtained from the NGI characterization for Run 4 and 10 duplicated from the DoE. Data are expressed as the mean ± standard deviation of two measurements.

Run	EF (%)	FPF (%)	MMAD (μm)	GSD (μm)
#4	92.04 ± 1.09	75.30 ± 8.61	2.21 ± 1.14	3.20 ± 0.97
#10	90.51 ± 0.51	72.09 ± 6.92	2.68 ± 1.25	2.92 ± 1.37

As shown in Table 12, both run #4 and run #10 showed acceptable emitted fractions, indicating good flowability. The fine particle fraction was around 75 % without significant differences between the two formulations, where the only varying factor being the inlet temperature during spray-drying process. These results agree with what was preliminarily observed during the DoE, which did not attribute a significant influence of the inlet temperature on the aerodynamic behavior expressed through the RF %. Furthermore, these findings underline their suitability for lung administration, in accordance with the criteria outlined by Sharma et al. [168]. Another crucial aspect characterizing the aerodynamic characteristics of microparticles designed for pulmonary delivery is the MMAD, which defines the diameter below which half of the particles are distributed. This metric was determined through interpolation from the inverse normal of the cumulative mass distribution. This interpolation was conducted in relation to the natural logarithm of the effective cut-off diameter of each stage using GraphPad Prism, Version 9 (Graphpad Software Inc., La Jolla, CA, USA) [119]. Referring to Table 12, the MMAD values for microparticles in run #4 and run #10 were 2.21 ± 1.14 and 2.68 ± 1.25 μm, respectively, suitable for pulmonary delivery. In both runs, a significant portion of the powder theoretically had the capability to reach the deeper airways and specifically the alveoli as MMAD values lower than 3 μm refer to

the extra-fine fraction of particles. However, it is worth noting that the MMAD in both cases was associated with a relatively broad Geometric Standard Deviation (GSD) of 3.20 and 2.92 for run #4 and run #10, respectively. Comparing these outcomes with the composition of the formulations, it is important to mention that a previous study demonstrated that the variation in concentrations of L-leucine and mannitol can impact the MMAD size. Specifically, Saleem et al. reported that a high concentration of mannitol could increase the MMAD, while elevated amounts of leucine led to its reduction. In the case of these formulations, the right balance of mannitol and leucine was found to result in a favorable MMAD, as well as a deposition and aerosolization profile [166–168]. The deposition profile of WLBU2 spray-dried microparticles is presented in Figure 29. A higher deposition of Run #10 powder was observed at the throat level, possibly indicating oropharyngeal impact of a fraction of the formulation. However, a considerable fraction of particles was also detected at stages 2 and 3, as well as at the MOC level. Taking these findings into consideration, it was concluded that the spray-dried powders related to run #4 and #10 were suitable for inhalation. Nonetheless, further *in vivo* testing is essential to determine the appropriate doses for pulmonary administration.

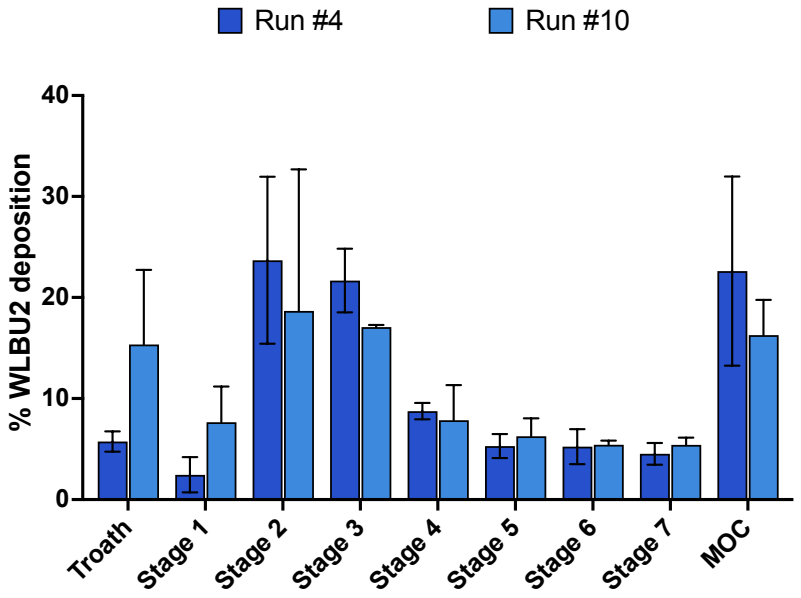

Figure 29. *In vitro* aerosolization profile of WLBU2 spray-dried powders run #4 and run #10 obtained using the Next Generation Impactor (NGI). Data are presented as mean ± standard deviation (n = 2) in the bar graph.

4.4 LL37 and hLF1-11 Dry powder formulations

During the preliminary screening for the formulation development of LL37 via spray-drying technique, three of the main excipients used in inhalation applications were studied for their impact on process yield and peptide content within the resulting powders. The spray-drying process exposes molecules, particularly peptides and proteins, to thermal and mechanical stresses [26]. In this regard, the choice of excipient is closely linked to the intended functionality of the powder, peptide characteristics, and aerosolization properties to ensure effective pulmonary deposition [153]. Mannitol, as previously elucidated in the section for WLBU2 SD, belongs to the class of reducing sugars and exhibits low hygroscopicity [95,102]. On the other hand, trehalose is a disaccharide characterized by a high glass transition temperature (T_g 110-115°C), resistance to acid hydrolysis, and a tendency to form an amorphous microparticle matrix during spray-drying [133,169]. During the formulation study, trehalose was favored due to its efficiency in stabilizing peptides and proteins compared to other sugars [95]. This preference is attributed to its superior capacity to form hydrogen bonds and generate powders with higher glass transition temperatures (T_g) [102]. Nevertheless, two primary drawbacks associated with trehalose are reported in the literature. The first is about its interaction with leucine: in the proposed formulation, the presence of this amino acid was found to be critical in enhancing powder dispersion [166]. Nonetheless, it is known that trehalose and leucine can interact accelerating the crystallization process. This interaction predominantly occurs at temperatures above 130°C, and therefore, given the drying conditions in this study at 120°C, it is unlikely to have adversely affected the peptide's integrity [97,158]. The second limitation relates to the risk of recrystallization and the potential loss of trehalose's bioprotective effect [170]. Indeed, both trehalose and raffinose, due to their high T_g values, tend to remain in an amorphous state during drying, leading to the absorption or adsorption of significant amounts of water vapor during processing and storage. Such sorption can alter the chemical and physical properties of the sugar, accelerating its hydrolytic degradation, and inducing isomerization or crystallization. These transformations can have a notable impact on the preservation and functionality of peptide and/or protein-based powders [134,170].

The results from the formulation study for LL37 SD are presented in Table 13. Comparing the data from formulations A and B, both of which contain the same percentage of mannitol, the percentage yield is higher for formulation B, achieved by using a lower feed rate of the spray solution than that used for formulation A. In contrast, about the spray-dried powders C and D, which contain the same percentage of trehalose, the yield was higher as the feed rate increased. Although we changed the spray rate between 3 and 5 ml/min in both the mannitol and trehalose formulations, the yield did not correlate proportionally with the feed rate. Table 13 also reported the process yield % of the two hLF1-11 formulation (G, H) with mannitol and trehalose. The yields of hLF1-11 formulations are in line with what observed for formulations containing LL37.

Table 13. Yield of the formulation study for spray-dried powders of LL37 (A to F) and for the powder loaded with hLF1-11 (G and H).

Formulation	LL-37 (%)	hLF1-11 (%)	Mannitol (%)	Trehalose (%)	Leucine (%)	Feed rate (ml/min)	Yield of drying (%)
A	5	-	85	-	10	5	47.95
B	5	-	85	-	10	3	51.79
C	5	-	-	85	10	5	59.19
D	5	-	-	85	10	3	50.58
E	15	-	-	75	10	5	55.32
F	15	-	-	75	10	3	61.16
G	-	15	75	-	10	3	53.8
H	-	15	-	75	10	3	62.16

4.4.1 UHPLC quantification of LL37 and hLF1-11

The drug content determination of LL37 and hLF1-11 in the spray-dried microparticles was performed according to UHPLC method described in Chapter III, section 3.1.4. The results obtained are shown in Table 14. The LL-37 and hLF1-11 peptides recovery in the spray-dried powders was calculated as the percentage ratio of the amount of

peptide present in the spray-dried powder to the amount of peptide weighed for the preparation of the spray solution [84,171].

Looking at the results in Table 14, the LL37 recovery was around 85 – 90 % w/w in most formulations with minor differences with regard of the theoretical LL37 content and the type of excipient.

The hLF1-11 recovery was 75 % for powders with mannitol and 105 % in the presence of trehalose. Similarly, to the above, a superiority of trehalose in stabilizing these peptides was observed. Unlike the WLBU2 peptide, which has been engineered to be more stable itself, they tend to be more fragile when exposed to thermal and mechanical stress [70,172,173].

Table 14. LL37 and hLF1-11 content within spray-dried powders.

Formulation	LL-37 (% w/w)	hLF1-11 (% w/w)	Mannitol (%)	Trehalose (%)	Drug recovery (%)
A	5	-	85	-	85.20 ± 6.37
B	5	-	85	-	91.45 ± 5.13
C	5	-	-	85	97.08 ± 2.11
D	5	-	-	85	84.96 ± 0.14
E	15	-	-	75	83.14 ± 0.50
F	15	-	-	75	88.88 ± 0.50
G	-	15	75	-	67.53 ± 0.19
H	-	15	-	75	93.33 ± 2.90

4.4.2 Particle size distribution

Utilizing laser diffraction analysis, the size distribution of the spray-dried microparticles was characterized. In terms of LL37 SD, after examining the size distribution of all six spray-dried powders presented in Table 15, it can be concluded that there is no significant difference in size. Therefore, it can be stated that both the composition and the change in peptide concentration (from 5% w/w to 15% w/w) did not affect the particle size distribution of the powders [96]. The spray-drying process yielded

microparticles spanning a size range from 1.25 µm to 6.26 µm, acceptable for pulmonary delivery.

Table 15. Volumetric percentile diameters of 10%, 50% and 90% of the total particle volume and span for LL37 SD (from A to F) and hLF1-11 SD (H). Each powder was analyzed in triplicates and the D_v values obtained are the average ± standard deviation.

Formulation	Dv_{10} (µm)	Dv_{50} (µm)	Dv_{90} (µm)	Span
A	1.46 ± 0.02	3.1 ± 0.01	6.26 ± 0.25	1.54 ± 0.06
B	1.60 ± 0.11	3.06 ± 0.13	5.53 ± 0.11	1.28 ± 0.05
C	1.46 ± 0.01	2.54 ± 0.01	4.45 ± 0.04	1.17 ± 0.01
D	1.46 ± 0.01	2.57 ± 0.03	4.58 ± 0.23	1.21 ± 0.07
E	1.38 ± 0.01	2.36 ± 0.01	4.08 ± 0.12	1.14 ± 0.04
F	1.25 ± 0.01	2.18 ± 0.01	3.94 ± 0.02	1.24 ± 0.06
H	4.01 ± 0.09	7.27 ± 0.18	13.8 ± 0.66	1.34 ± 0.04

4.4.3 Morphology of LL37 SD and hLF1-11 SD

The morphological characterization of LL37 and hLF1-11 spray-dried microparticles was performed with SEM as previously described in Chapter III, section 3.1.7.
Observing the images obtained for LL37 and hLF1-11 raw materials in Figure 30, the particles appeared partially spherical and fragmented, but also plates-like without any specific shape [138]. This morphology indicates that the peptides need to be formulated to be administered, as their morphology does not meet the requirements for adequate inhalation. Following drying, LL37 SD microparticles were spherical, smooth, and approximately 1 micrometer in size, without significant differences compared to the excipient-only system and in agreement with the information obtained by laser diffraction as all powders were in a size range suitable for pulmonary administration [174]. Despite the presence of leucine, which, according to the literature, crystallizes on the surface of the particles during spray-drying by wrinkling

them, the particles were smooth [175]. As investigated by Kwok et al., the type and concentration of peptide can also influence the surface of the particles, making them both smooth and corrugated regardless of the presence of leucine [84]. This is evident in the hLF1-11 microparticles, which, despite being formulated in the same system, exhibit a slightly rougher surface. This difference can be attributed to the distinct properties of both peptides. Furthermore, the spray-dried microparticles appeared cohesive and partly agglomerated. This effect can be traced back to the surface enrichment due to the hydrophobicity of leucine and to the smaller size that increases the surface area favoring inter-particle interaction [96].

In addition to composition, another factor to consider is a process parameter, specifically the feed rate. Xu Y. et al., reported an increase in spray-dried particles roughness proportional to the increase in feed rate. Particles produced at a pump feed rate of 10 % corresponding to 3 ml/min for an aqueous solution were spherical, while at a 100 % feed rate, they were rough. This agreed with the results obtained for LL37 SD produced at a feed rate of 3 ml/min [174].

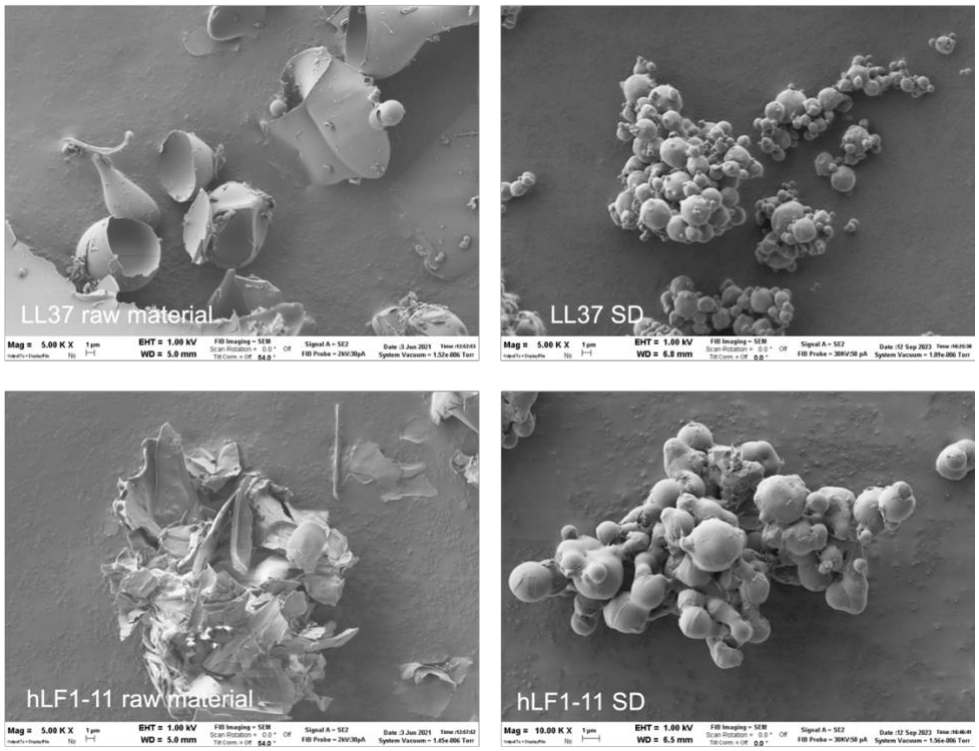

Figure 30. Scanning Electron Microscopy images taken at 5,000 kV of magnification.

4.4.4 Thermal behavior of LL37 SD and hLF1-11 SD

Thermograms of LL37, LL37 SD, trehalose and leucine are shown in Figure 31 and Figure 32. LL37 raw material exhibited a broad endothermic band in the 30 – 100° temperature range, corresponding to the evaporation of unbound water. This loss was about 0.2 % indicating a low water content. Two endothermic peaks of small entity at about 130 °C and 158 °C could be attributed to a solid-solid reorganization of LL37. Then, an endothermic peak at around 230 °C (ΔH_f = - 49.09 J/g) associated to the peptide melting, immediately followed by decomposition, was observed. The characteristic melting peak of LL37 remained present in the thermogram of the spray-dried formulation but the thermal behavior of trehalose can be modified during the spray-drying process, as observed in the literature [178]. The thermogram of trehalose in Figure 32 presented three characteristic endothermic peaks related to different phases of transition from order to disorder [176]. The first intense peak at about 100 °C was associated with the evaporation of unbound water, followed by a second evaporation event at 135 °C due to the evaporation of bound water [177,178]. In the temperature range 210 – 270 °C the fusion of the anhydrous β form of trehalose and its decomposition are observed. In the spray-dried formulation, on the other hand, the characteristic dehydration peaks are not present, probably due to the dehydration process that occurred during the production of the powder by spray-drying [96,138].

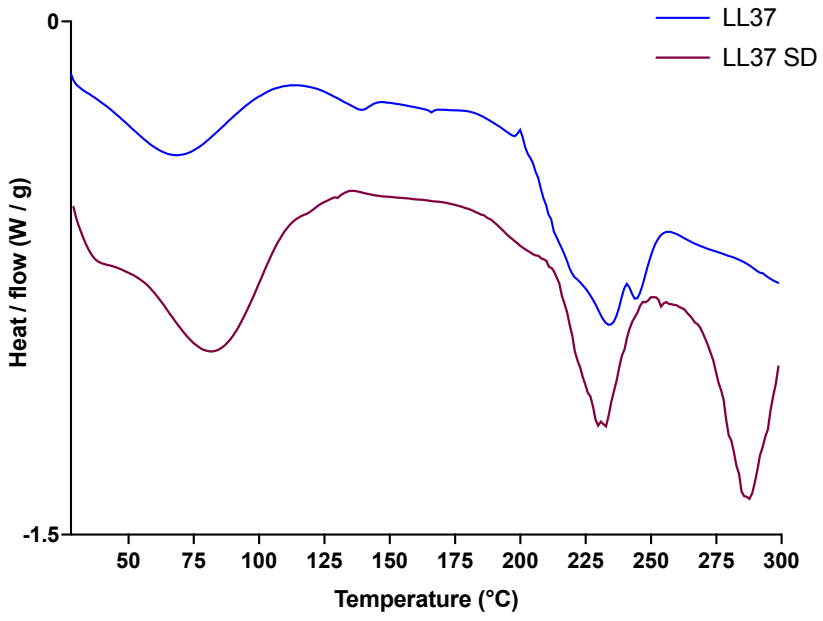

Figure 31. Thermograms for LL37 raw material and LL37 SD (^exo).

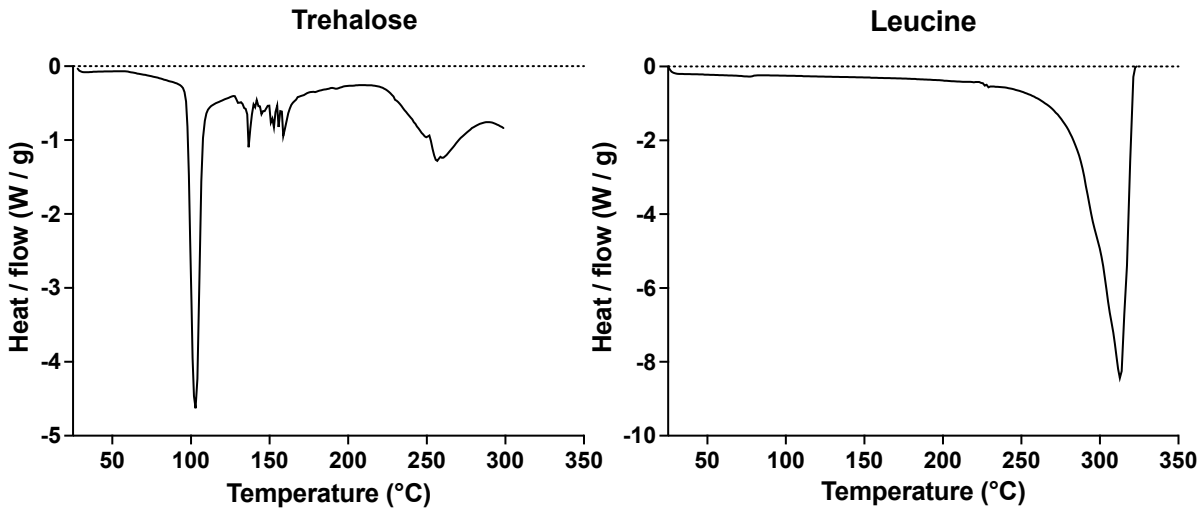

Figure 32. DSC thermogram of trehalose on the left and leucine on the right (^exo).

hLF1-11 raw material peptide presented a broad endothermic band at 30 – 90 °C, associated with the loss of unbound water. Two endothermic peaks at about 210 °C and 230°C, attributed to the peptide melting (ΔH_f -115 J/g), followed by a decomposition event, were present in the thermogram (Figure 33). When formulated, the fusion of the LF1-11 is represented by a single peak with an enthalpy like that described for the raw material hLF1-11. Trehalose also shown its characteristic dehydration peak at 100 °C, while its melting peak was not distinguishable as fell within the melting range of the peptide [179].

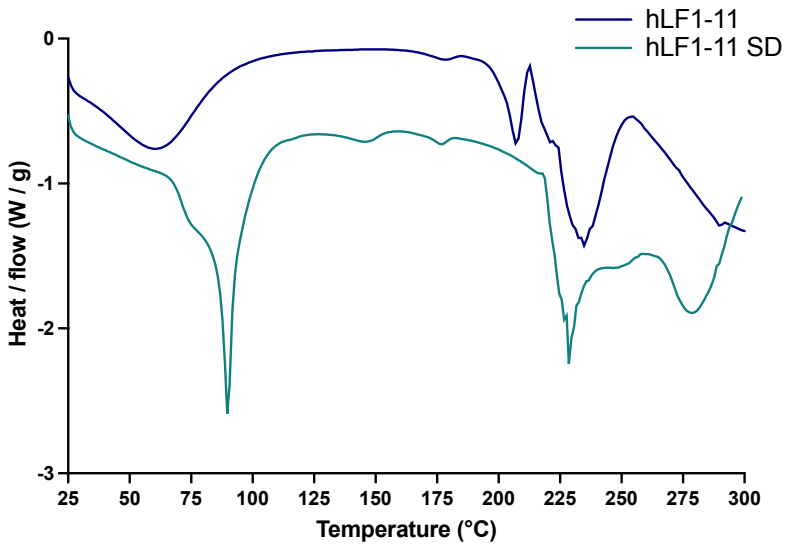

Figure 33. Thermograms for hLF1-11 raw material and hLF1-11 SD (^exo).

4.4.5 *In vitro* aerodynamic performance with Next Generation Impactor

In vitro pulmonary deposition of selected spray-dried LL37 formulations (#F) was assessed using a Next Generation Impactor (NGI), as previously described in Chapter III, section 3.1.9. The *in vitro* NGI deposition profiles are presented in Figure 34. DPI formulation exhibited favorable dispersion with EF% around 90 % with a minimal loss of drug in the capsule. The MMAD value was 3.58 ± 0.02 μm associated with a GSD around 2 and a FPF % value of 67.30 ± 0.16 %, in acceptable range for lung deposition. These values also agree with the previous assessment of the geometric size shown before.

Since the spray-dried hLF1-11 powders showed a $Dv5_0$ > at 7 um and Dv_{90} > 10 um following analysis by laser diffraction, their aerodynamic properties have not been approved to date as potentially unsuitable for pulmonary administration because they are easily susceptible to impact along the upper airways due to their size.

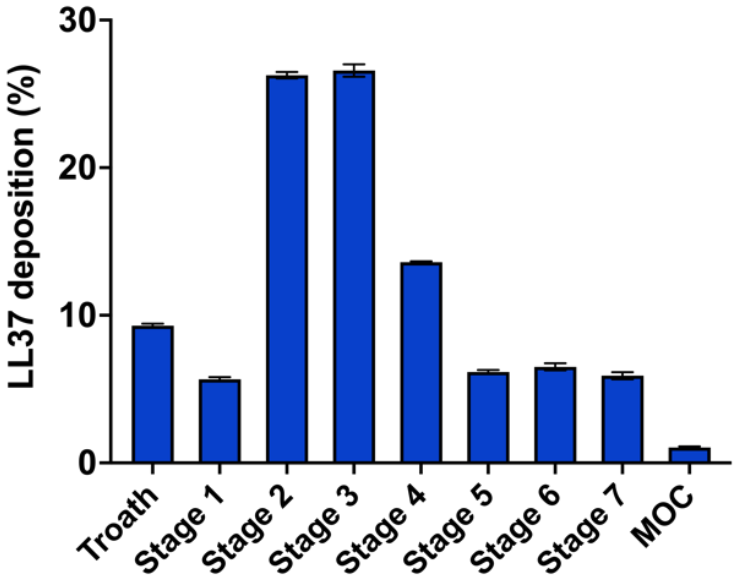

Figure 34. *In vitro* aerosolization profile of LL37 spray-dried powders run #F obtained using the Next Generation Impactor (NGI).

4.5 Structural studies by Circular Dichroism spectroscopy

Studying the interaction of antimicrobial peptides with bacterial membranes is crucial as their mechanism leads to their destabilization [180]. Through circular dichroism studies using suitable molecules capable of mimicking the bacterial outer wall, *i.e.* lipids, lipopolysaccharide, and/or detergents (SDS), it is possible to understand the action of the peptide, which may fall into one of the three typical mechanisms proposed: the barrel stave, toroidal pore or carpet model. Conducting a biophysical study of cellular dichroism in this way provides the opportunity to determine the secondary structure of the peptide when in contact with bacterial membranes. The use of lipid mixtures is a widely used but highly simplified method as the envelope of bacteria is very complex. Indeed, when reference is made to *Pseudomonas*, it must be remembered that as a gram bacterium, it possesses an asymmetrical double layer with an inner wall consisting of phospholipids and an outer wall of LPS and proteins [181]. The structural characteristics of WLBU2, LL37, and hLF1-11 were analyzed by far-UV circular dichroism spectroscopy in different media, *i.e.* LPS (0.03 %), LPSD (0.083 %), and SDS (50 mM), to mimic their interaction with bacterial surfaces. As regard the formulation, only WLBU2 SD was tested while studies on LL37 and hLF1-11 SD are currently ongoing, awaiting to conclude the investigation of their antimicrobial properties. The peptide WLBU2, in Figure 35, showed a typical random coil conformation in an aqueous solution with a negative band at 204 nm. In the presence of anionic SDS micelles, the peptide acquired a well-defined α-helix structure, with a positive band at 196.5 nm and two negative bands at 209.5 nm and 221 nm. The interaction with LPS and LPSd promoted the shift of the negative band to 208 nm and increased negative intensity from 210 nm to 240 nm. The differential analysis of WLBU2 spectra in an aqueous solution in the presence of LPS and LPSd revealed the peptide's inclination to interact with mimetics of the bacterial wall (insert Figure 35) with the acquisition of helical conformation. Likewise, WLBU2 SD in aqueous solution showed a random coil conformation with a negative band at 199 nm. In the presence of SDS micelles, WLBU2 SD acquired a typical α-helix conformation with a positive band at 195 nm and two negative bands at 220.5 nm and 210 nm (Figure 36). In the presence of LPS and LPSd, WLBU2 SD interacted with both acquiring helical conformation. This conformation was more marked with LPSd, the

polysaccharide portion of LPS, demonstrating that this bacterial wall component was responsible for the peptide interaction. By comparing the CD spectra of WLBU2 and WLBU2 SD (Figure 37), the formulation contributed to the acquisition of a higher content of WLBU2 helical conformation (insert Figure 37).

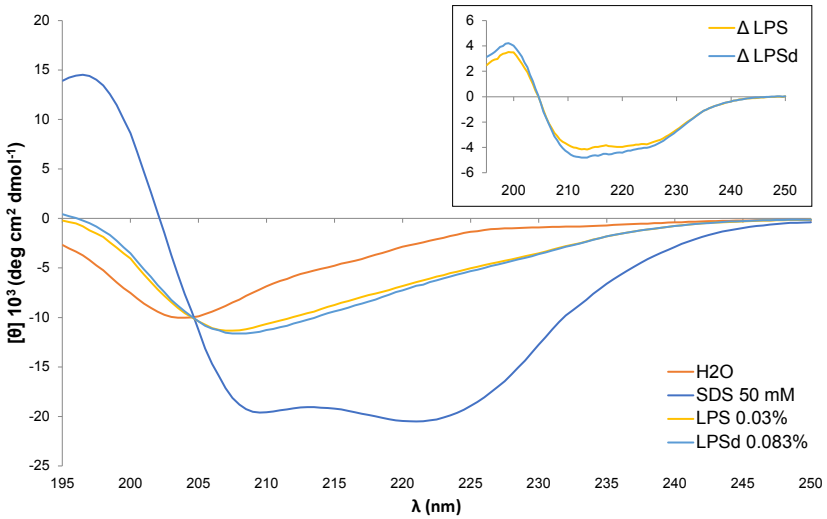

Figure 35. Far UV-CD spectra of 100 μM WLBU2 peptide in aqueous solution (orange line) and in the presence of 50 mM SDS (dark blue line), 0.03% LPS (yellow line), and 0.083% LPSd (light blue line) at 20 °C. The inset shows the difference spectrum (Δ) between the WLBU2 in aqueous solution and in the presence of LPS and LPSd.

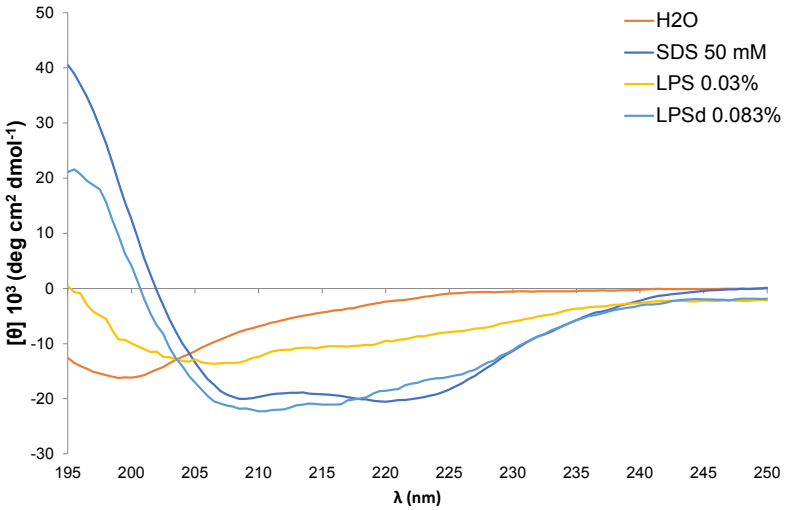

Figure 36. Far UV-CD spectra of 50 μM WLBU2-SD in aqueous solution (orange line) and in the presence of 50 mM SDS (dark blue line), 0.03% LPS (yellow line), 0.083% LPSd (light blue line), at 20 °C.

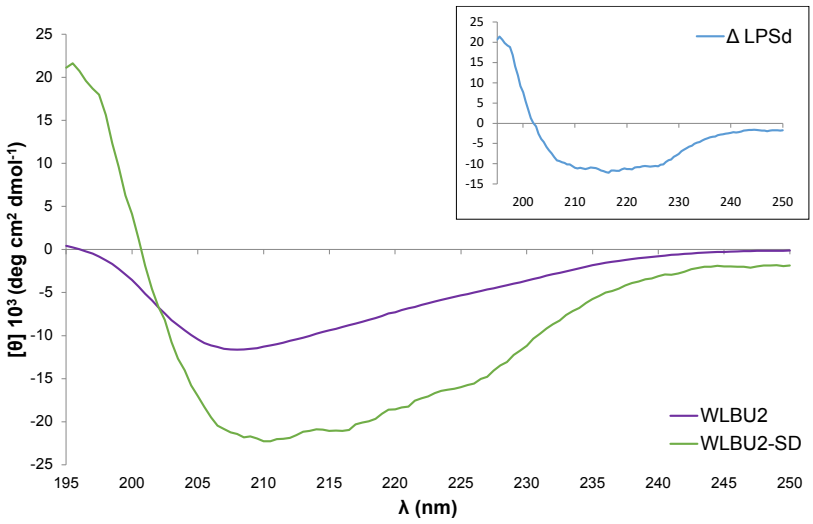

Figure 37. Far UV-CD spectra of 100 μM WLBU2 (purple line) and 50 μM WLBU2-SD (green line) in the presence of 0.083% LPSd, at 20 °C. The inset shows the difference spectrum (Δ).

Just like the observation made with WLBU2, the peptide LL37 exhibited a characteristic random coil structure when placed in an aqueous solution, featuring a negative band at 200 nm. As shown in Figure 38, in the presence of anionic SDS micelles, the peptide underwent a distinct transformation into an α-helix structure, as indicated by a positive band at 196.5 nm and two negative bands at 209.5 nm and 221 nm (refer to Figure 38). When interacting with LPS and LPSd, differently from WLBU2 in the presence LL37 did not adopt any helical conformation, as shown in the Figure 39.

As for hLF1-11, no structural change was evidenced once in contact with molecules capable of mimicking the bacterial wall (Figure 40).

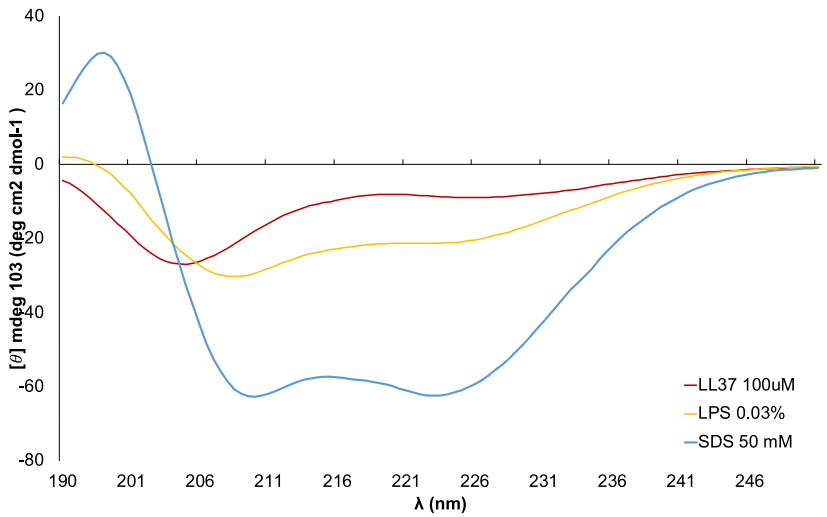

Figure 38. Far UV-CD spectra of 100 μM LL37 in aqueous solution (red line) and in the presence of 50 mM SDS (dark blue line), and 0.03% LPS (yellow line).

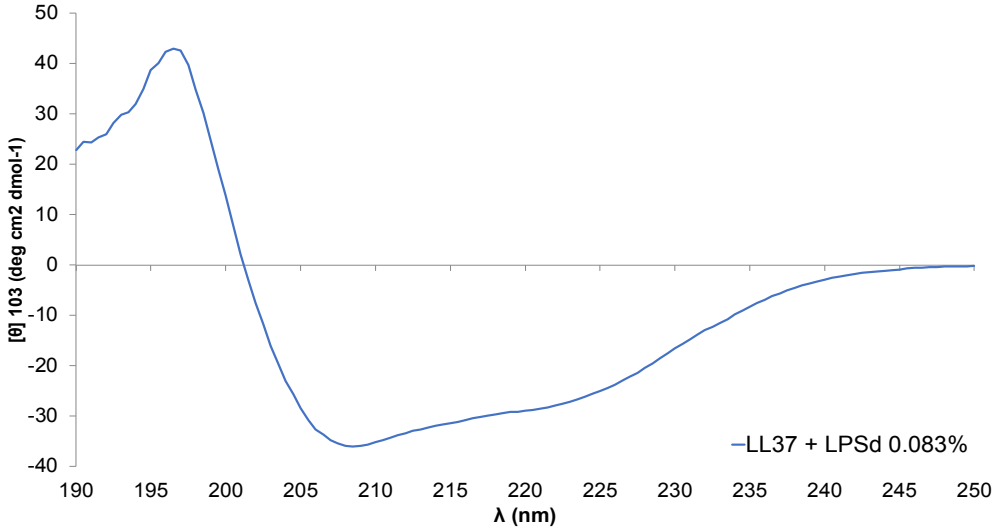

Figure 39. Far UV-CD spectra of LL37 in the presence of LPSd 0.083 %.

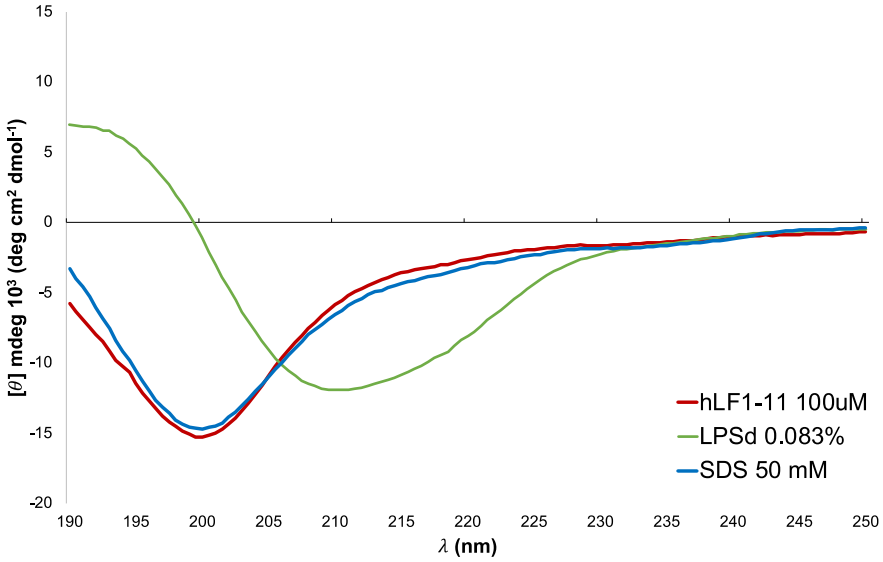

Figure 40. Far UV-CD spectra of 100 μM hLF1-11in aqueous solution (red line) and in the presence of 50 mM SDS (dark blue line), and 0.083 % LPSd (green line).

4.6 *In vitro* cytotoxicity assays on peptide-loaded microparticles

4.6.1 Crystal violet staining for cytotoxicity assays on BEAS 2B cell line

In addition to being effective, a formulation must also be biocompatible and non-toxic at least in the expected range of therapeutic activity and in the case of these peptides in the range of effective concentrations on the bacterium [165]. Consequently, the cytotoxicity of unprocessed and formulated peptides was first assessed by measuring the metabolic activity of the epithelial bronchial cells BEAS-2B following exposure for 72 h and by applying a crystal violet staining assay. The human lung-derived BEAS-2B cell line was first described in 1988 and obtained by immortalizing normal human bronchial epithelial cells with the A12-SV40 virus [182]. They resemble primary basal cells, and express proteins typical of epithelial cells, such as cytocheratin 8 and 18, but do not differentiate and are unable to form tight junctions [83,183]. Epithelial cells cover the surface of the airways and alveoli representing the first target of all that is inhaled and playing a protective role towards toxic substances or pathogenic microorganisms that might be inhaled [83].

For each peptide, the formulation that proved to be most successful in terms of aerosolization was selected and was solubilized in RPMI-1640 medium, as for the peptide, to obtain a final active concentration of 0, 5, 10, 15, 20, 25, 30 μg/ml for WLBU2 / WLBU2 SD (Run 10) and 0, 5, 10, 30, 50, 75, 100 μg/ml for LL37 / LL37 SD (#F) and hLF1-11 / hLF1-11 SD (#H). Results are presented in Figure 41 and Figure 42 and expressed as half maximal inhibitory concentration IC_{50}, *i.e* drug concentration capable of inhibiting 50 % of cells *in vitro* [141]. From the viability curves, no significant differences were observed between the effect of the raw material peptide and its corresponding formulation at the tested concentrations, well above the active concentration on the bacterial strain *P. aeruginosa.* It can therefore be stated that the formulation process did not alter the cytotoxicity profile of the peptides considered [138]. The effect on cell proliferation of the microparticulate matrix consisting of mannitol/leucine or trehalose/leucine (blank microparticles) was also investigated, and even at the highest concentration, antiproliferative effects were absent. Similarly, even at the highest concentrations applied, *i.e.* 30 μg/ml for WLBU2 / WLBU2 SD and 100 μg/ml for LL37/LL37 SD and hLF1-11/hLF1-11 SD, only a 10 % cell viability reduction was observed. According to the ISO guidelines, which define a compound as cytotoxic if it reduces viability below 70%, the peptides and their formulations are not considered cytotoxic in the presented cell model [184,185].

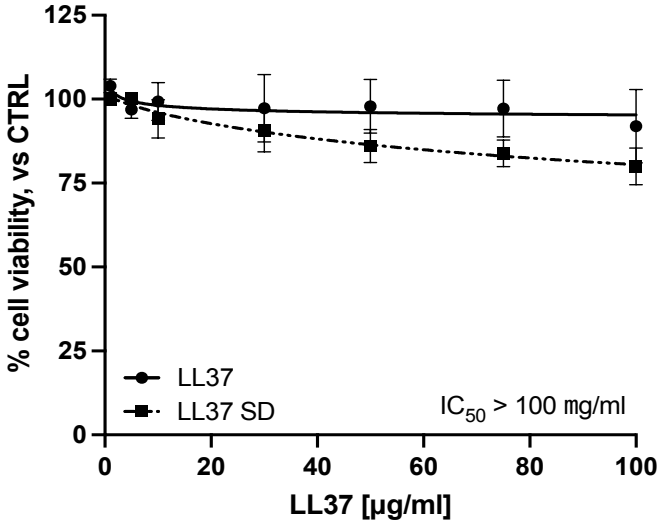

Figure 41. Crystal violet staining of LL37/LL37 SD on BEAS2B cell line. Results are expressed as cell viability curve and each point represents the mean ± standard deviation of three different experiments.

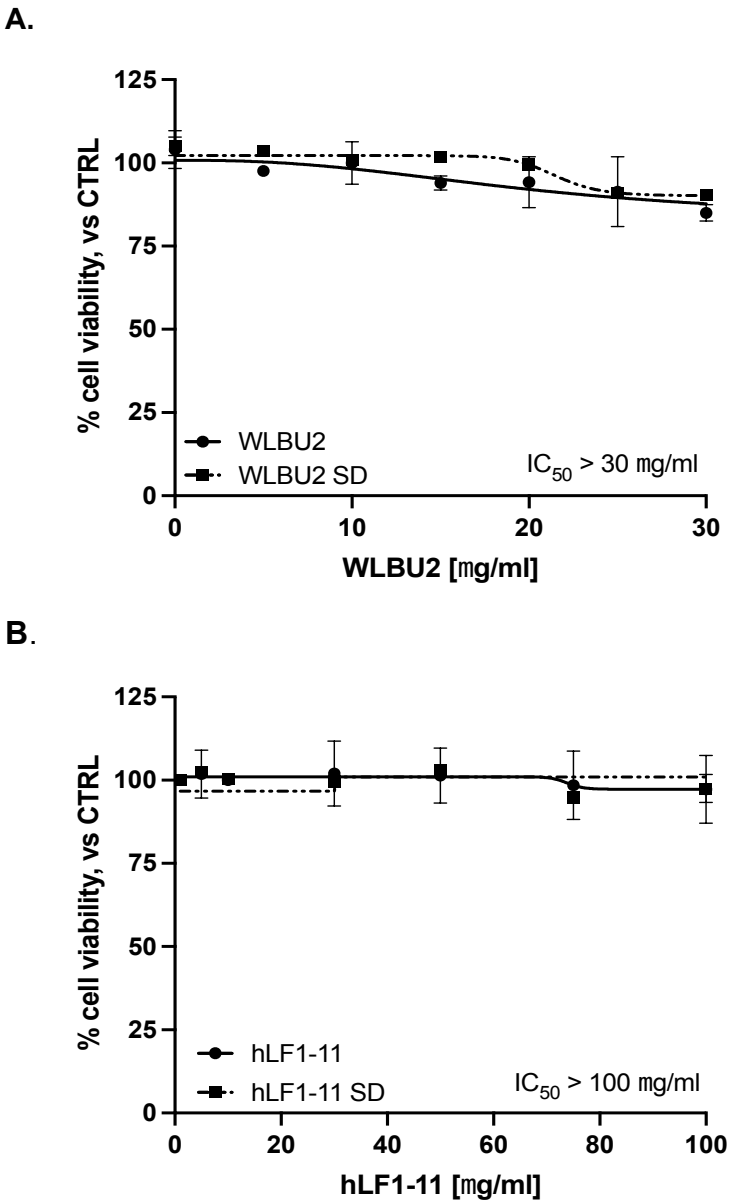

Figure 42. Crystal violet staining on BEAS 2B. Results are expressed as cell viability curve and each point represents the mean ± standard deviation of three different experiments. A) WLBU2/WLBU2 SD, B) hLF1-11/hLF1-11 SD.

4.6.2 Crystal violet staining for cytotoxicity assays on A549 cell line

The cytotoxicity of the peptides and their formulations was assessed in a second cell line, A549, by applying the same procedure as described above. A549 are human adenocarcinoma cells that constitute a tumor line used as a model for alveolar epithelial cells [186]. This line consists of hypotriploid basal epithelial alveolar cells,

and it was first isolated by D. J. Giard et al in 1972 from a 58-year-old Caucasian man with cancer. They have been used extensively to study lung cancer but also represent a model of type II alveolar epithelium since they express certain proteins that link them to AT2 cells [187]. As for BEAS-2B cells, for each peptide, the formulation that proved to be most successful in terms of aerosolization was selected and was solubilized in RPMI-1640 medium, as for the peptide, to obtain a final active concentration of 0, 5, 10, 15, 20, 25, 30 μg/ml for WLBU2 / WLBU2 SD (Run 10) and 0, 5, 10, 30, 50, 75, 100 μg/ml for LL37 / LL37 SD (#F) and hLF1-11 / hLF1-11 SD (#H). Results are presented in Figure 43 and Figure 44 and expressed as half maximal inhibition concentration IC_{50}. For peptides LL37 and WLBU2 (Figure 43 and Figure 44), no significant differences in the cell viability profile were identified. Even at the highest concentrations of 100 μg/ml and 30 μg/ml, an inhibition of cell proliferation of only 10 % was observed for both treatments. When the profile of formulated WLBU2 was further investigated, however, a slight reduction in the already low cytotoxicity was observed at 25 μg/ml. At this concentration of unprocessed peptide, viability was 90 %, whereas it was 100 % when the peptide was formulated. The same was observed for hLF1-11 peptide (Figure 44 B) with a reduction of approximately 10 % in cell viability at high concentrations and an IC_{50} higher at the highest concentration tested (100 μg/ml) than the one active on bacterial strains. Again, the process did not significantly alter the proliferative effect of the compounds on this cell line.

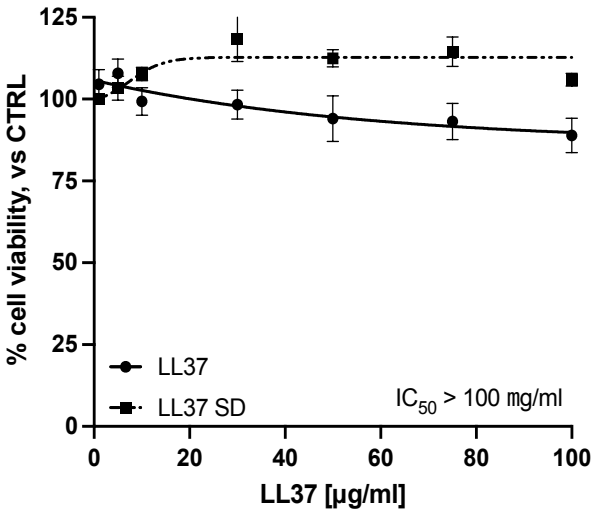

Figure 43. Crystal violet staining on A549 for LL37 and LL37 SD. Results are expressed as cell viability curve and each point represents the mean ± standard deviation of three different experiments.

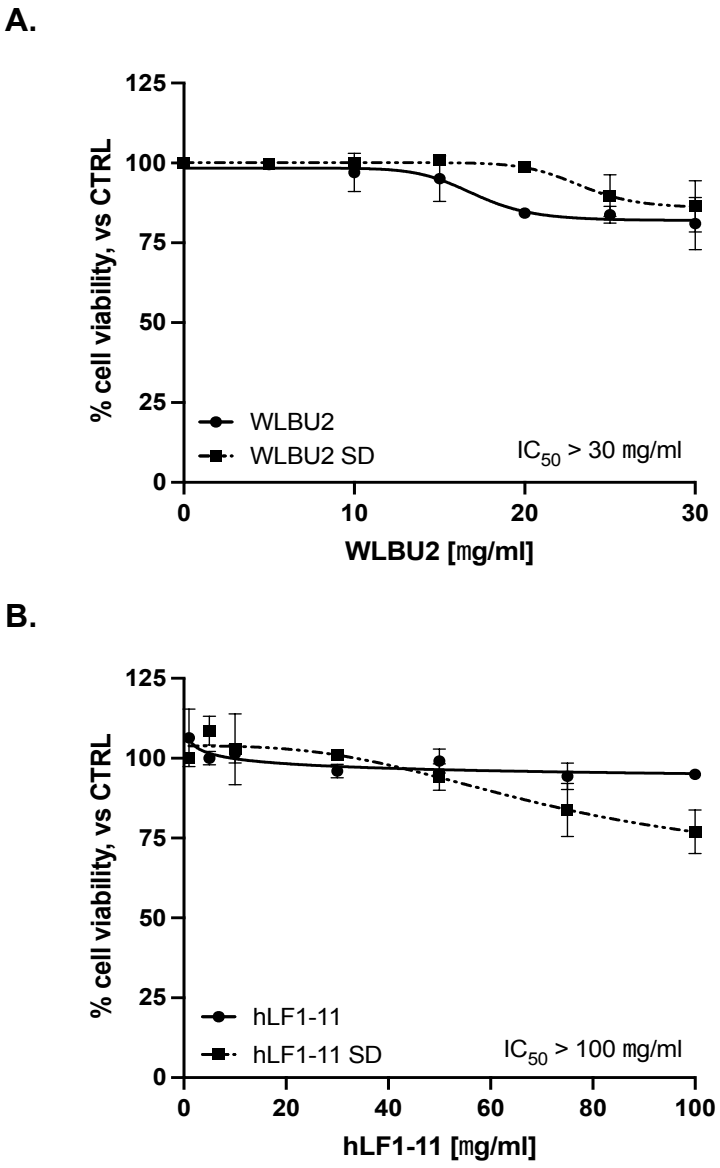

Figure 44. Crystal violet staining on A549. Results are expressed as cell viability curve and each point represents the mean ± standard deviation of three different experiments. A: WLBU2/WLBU2 SD, B: hLF1-11/hLF1-11 SD.

4.7 In vitro antimicrobial studies on peptide-loaded microparticles

4.7.1 Antibacterial activity against planktonic cells and killing kinetics

The experiments were carried out on planktonic bacterial cells by the CFU assay. WLBU2 was proven to have direct bactericidal activity against the investigated strains with EC_{50} values of 0.127 μM for *P. aeruginosa* PECHA 4. Instead, WLBU2 SD

significantly increased antibacterial activity, with EC_{50} value of 0.100 μM. The strong activity was also confirmed by dichroism studies where the interaction with membrane-like substances induced a clear conformation change from unstructured peptide to α-helical, as shown before.

The rates of *P. aeruginosa* killing by WLBU2 over time are shown in Figure 45. The bactericidal activity of WLBU2 was very fast against all the investigated strains. Indeed, after 2 minutes the killing was over 99 %. The same behavior was observed for WLBU2 SD.

Table 16. *In vitro* antibacterial activity of WLBU2 peptide and WLBU2-SD against planktonic cells.

Bacterial strains	**EC_{50} (95% Confidence Intervals) [mol/L]**	
	WLBU2	**WLBU2-SD**
P. aeruginosa ATCC 27853	0.119 (0.110 – 0.129) × 10^{-6}	0.095 (0.088 – 0.102) × 10^{-6}
P. aeruginosa PECHA 4	0.127 (0.113 – 0.142) × 10^{-6}	0.100 (0.096 – 0.106) × 10^{-6}

EC_{50}, half-maximal effective concentration.

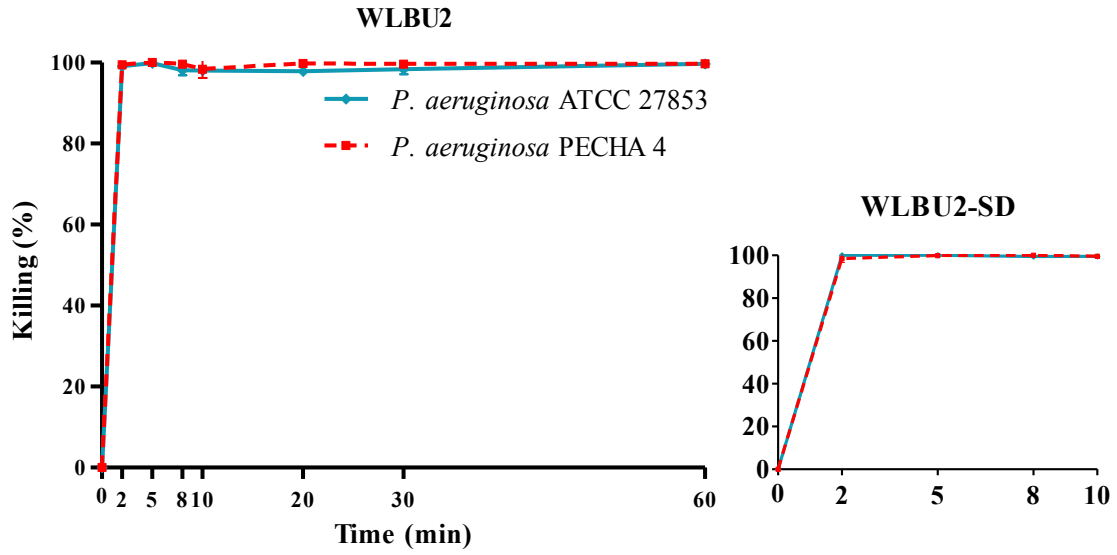

Figure 45. Time kinetics of *in vitro* activity of WLBU2 against *P. aeruginosa* ATCC 27853 and *P. aeruginosa* PECHA 4. Peptide concentration was equal to its minimal bactericidal concentration values (5 μg/mL). The inset shows time kinetics of WLBU2-SD. The activity is expressed as percentual killing, reported data represent mean values ± standard deviation.

LL37 and hLF1-11 have so far only been tested on the clinic isolate strain *P. aeruginosa* PECHA 4 and their formulations have been characterized biologically by preliminary analysis. LL37 showed a direct bactericidal activity against *P. aeruginosa* PECHA 4 with EC_{50} of 0.346 μM. When the peptide was formulated, a preliminary screening of its activity showed inhibition of 99 % and 85 % at 2 μg/ml and 5 μg/ml, respectively.

The rate of killing of *Pseudomonas* by LL37 over time is presented in Figure 46. More than 99 % inhibition of bacterial growth was observed within 8 minutes, indicating a probable mechanism of action by pore formation as in the case of WLBU2. Regarding spray-dried formulations of LL37, preliminary data were obtained that need to be further confirmed and investigated.

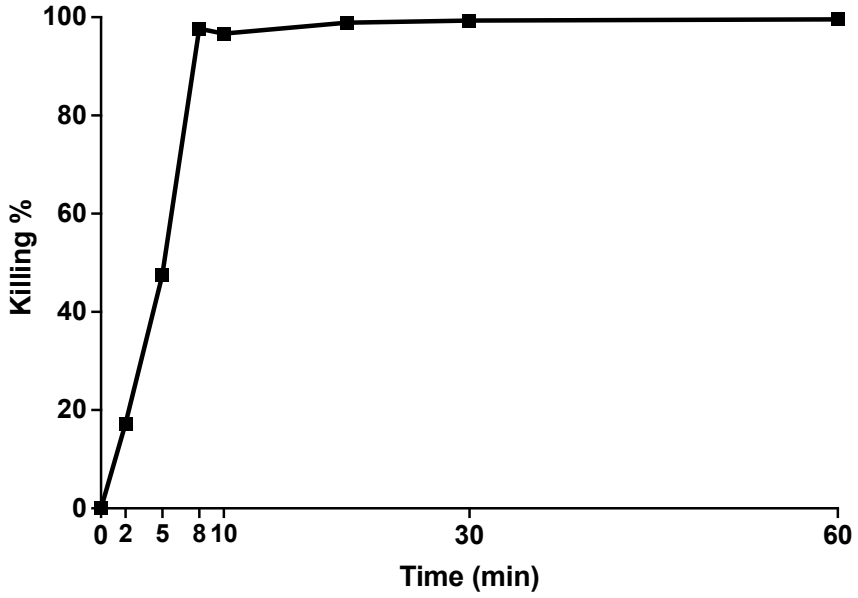

Figure 46. Time kinetics of *in vitro* activity of LL37 against *P. aeruginosa* PECHA 4. Peptide concentration was equal to its minimal bactericidal concentration values (5 μg/mL). The activity is expressed as percentual killing, reported data represent mean values ± standard deviation.

hLF1-11 showed medium bactericidal activity with EC_{50} of 1.149 μM on *P. aeruginosa* PECHA 4 and maintained inhibitory activity (greater than 99 %) when formulated at 2 μg/ml. Although this peptide was the least potent, studies of the killing kinetics again showed very rapid killing with inhibition of over 99 % in 2 minutes (Figure 47).

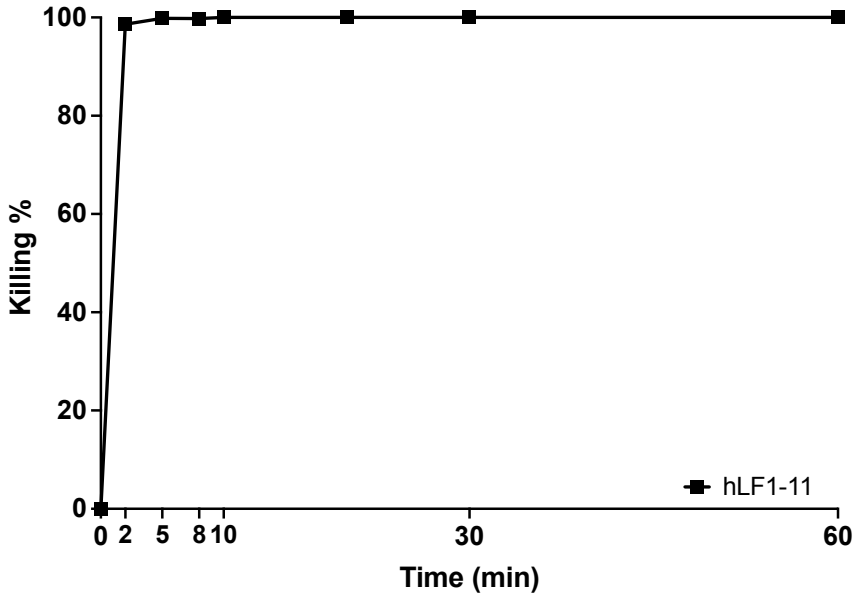

Figure 47. Time kinetics of *in vitro* activity of hLF-11 against *P. aeruginosa* PECHA 4. Peptide concentration was equal to its minimal bactericidal concentration values (5 µg/mL). The activity is expressed as percentual killing, reported data represent mean values ± standard deviation.

The antimicrobial activity of the formulated peptides was also evaluated 3, 6 and 9 months after production, confirming the results previously obtained.

4.7.2 Activity against P. aeruginosa strains' monomicrobial biofilm

The Crystal violet assay was used for microbial biomass quantification to evaluate the capability of unprocessed WLBU2 and WLBU2 SD to reduce the monomicrobial biofilm formed by the studied *Pseudomonas* strains in polystyrene multi-well plates. At the concentration used (5 µg/mL), WLBU2 and WLBU2 SD reduced mature biofilm biomass with a reduction more than 40% compared to the control. The highest activity was observed for WLBU2 SD against *P. aeruginosa* PECHA 4 at 24 h of treatment (72.38%). As reported in Table 17, the anti-biofilm activity of WLBU2 peptide was significantly diminished (*P. aeruginosa* ATCC 27853), with consequent biofilm re-growth, or unchanged (*P. aeruginosa* PECHA 4) after 24 h of treatment. On the contrary, the anti-biofilm activity of WLBU2 SD has been preserved and significantly increased after 24 h against all investigated strains.

Table 17. Reduction of monomicrobial biofilm biomass after treatment with WLBU2 peptide and its formulation.

Strain	% Reduction of Biofilm Biomass [1]			
	WLBU2		WLBU2-SD	
	5 h	24 h	5 h	24 h
P. aeruginosa ATCC 27853	56.72 ± 3.77	40.18 ± 5.11*	42.32 ± 5.95	53.57 ± 5.06*
P. aeruginosa PECHA 4	43.68 ± 5.11	55.85 ± 10.86	54.15 ± 2.17	72.38 ± 6.48**

[1] % reduction evaluated by CV assay with reference to untreated control. Statistically significant with respect to the 5 h treatment (*, p <0.05; **, p <0.01).

The antibiofilm activity of the LL37 peptide and its microparticle formulation was preliminarily evaluated towards mature *Pseudomonas aeruginosa* PECHA 4 biofilms. Significant impairment of the architecture of the mature biofilm was observed at the concentration of 50 µg/ml (11.128 µM), with a percentage reduction in biomass of 31.13 ± 20.60% and 44.52 ± 0.87%, respectively, compared to the untreated biofilm (Table 18). These preliminary results showed a better anti-biofilm activity of the LL37 SD, albeit not statistically significant, compared to the peptide alone. Further evaluation is needed to demonstrate these findings.

Table 18. Reduction of monomicrobial biofilm biomass after treatment with LL37 peptide and its formulation.

Strain	% Reduction of Biofilm Biomass [1]	
	LL37	LL37 SD
P. aeruginosa PECHA 4	31.13 ± 20.60	44.52 ± 0.87

Since the hLF1-11 peptide proved to be the least potent on planktonic cells, it was not considered for biofilm studies.

5 Conclusion

The first part of this project was dedicated to the fine-tuning of the spray drying process to create microparticle powders containing the peptide WLBU2, with a specific focus on their suitability for pulmonary administration. The central objective was to produce microparticles that possess ideal aerodynamic properties, particle size distribution, and moisture content while safeguarding the peptide's stability throughout the process. Employing the systematic approach of Design of Experiments (DoE), we have garnered essential findings.

The selection of excipients for the microparticle matrix was a pivotal step in ensuring the stability of WLBU2 during the spray drying process. Mannitol, as a non-reducing sugar, emerged as a robust protector against thermal stress, while leucine functioned as a surface modifier, reducing inter-particle cohesion, and improving flowability, a critical attribute for inhalable products. The application of the DoE was crucial in defining the optimal combination of process parameters for spray drying. Key factors under examination were feed concentration, feed rate, and inlet temperature. These factors were thoughtfully chosen due to their direct influence on the structure, size, and moisture content of the resultant spray-dried particles. The DoE results revealed that feed concentration and inlet temperature exerted a significant influence on process yield, with feed concentration emerging as particularly impactful. The particle size distribution fell within the acceptable range for pulmonary delivery. The Dv_{50} values spanned from 3.3 µm to 6.0 µm. Notably, the moisture content, a critical quality parameter, remained consistently below 6%, affirming the efficacy of the solvent evaporation process. DSC analysis confirmed the preservation of WLBU2's crystalline state post-spray drying. It also revealed changes in mannitol's crystallinity due to the presence of the peptide, marked by a reduction in enthalpy. This crystalline nature of WLBU2 SD could potentially enhance aerosolization while raising questions about its bioavailability. The *in vitro* aerodynamic assessment resulted in all formulations consistently achieving acceptable EF values, ranging from 85 % to 98 % and an acceptable RF %. This signifies their potential for effective lung deposition. To summarize, the optimization of the spray drying process for microparticles containing WLBU2 has yielded promising results. The systematic approach, encompassing critical quality attributes such as particle size distribution, moisture content, and

aerodynamic performance, has generated valuable insights for the development of inhalable peptide formulations.

The follow-up part of the WLBU2 project was the preliminary screening for the formulation development of LL37 and hLF1-11 through spray drying with a focus on understanding the impact of key excipients, crucial in inhalation applications, on both the process yield and the peptide content within the resulting powders. The choice of excipient is intimately tied to the intended functionality of the powder, the characteristics of the peptide, and the desired aerosolization properties necessary for effective pulmonary deposition.

Here, three commonly used excipients in the context of dry microparticle production through spray drying are taken into consideration: mannitol, trehalose, and lactose, as well as the amino acid leucine. Mannitol, characterized as a reducing sugar with low hygroscopicity, was an attractive candidate, as seen in our previous study with WLBU2. Lactose, another reducing sugar, posed concerns due to its potential to trigger Maillard reactions when it encounters amino groups in peptides and proteins. In contrast, trehalose, a disaccharide with a high glass transition temperature, exhibited resistance to acid hydrolysis and the ability to form an amorphous microparticle matrix during spray drying. In our preliminary study, we excluded lactose due to its Maillard reaction potential, ultimately favoring trehalose for its capacity to stabilize peptides and proteins more effectively. Moving on to the results from our study, the choice of feed rate significantly influenced the yield for both mannitol and trehalose formulations. However, this influence wasn't always linear, as altering the spray rate between 3 and 5 ml/min did not proportionally impact yield.

Subsequently, we assessed the drug content of LL37 and hLF1-11 in the spray-dried microparticles. We observed that LL-37 exhibited recovery percentage greater than or equal to 90% in most formulations, with exceptions in powders D and E. In contrast, hLF1-11 showed content of 75% in mannitol-based powders and an impressive 105% in trehalose-based formulations. This underscores trehalose's superiority in stabilizing these peptides, which are more sensitive to thermal and mechanical stress. To further characterize the microparticles, we performed laser diffraction analysis, revealing a size distribution suitable for pulmonary administration, with particle diameters ranging from 1.25 µm to 6.26 µm. Additionally, SEM revealed that LL37 SD and hLF1-11 SD

microparticles were spherical, smooth, and appropriately sized for inhalation, thanks to the formulation and leucine's presence.

In vitro pulmonary deposition assessment through the Next Generation Impactor (NGI) demonstrated favorable dispersion trends for DPI formulations with EF% of around 90%. The MMAD values fell within an acceptable range for lung deposition. The respirable fraction exceeded 50%, with powder F, containing 75% trehalose, 15% LL37, and 10% leucine, exhibiting the highest value.

In our quest to understand the interaction between antimicrobial peptides and bacterial membranes, we delved into crucial aspects of their mechanisms, with a particular focus on the destabilization of bacterial membranes. This understanding is pivotal as it forms the basis for the antimicrobial action of these peptides. We employed circular dichroism studies using molecules that mimic bacterial outer walls, such as lipids, LPS, and detergents (SDS), to shed light on how these peptides act. Their mechanism can typically be categorized into three models: the barrel stave, toroidal pore, or carpet model. By conducting biophysical studies via circular dichroism, we gained insights into the secondary structure of the peptides when in contact with bacterial membranes. In our study, we investigated the structural characteristics of peptides WLBU2, LL37, and hLF1-11, as well as WLBU2 SD through far-UV circular dichroism spectroscopy. When examining WLBU2, we observed that in an aqueous solution, it exhibited a typical random coil conformation. However, in the presence of anionic SDS micelles, it transitioned into a well-defined α-helix structure. Additionally, interaction with LPS and LPSd further promoted helical conformation. This confirmed WLBU2's tendency to interact with bacterial wall mimetics, adopting a helical structure during this interaction. Similarly, WLBU2 in its spray-dried (SD) form showed a random coil conformation in an aqueous solution, transitioning into an α-helix structure when in the presence of SDS micelles. Interaction with LPS and LPSd led to even more pronounced helical conformation. Comparatively, the SD formulation contributed to a higher content of WLBU2's helical conformation. A similar behavior was observed for LL37, but not for hLF1-11, which retained its random coil structure when in contact with substances mimicking the composition of the bacterial wall.

Furthermore, we considered the crucial aspect of cytotoxicity. For a formulation to be effective, it must also be biocompatible and non-toxic within the expected therapeutic concentration range. Our assessment involved measuring the metabolic activity of

bronchial epithelial cells BEAS-2B after exposure to unprocessed peptides and their formulations. The results from this cytotoxicity assessment revealed that, at concentrations well above the active concentration against *P. aeruginosa*, neither the unprocessed peptides nor their formulations exhibited significant differences in cytotoxicity. The formulations did not alter the cytotoxicity profiles of the peptides. We extended cytotoxicity evaluation to another cell line, A549, which represents a model for alveolar epithelial cells. Here, we observed no significant differences in the cell viability profile between the unprocessed peptides and their formulations, even at high concentrations.

Moving on to the bactericidal activity of these peptides, WLBU2, LL37 and hLF1-11 displayed direct bactericidal activity against the tested strains of *P. aeruginosa*, albeit with some differences in terms of potency. For WLBU2 an increased antibacterial activity was also observed when formulated into spray-dried microparticles. Moreover, the killing of *Pseudomonas* by WLBU2 was remarkably rapid, with over 99% inhibition within just 2 minutes. LL37 also exhibited potent bactericidal activity against *P. aeruginosa*, with its spray-dried form showcasing similar efficacy once preliminary tested. The kinetics of *Pseudomonas* killing demonstrated rapid inhibition of bacterial growth, with over 99% inhibition within 8 minutes. hLF1-11, although less potent, still displayed moderate bactericidal activity, with rapid inhibition of over 99% within 2 minutes.

In summary, this project advances our knowledge of spray drying for inhalable peptide formulations and enhances our understanding of the interactions and activities of antimicrobial peptides. These findings pave the way for the development of effective treatments for respiratory infections and underscore the potential of inhalable peptide-based therapies.

Chapter IV

PLGA Nanoparticles for Antimicrobial Peptides delivery

1 Introduction

The clinical utility of AMPs is often hindered by issues related to stability, controlled release, and targeted delivery. To address these challenges, nanotechnology-based approaches have gained significant attention [188]. The encapsulation of pharmaceutical molecules in nanoparticle systems aims to aid the dissolution of poorly soluble molecules, prevent enzymatic degradation processes, or control drug delivery [120]. Among the various materials with which nanoparticles can be manufactured, polymers such as PLGA have attracted great interest over the years for their ability to assert the problems described above [189]. There are different techniques that allow the manufacturing of these systems. The first procedure developed was the nanoprecipitation or solvent displacement, especially applied for the encapsulation of hydrophobic compounds. It is an easy method, patented in 1989, whose major advantages over the emulsification process are simplicity and reproducibility [190]. Nanoprecipitation occurs by interfacial deposition*, i.e.* by the transport of a polymer dissolved in an organic water-miscible phase into a non-solvent or aqueous phase [191]. Particle formation occurs by nucleation, growth, and aggregation where the driving force is the interfacial turbulence created by differences in the surface tension of the aqueous phase (high) and the organic phase (low). This turbulence induces the diffusion of the organic solvent from low surface tension sites causing the precipitation of the polymer in the form of nanoparticles [115,190,192]. When a hydrophobic molecule such as PLGA is solubilized in a polar solvent, *i.e.* acetone, and subsequently added to a large volume of water, the concentration of the solute exceeds the thermodynamic solubility limit, defining a supersaturation condition. From the supersaturation of the solute, the system evolves with nucleation and spontaneous growth. Nuclei that exceed a critical size can continue to grow by attracting solute

molecules from the surrounding solution until the remaining solute concentration reaches equilibrium. The speed of particle growth is influenced by the degree of supersaturation and the diffusion coefficient of the solute molecules [193]. Particles obtained by nanoprecipitation are collected in suspension together with other impurities, such as excess stabilizers, thus requiring a purification step, usually by centrifugation, ultracentrifugation and/or dialysis after the removal of the organic solvent by room temperature evaporation or under pressure [194]. The effectiveness of the nanoprecipitation process depends on several factors that influence the characteristics of PLGA nanoparticles. These factors include the type of solvent and non-solvent, mixing technique, and environmental conditions. How these variables interact determines key attributes such as nanoparticle size, shape, drug encapsulation efficiency, and release behavior. It is crucial to manage these factors to tailor PLGA nanoparticle formulations [195]. The first element to consider is the polymer concentration used for encapsulation and formation of the nanoparticle system. It affects the viscosity of the organic phase, and when this viscosity becomes too high, it hampers the proper diffusion of the polymer within the non-solvent. This, in turn, hinders successful nanoprecipitation and leads to the formation of larger particles [115,196]. To address this issue, researchers have explored the use of stabilizing materials like polyvinyl alcohol (PVA), as mentioned by Bilati [196]. For instance, Alkholief et al. opted for PVA as a stabilizer to produce spherical nanoparticles with a narrow size distribution, even at higher concentrations. As an alternative, they proposed the polyvinylpyrrolidone (PVP), which appears to facilitate the encapsulation of large molecules such as proteins [195]. Overall, PVA is recognized as one of the most well-known stabilizers. However, it is worth noting that several studies have pointed out the mucoadhesive properties of PVA when it interacts with polymeric nanoparticles, potentially affecting the efficacy of the pulmonary delivery of these formulations into the deep lung. Popov et al. demonstrated that the mucoadhesive properties of PVA are closely linked to its degree of hydrolysis. Specifically, a degree of hydrolysis ranging from 75 to 95% allows nanoparticles to penetrate mucus because the PVA corona formed is sufficiently hydrophilic, preventing stable hydrogen bond formation with mucins [197]. The main characteristics affected by the presence of PVA are the size and the zeta potential. Indeed, it has been reported that an increase in PVA concentration, as in the case of PLGA, induces an increase in viscosity that

hinders polymer diffusion. As regards the zeta potential, the stabilizer forms a coating on the PLGA nanoparticle surfaces that results in a decreased negative charge [195]. The zeta potential of PLGA nanoparticles typically becomes more negative in the presence of PVA as it is a hydrophilic polymer that carries a net negative charge in aqueous solutions. When PVA is used to coat the surface of PLGA nanoparticles, it introduces additional negatively charged groups to the nanoparticle surface, leading to a decrease in the zeta potential. This change in zeta potential can influence the stability, dispersion, and interactions of the nanoparticles in solution [120,197].

The type of organic solvent used is also a critical factor in the production of polymeric nanoparticles through nanoprecipitation. Acetone is the most frequently employed solvent, as it offers full solubility for PLGA and has been linked by multiple authors to a reduction in nanoparticle size when compared to alternative solvents [120,198]. Acetone is miscible with water, has a low boiling point of 56 °C and a dielectric constant of 20.7, making it sufficiently polar to ensure good diffusion into the non-solvent phase [115,199]. In addition, the affinity of the polymer for the solvent plays a crucial role, as a higher affinity between polymer and solvent increases the likelihood of the solvent remaining within the supersaturation region, again hindering the diffusion process [196,199]. Nevertheless, relatively modest encapsulation efficiencies have been documented, together with low drug loading (approximately 20% of the theoretical loading), indicating a dependence on factors such as drug-polymer interaction and the drug's miscibility within the polymer matrix [200,201]. As observed by Chew et al. when encapsulating the highly water-soluble levofloxacin in PLGA nanoparticles, the reduced encapsulation efficiency of these systems was related to the solubility of the drug in the organic and/or aqueous phase[101,202]. These limits might be overcome with the help of the microfluidics technique where a greater control over nanoparticle production can be achieved [203]. Moreover, the mechanical stress to which the active molecules are exposed is less than in batch-to-batch processes such as emulsification, ultrasonic emulsification, or nanoprecipitation, which often require sonification steps [204]. With microfluidics, it is also possible to implement phase mixing efficiency by incorporating passive mixers into the channels [121,123]. An example is the staggered herringbone micromixer chip used in this study. It represents one of the most common passive mixers where mixing is induced by chaotic advection, increasing efficiency in terms of both final product quality and time [205]. This chip is

characterized by a microchannel geometry that increases the interfacial contact area between the species, which are mixed quickly and efficiently thanks to the chaotic flow created [206].

Since PLGA often requires the use of acetone that can damage the structure of the microchips, a chip made of zeonor, a transparent, highly pure olefinic cyclic polymer, resistant to most organic solvents, was used [207,208]. Using this chip, the characteristics of the nanoparticles being formed within the microchannels are influenced solely by the composition of the nanoparticle system and the settings of the microfluidic procedure, including the concentration of PLGA, the peptide, the stabilizer, the flow rate of the two phases, their ratio and the total flow rate applied. A typical microfluidic setup is composed of two syringe pumps for the organic phase (PLGA + drug + acetone) and the aqueous phase (stabilizers + water). In this part of the PhD project, carried out at the Lüdwig Maximilians Universität (Munich, Germany), the objective was to investigate and compare the formulation of antimicrobial peptides into PLGA nanoparticles using the above-mentioned techniques. Starting with the formulation development carried out in bulk with a formulation composed of PLGA, PVA as stabilizer and peptides, the study proceeded with the formulation optimization using microfluidics by investigating the influence of various process parameters on the chemical-physical and loading properties of the obtained systems.

2 Materials

Polyvinylalcohol (PVA) Mowiol 4-88 (Mw 31 000 g/mol) and Resomer RG 502 H (PLGA) acid terminated (MW 7.000-17.000) were purchased from Merck (Merck KGaA, Darmstadt, Germany). Acetone and all the organic solvents were of analytical grade. LL37 (LLGDFFRKSKEKIGKEFKRIVQRIKDFLRNLVPRTES, MW 4493.29 Da), WLBU2 (RRWVRRVRRWVRRVVRVVRRWVRRU24, MW 3400.12 Da), hLF1-11 (GRRRRSVQWCA, MW 1374.58 Da) were purchased from GenScript (Piscataway, USA) as white lyophilized powders (TFA salt), without any further chemical modification in the amino acidic sequence, with > 90% purity. The microchip Fluidic 187 was purchased from ChipShop (Jena, Germany) together with polyethylene (PTFE) tubing intrametric, I.D. 38 mm, O.D. 1.09 mm.

3 Methods

3.1 Nanoprecipitation

PLGA nanoparticles (PLGA NPs), loaded with LL37, WLBU2 or hLF1-11, were prepared by the nanoprecipitation technique (Figure 48).

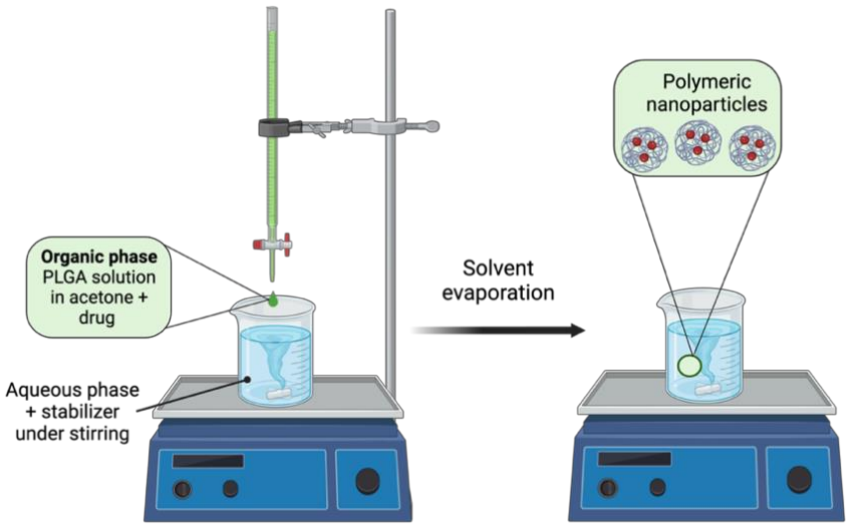

Figure 48. Nanoprecipitation experimental setup (created with Biorender.com).

PLGA was weighed and dissolved in 1 ml of acetone to reach a final concentration of 5 mg/ml. Each peptide was first solubilized in 100 μL of ultrapure water and then added to the PLGA phase to reach a final active concentration of 1.5 mg/ml, 0.5 mg/ml and 0.1 mg/ml. The resulting theoretical peptide loadings (%), calculated as the amount of peptide relative to the mass of the initial system (polymer + peptide), were 20 % w/w, 10 % w/w, and 2 % w/w, respectively. The organic solution, composed of PLGA and LL37, WLBU2, or hLF1-11 in acetone, was then added dropwise in 10 ml of an aqueous solution of PVA 1.5 % w/v. Acetone was evaporated under stirring at 300 rpm for 3 hours at room temperature. The evaporation time was determined based on the evaporation rate of a volume of acetone equal to that in the formulation (1 ml). NPs were then purified and washed with ultrapure water from exceeding reagents by centrifuging twice for 30 minutes at 18,000 rcf and 4 °C. Before the first centrifugation step, nanoparticle suspension was divided into 2 ml aliquots and transferred into multiple Eppendorf tubes added with 30 μl of glycerol at the bottom. The inclusion of

glycerol facilitated the resuspension of the nanoparticle pellet after the purification process. Then nanoparticles were resuspended in a final volume of 2 ml of ultrapure water and freeze-dried for 16 h (Epsilon 2-6D LCSplus, Martin Christ Gefriertrocknungsanlagen GmbH, Germany where shelf temperature was decreased down to - 50 °C and 0.2 mBar, and then primary drying was carried out at – 20 °C and 0.1 mBar.

3.1.1 Physical characterization

Nanoparticle's hydrodynamic diameter (d_H), polydisperse index (PDI), and ζ potential were measured by dynamic light scattering (DLS) using a Zetasizer Nano ZS instrument (Malvern Instruments Ltd., Worcestershire, United Kingdom). The refractive index used in the analysis was 1.33 and water was used as a dispersant for both size and ζ potential measurements. Size averages and ζ potential values were measured after NP's purification. For the former, the nanoparticle's dispersion was diluted 1:10 with ultrapure water and measured using a polystyrene disposable cuvette ZEN0040. Instead, for the latter, a folded capillary zeta cell DTS1070 was used. Analysis was carried out in triplicate with at least 13 runs at a constant temperature of 25 °C.

3.1.2 HPLC analytical quantification of peptides

An analytical method for the determination of LL37 and WLBU2 within nanoparticles was developed using a Dionex UltiMate™ 3000 HPLC system (Thermo Fischer Scientific, Dreieich, Germany) coupled with Chromeleon™ 7 Chromatography Data system (CDS) software. The separation was carried out in reverse phase chromatography with an INERTSIL 5 ODS-3 150 x 3 mm column coupled with a guard column. The elution was performed in a gradient mode with 100 % ultrapure water + 0.05 % v/v trifluoroacetic acid (TFA) as mobile phase A and acetonitrile:H_2O + 0.05 % TFA 95:5 v/v as mobile phase B (from 5 % to 95 % of mobile phase B) as shown in Table 19. Flow rate was set to 0.4 ml/min, injection volume of 30 µL, run time 20

minutes, and room temperature. The detection wavelength was set at 210 nm for both peptides.

Table 19. Gradient regime for High-Performance Liquid Chromatography (HPLC) analysis.

% mobile phase B	Minutes
5	0
65	13.6
95	13.61
95	14.60
5	14.61
5	20

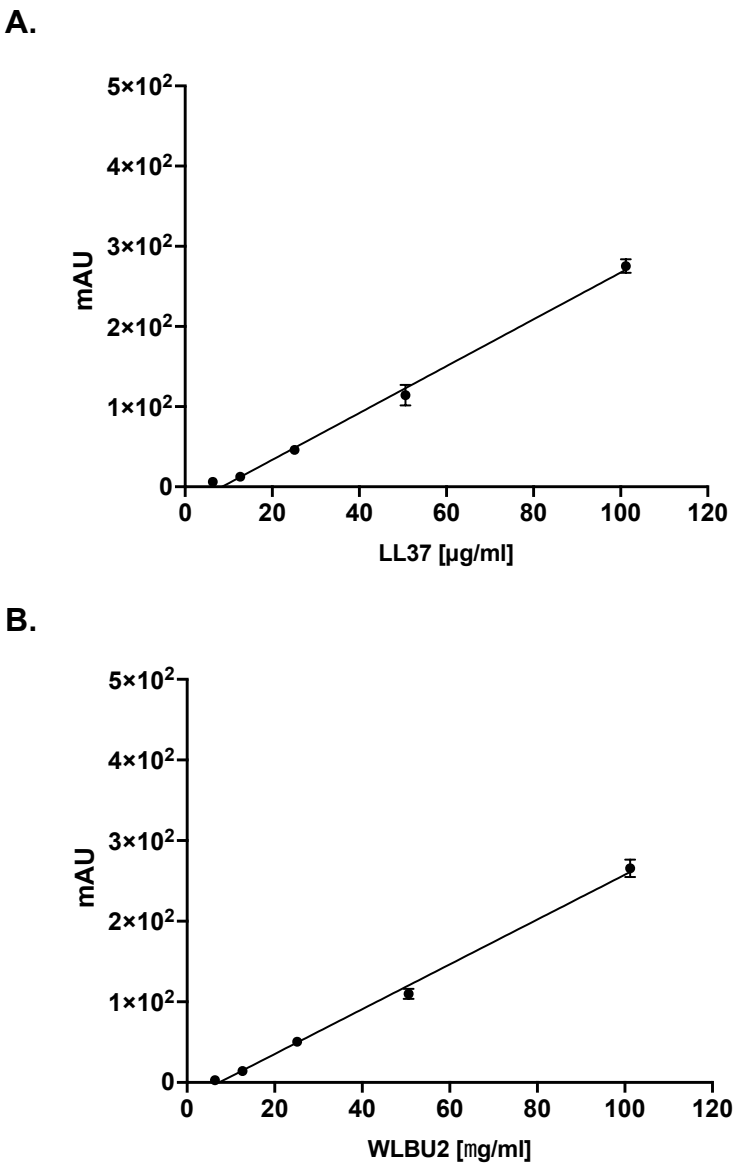

Figure 49. Calibration curve for LL37 (A) and WLBU2 (B). Linearity was assessed in the range of 6.3 – 100 μg/ml (mean ± standard deviation of two measurements (n = 2)).

LL37 calibration curve (Figure 49 A) was obtained by plotting the peak's area referred to 5 solutions from 6.3 µg/ml to 100 µg/ml. Linearity was assessed in this range with R^2 = 0.99. The LOD and LOQ were found to be 0.393 µg/ml and 1.19 µg/ml, respectively. Linearity was represented by R^2 = 0.99 also when WLBU2 was quantified. From the calibration curve, for WLBU2 the LOD and the LOQ were found to be 0.78 µg/ml and 2.78 µg/ml, respectively (Figure 49 B).
hLF1-11 calibration curve (Figure 50) was obtained by plotting the peak's area referred to 5 solutions from 6.3 µg/ml to 100 µg/ml. Linearity was assessed in this range with R^2 = 0.99. The LOD and LOQ were found to be 0.23 µg/ml and 1.42 µg/ml, respectively.

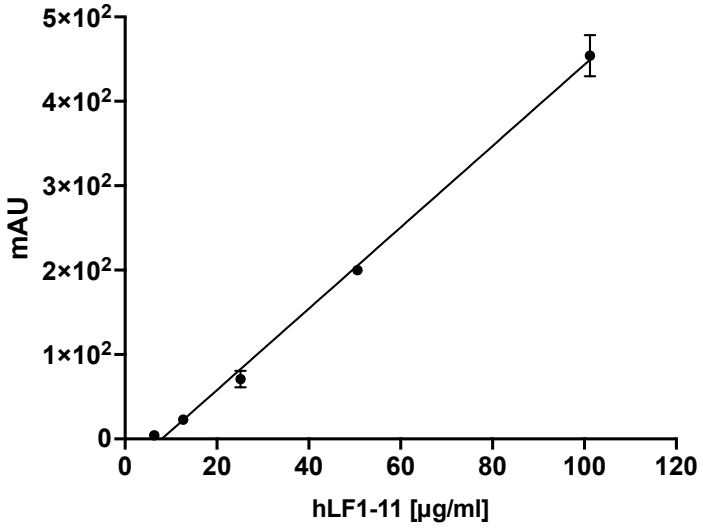

Figure 50. Calibration curve for hLF1-11 peptide. Linearity was assessed in the range of 6.3 – 100 µg/ml. Each point represents the mean ± standard deviation of two measurements (n = 2).

3.1.3 Encapsulation Efficiency and Drug Loading

The encapsulation efficiency (EE %) and drug loading (DL %) were determined through an extraction procedure applied to lyophilized nanoparticles. Specifically, approximately 2 mg of freeze-dried particles were treated with 1 ml of acetonitrile, which triggered the dissolution of the polymeric nanoparticle matrix. Subsequently, the resulting solution was vigorously vortexed and supplemented with 50 µL of ultra-pure

water, inducing the precipitation of PLGA and the simultaneous dissolution of the loaded peptide. After a centrifugation cycle for 30 minutes at 18,000 rcf and 4 °C the supernatant was analyzed for the amount of encapsulated peptides by applying the HPLC method described in Chapter IV, in section 3.1.2. The DL% and EE% were determined using the following equations:

$$\text{DL (\%)} = \frac{Peptide\ amount\ loaded\ in\ NP\ (\mu g)}{initial\ amount\ of\ NP(\mu g)}\ \text{x 100}$$

$$\text{EE (\%)} = \frac{Peptide\ amount\ loaded\ in\ NP\ (\mu g)}{Initial\ total\ peptide\ used\ \ (\mu g)}\ \text{x 100}$$

where the initial amount of NP (μg) refers to the initial total amount of solid used for the preparation of the system (polymer + peptide); the peptide amount loaded in NP refers to the encapsulated peptide found after the extraction procedure from the freeze-dried NPs.

3.2 Microfluidic-assisted PLGA Nanoparticles manufacturing

3.2.1 Nanoparticles synthesis

PLGA nanoparticles were prepared using a zeonor, single-phase staggered herringbone mixer chip (Microfluidic ChipShop, Jena, Germany). The chip was composed of two inlet channels with a depth of 200 μm and width of 300 μm, a channel width mixer of 600 μm and a channel width outlet of 600 μm. The chip was connected to two NE - 1600 syringes pumps (Darwin Microfluidics, Paris, France) via polytetrafluoroethylene (PTFE) tubing (internal diameter 0.38 mm, outer diameter 1.09 mm). A schematic representation of the microfluidic setup is presented in Figure 51. In practice, microfluidics involves the use of two syringes filled with the aqueous phase and the organic phase. Once connected to the pumps, these allow the controlled delivery of the two phases, thus the solutions are dispensed and mixed within the channels of the chip. By varying the flow rates, the ratio between the water and

aqueous phase, and the total flow rate applied, particles with different characteristics can be obtained.

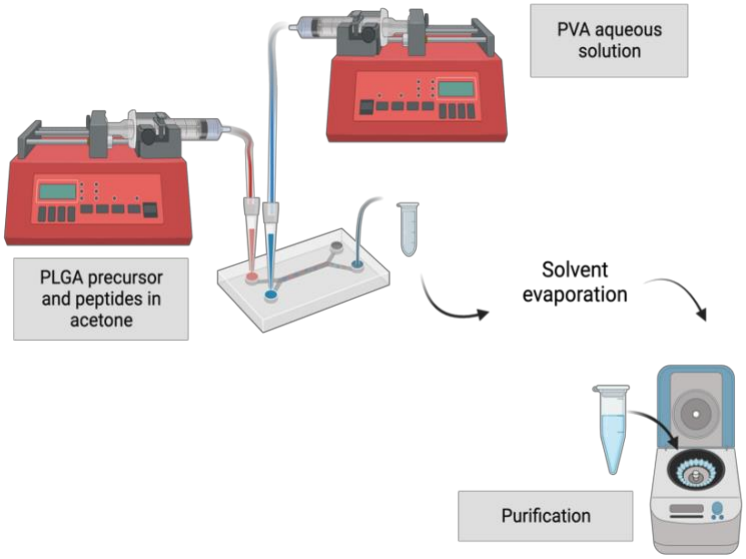

Figure 51. Microfluidic setup with syringe pumps, tubing and the chip (created with Biorender.com).

The manufacturing of the PLGA NPs was divided into two phases and it was only applied for the encapsulation of LL37 and WLBU2. The first phase aimed to screen the influence of microfluidic parameters on physical-chemical NPs properties, while the second one consisted of a formulation optimization.

Preliminary phase

NPs were first prepared by dissolving PLGA at 5 mg/ml in a water-miscible organic solvent*, i.e.* acetone, as for bulk nanoprecipitation. LL37 or WLBU2 solution at 0.1 mg/ml (2 % w/w of the initial total solid amount) was added to the PLGA phase and pumped into the microfluidic channel against PVA 1.5 % w/v to induce polymer precipitation in nanosized particles. The flow rate of the organic phase (FRop) was kept constant at 0.2 ml/min, while for the PVA-aqueous phase the flow rate (FRwp) was changed on three level, *i.e*. was set at 1.6 ml/min to 2 ml/min and 3.2 ml/min. Therefore, we considered as process variables the Flow Rate Ratios (FRR) given by FRwp/FRop and the Total Flow Rate (TFR) given by the sum of the FRop and FRwp.

Therefore, FRR tested were 1:8 (v/v), 1:10 (v/v), and 1:16 (v/v) with TFR of 1.8 ml/min, 2.2 ml/min, 3.4 ml/min, respectively. Immediately following the synthesis of the nanoparticles, they were purified and washed with ultrapure water as described in Chapter IV, section 3.1.1. The effect of passive mixing and preparation conditions (FRR, TFR) on particle size, surface charge, and ζ potential was investigated (Table 20).

Table 20. Microfluidic process parameters were investigated to produce PLGA nanoparticles FRR: flow rate ratio; FRop: flow rate organic phase; FRwp: flow rate water phase; TFR: total flow rate.

FRR [ml/min]	FRop [ml/min]	FRwp [ml/min]	TFR [ml/min]
1:8	0.2	1.6	1.8
1:10	0.2	2	2.2
1:16	0.2	3.2	3.4

Optimization phase

Based on the physical characterization of NPs in the preliminary study, the FRR of 1:10 was selected to produce NPs to be tested *in vitro* in cell culture models. In the beginning, the formulation composition was the same as in the preliminary study, *i.e.* 5 mg/ml PLGA, 1.5 % w/v PVA, and 0.1 mg/ml peptide (5_PLGA NPs). However, subsequent cytotoxicity studies revealed the need to optimize the NPs composition. As a result, efforts focused on reducing the PLGA concentration to 2.5 mg/ml, adjusting the PVA concentration to 0.55 % w/v, and keeping at 0.1 mg/ml the peptide amount (2.5_PLGA NP). Microfluidic parameters such as FRop, FRwp, FRR, and TFR were kept constant at 0.2 ml/min, 2 ml/min, 1:10 v/v, and 2.2 ml/min, respectively. After the nanoparticle's synthesis, the same purification steps described in Chapter IV, section 3.1.1 were applied.

To further investigate the *in vitro* cellular uptake of 2.5_PLGA NPs formulations, coumarin 6 (C6) fluorescently labeled nanoparticles were prepared as described above, by adding C6 100 μg/ml in the PLGA phase achieving a final C6 concentration in acetone of 6 μg/ml.

3.2.2 Physical characterization

The d_H, the PDI, and ζ potential were measured by dynamic light scattering using a Zetasizer Ultra instrument (Malvern Instruments Ltd., Worcestershire, United Kingdom) as described in Chapter IV, section 3.1.1.

3.2.3 Encapsulation Efficiency % and Drug Loading %

EE % and DL % were calculated after purification by applying a peptide extraction process. Briefly, a volume of 500 μl of nanoparticle suspension was centrifuged at 18,000 rcf at 4 °C for 30 minutes. 450 μl of supernatant was removed and replaced by 450 μl of acetonitrile, which allowed the nanoparticle system to be dissolved. The presence of a water residue allowed the precipitation of PLGA. Following centrifugation at 18,000 rcf, 4 °C, 15 min, the supernatant was analyzed by HPLC for peptide content by applying the method above described. DL (%) and EE (%) were determined as described in Chapter IV, in section 3.1.2.

3.2.4 Transmission Electron Microscopy

The surface morphology of LL37 loaded, WLBU2 loaded and blank PLGA nanoparticles was visualized via transmission electron microscopy (TEM) using a FEI Titan Themis 60-500 microscope (Thermo Fischer Scientific, Schwarte, Germany). NPs were prepared as described in Chapter IV, section 3.2.1 and 2 μL of each sample was placed on a copper grid and dried. The dried layer was then stained with 2 % w/v phosphotungstic acid and examined.

3.2.5 MTT cytotoxicity assay

The *in vitro* cell compatibility of LL37, WLBU2, the respective nanoparticles formulations and blank PLGA NPs was evaluated via MTT assay. In brief,

16HBEC14o^{-} and murine alveolar macrophages MHS cells were seeded in 96-well plates (10,000 and 5,000 cells per well, respectively) for 24 h. For 16HBEC14o- cells, Dulbecco's Modified Eagle Medium (DMEM) supplemented with 2 mM glutamine, 10 % fetal bovine serum (FBS Gibco, Life Technologies), and antibiotics as penicillin 100 U/ml and streptomycin 100 mg/ml was used. For murine alveolar macrophages MHS, RPMI-1640 supplemented with 2 mM glutamine, 10 % fetal bovine serum (FBS, Gibco, Life Technologies), 2-mercaptoethanol 50 mM, and antibiotics as penicillin 100 U/ml and streptomycin 100 mg/ml was used.

After 24 h attachment, peptides and nanoparticles diluted in RPMI-1640 or DMEM complete medium were added to the plate (100 µL per well) at different concentrations. Briefly, a preliminary screening of LL37 and WLBU2 cytotoxicity over 24 h and 72 h was carried out by testing peptides from 1.5 μg/ml to 75 μg/ml and 0.5 μg/ml to 32 μg/ml, respectively.

Formulations 5_PLGA NPs were tested at varying concentrations in the range of 0.1 – 2.5 μg/ml of LL37 or WLBU2 in nanoparticle's suspension for 24 h and 72 h, while formulation 2.5_PLGA NPs in the range of 0.1 – 5 μg/ml for 24 h. Control groups included cells treated with blank nanoparticles at equivalent concentrations to the treatment groups and untreated cells.

After 24 h or 72 h incubation based on the experiment, the medium was removed and replaced with MTT solution (0.5 mg/ml) in serum-free RPMI-1640 or DMEM and incubated for 3 h. Finally, the MTT solution was discarded, 100 µL per well of DMSO was added and incubated at room temperature for 30 min under mild shaking. The optical density was determined at 570 nm using a microplate reader (TECAN, Switzerland). Each experiment was performed in triplicate.

3.2.6 CCK-8 cytotoxicity assay

The viability of cells exposed to 2.5_PLGA NPs was additionally assessed through a second and practical colorimetric assay known as the Cell Counting Kit 8 (WST-8/CCK8). This method offers distinct advantages over MTT, primarily because it results in the generation of a water-soluble tetrazolium salt, unlike MTT. Viable cells metabolize these crystals, generating an orange formazan dye, whose absorbance

can be promptly measured. As for the MTT, the assay was carried out on human bronchial 16HBEC14o$^-$ cells and murine alveolar macrophage MHS cells. Briefly, 10 000 cells per well and 5 000 cells per well for 16HBEC14o$^-$ and MHS respectively were seeded in a 96-well cell culture plate. Then, after 24 h incubation at 37 °C in a humidified atmosphere with 5 % CO_2, the cell culture medium was replaced by a series of dilutions of peptides or nanoparticles in complete medium. Specifically, unprocessed peptides were tested in the range of concentration from 0.5 μg/ml to 15 μg/ml and each experiment was repeated in triplicate. Cells were then tested at varying concentrations in the range of 0.1 to 3.5 μg/ml of LL37 and WLBU2 in the PLGA nanoparticles suspension for 24 h. After 24 h treatment, 10 μL of the CCK-8 reagent (MedChemExpress Ltd.) was added to each well and the OD was measured at 450 nm with a microplate reader (TECAN, Switzerland). Control groups included cells treated with blank nanoparticles at equivalent concentrations as the treatment groups and untreated cells.

3.2.7 Cellular Uptake by Flow Cytometry

Since both the peptides and the PLGA polymer are non-fluorescent molecules, coumarin-6 was incorporated in the 2.5_PLGA NP as a fluorescent dye to study cellular uptake. Fluorescently labeled nanoparticles were prepared as described in Chapter IV, section 3.2.1. 16HBEC14o$^-$ and alveolar murine macrophage MHS cells were seeded (100 000 and 50 000 cells per well) in 24-well plates in triplicates and incubated 24 h at 37 °C with 5 % CO_2. The cells were treated with loaded nanoparticles to achieve an active concentration of 0.2 μg/ml corresponding to a nanoparticulate system concentration of 5 μg/ml. After 24 h, the cell medium was discarded, cells were trypsinized and washed with PBS twice. Cellular uptake was assessed using a flow cytometer (Attune NxT flow cytometer, Thermo Fisher Scientific, Waltham, MA, USA) with an excitation wavelength of 488 nm and fluorescence detection at 525 nm. A total of 10,000 gated events per sample were recorded [209].

4 Results and Discussion

4.1 Nanoprecipitation

PLGA NPs loaded with LL37, WLBU2, and hLF1-11 were prepared at different theoretical drug loading, expressed as the % w/w of peptide added in the beginning with regard of the total solid amount used. Specifically, PLGA concentration was kept constant at 5 mg/ml, while peptide initial concentrations were varied from 1.5 mg/ml to 0.5 mg/ml and 0.1 mg/ml, corresponding to a 20 %, 10 %, and 2 % w/w theoretical drug loading, respectively. Peptide solutions were added to the PLGA phase composed of 1 ml of acetone and dropwise poured into 10 ml of PVA 1.5 % w/v as the aqueous phase. Following the evaporation and the purification steps, particles were freeze-dried. Table 21 shows the yield of the nanoparticle production by nanoprecipitation.

Table 21. The yield of nanoparticle production prepared by nanoprecipitation after freeze-drying. Blank or empty NPs refers to the unloaded nanoparticles.

Theoretical peptide loading (% w/w)	**Yield (%)**		
	20	**10**	**2**
Empty PLGA NP		53.30 ± 2.54	
LL37_PLGA NP	67.17 ± 0.38	74.25 ± 3.51	67.77 ± 3.40
WLBU2_PLGA NP	54.81 ± 0.61	53.34 ± 6.70	-
hLF1-11_PLGA NP	55.61 ± 0.92	72.04 ± 3.80	61.80 ± 2.70

When considering LL37_PLGA NPs, it can be noted that the yield increased as the theoretical peptide loading changed from 2 % w/w to 10 % w/w and then decreased again with 20 % w/w. This increase in yield with higher initial peptide loading might be due to enhanced interactions between the peptide and PLGA, promoting nanoparticle formation. However, it's important to note that the yield started to decrease when the theoretical peptide loading exceeded a certain threshold (20 % w/w). This reduction in yield might be attributed to factors like polymer saturation or particles aggregation [196].

For WLBU2_PLGA NPs, the yield remained relatively stable and did not significantly change with varying theoretical peptide loading, while slight variations were observed

for hLF1-11_PLGA NPs. Like LL37_PLGA NP, a 10 % w/w theoretical peptide loading resulted in a higher yield (72.04 ± 3.80 %). However, it's worth noting that no significant correlation was observed regarding the theoretical loading and the yield of nanoparticle production.

4.1.1 Physical characterization

Particle size was assessed using dynamic light scattering (DLS) and the values were expressed as the average of the hydrodynamic diameter (d_H) of three independent measurements. DLS is a non-destructive technique based on the random Brownian motions of particles in the dispersing medium [210,211]. A laser beam illuminates the sample, and the fluctuations in light intensity resulting from the Brownian motion of the particles induce light scattering. These fluctuations are captured and quantified by a detector, employing an autocorrelation algorithm to determine the rate of intensity fluctuations and the scattering coefficient (D). Subsequently, the diffusion coefficient is transformed into a hydrodynamic diameter using the Stokes-Einstein equation as follows:

$$d_H = \frac{kT}{3\pi\eta D}$$

Under identical temperature conditions, small particles move faster, leading to rapid fluctuations in scattering intensity, whereas larger particles exhibit slower motion, resulting in comparatively minor changes in scattered light intensity [211,212].
The nanoparticles obtained by nanoprecipitation, whose characteristics are shown in Table 22 presented an average size of 200 nm, with PDI between 0.02 and 0.2 and a negative ζ potential of approximately -15 mV, with slight variation between the different peptides encapsulated in the nanoparticulate system. These results agree with previous published studies focusing on the development of polymeric PLGA nanoparticles for drug encapsulation, applying similar concentrations of PLGA (5 mg/ml) and the stabilizing agent PVA (1.5 % w/v) [91,120,209].

Table 22. Physical chemical properties of PLGA nanoparticles prepared by nanoprecipitation with different theoretical peptide loadings.

	Theoretical peptide loading (% w/w)	**d_H (nm)**	**PDI**	**ζ potential (mV)**
Empty PLGA NPs	-	164.63 ± 3.60	0.02 ± 0.01	-16.60 ± 0.48
LL37_PLGA NPs	20	258.40 ± 11.47	0.16 ± 0.03	-16.40 ± 6.08
	10	216.10 ± 5.97	0.09 ± 0.00	-18.78 ± 2.10
	2	206.10 ± 5.08	0.08 ± 0.01	-17.35 ± 1.23
WLBU2_PLGA NPs	20	212.63 ± 5.08	0.03 ± 0.03	-12.5 ± 2.50
	10	184.40 ± 6.58	0.05 ± 0.01	-15.78 ± 2.30
	2	-	-	-
hLF1-11_PLGA NPs	20	212.40 ± 3.90	0.28 ± 0.02	-17.33 ± 0.57
	10	226.87 ± 1.68	0.06 ± 0.03	-15.50 ± 1.90
	2	208.50 ± 3.40	0.13 ± 0.08	-11.92 ± 4.35

Higher theoretical peptide loadings tend to result in larger nanoparticles [200]. This trend was observed across all peptide formulations. For example, in the LL37_PLGA NPs, at a theoretical peptide loading of 20% w/w, the d_H was significantly higher (258.40 ± 11.47 nm) compared to when the loading was reduced to 2% w/w (206.10 ± 5.08 nm). A similar pattern was observed for WLBU2 and hLF1-11 peptides.

PDI values provide insight into the uniformity of nanoparticle size distribution. Interestingly, variations in theoretical peptide loading seemed to have minimal impact on PDI such as in the case of LL37_PLGA NPs. This suggests that altering peptide concentrations may not significantly affect the uniformity of nanoparticle size distribution. However, in other cases, such as hLF1-11_PLGA NPs, at a theoretical peptide loading of 20% w/w (PDI = 0.28 ± 0.02) a broader size distribution, indicating some degree of heterogeneity in particle size.

The surface charge of nanoparticles, as indicated by ζ potential, is crucial for nanoparticle stability and interactions with biological systems. This is an index of dispersion stability, and the measurement is based on the determination of the electrophoretic mobility of particles in an electric field following illumination of the sample by a laser beam [213]. The charged particles move towards the electrode of the opposite sign, thus creating a change in the scattering frequency of the sample proportional to the electrophoretic mobility. From this, by applying Henry's equation,

the ζ potential is calculated. A high value (*i.e.* - 30 mV and + 30 mV) causes the nanoparticles to stay away from each other, repelling each other enough to eliminate the possibility of agglomeration, aggregation, and/or flocculation [211].

Varying ζ potential values across different peptide-loaded nanoparticles were observed. For example, LL37_PLGA NPs exhibited ζ potential values around -16 mV, indicating negatively charged nanoparticles. hLF1-11_PLGA NPs showed ζ potential values from -17 mV to -11.92 mV, with some variability based on the theoretical peptide loading. The ζ potential values within this range suggest a moderately negative surface and they agree with previously reported values. Indeed, Mura et al. studied the influence of the surface charge of PVA/PLGA nanoparticles on toxicity effects on Calu-3 cells, and by using partially hydrolyzed PVA, they obtained nanoparticles with a size around 200 nm, narrow size distributions with PDI 0.1 - 0.2 and negative ζ potential [214].

Considering the influence of these properties on the applicability of NPs, here the designed particles should aim to facilitate the release of LL37, WLBU2, and hLF1-11 peptides precisely within the lung parenchyma, where the presence of *P. aeruginosa* can lead to progressive damage following airway colonization and infection [215]. This bacterial strain is a major contributor to morbidity and mortality among cystic fibrosis patients, whose compromised immune systems make them susceptible to such infections [216]. In these patients, the primary challenge for drug delivery lies in the nature of the mucus, which is dense and viscous. It acts as a selective barrier due to the porous matrix formed by mucins, featuring pores ranging from 300 to 400 nm [217]. Therefore, an ideal delivery system must have a size of less than 500 nm to navigate the gaps between mucins effectively while avoiding entrapment within the mucus layer. Additionally, as discussed in the introduction, the particles need to be small enough to evade immune system clearance and tissue accumulation, yet sufficiently large to prevent exhalation after administration [131,202].

4.1.2 Encapsulation Efficiency and Drug Loading

Encapsulating hydrophilic and amphiphilic molecules within PLGA nanoparticles poses a significant challenge due to the susceptibility of the drug to partition into the aqueous phase, which typically has a much larger volume than the organic phase. Therefore, achieving high EE % and DL % with antimicrobial peptides is critical [196,218]. Encapsulation efficiency quantifies the proportion of drug successfully encapsulated relative to the total drug amount used for encapsulation. Drug loading, also referred to as Actual Drug Loading to distinguish it from the theoretical loading described in the previous section, indicates the quantity of drug encapsulated compared to the total weight of the system (comprising both polymer and drug) used during the NPs preparation. In this work, the actual loading properties were investigated by extraction of the peptides from the lyophilized nanoparticles. Briefly, the freeze-dried nanoparticles were treated with acetonitrile to dissolve the polymer system and ultrapure water to induce polymer precipitation, which was completed by centrifugation. The supernatant was analyzed for encapsulated peptide by high-performance liquid chromatography using the analytical method indicated in Chapter IV, section 3.1.2. The results are shown in Table 23.

Table 23. Loading properties of PLGA nanoparticles prepared by nanoprecipitation with a different theoretical drug loading.

	Theoretical peptide loading (% w/w)	**DL (%)**	**EE (%)**
LL37_PLGA NPs	20	1.50 ± 0.40	7.38 ± 0.05
	10	2.17 ± 0.03	19.52 ± 0.03
	2	0.44 ± 0.03	23.70 ± 1.66
WLBU2_PLGA NPs	20	1.58 ± 0.04	6.99 ± 0.18
	10	1.82 ± 0.21	19.75 ± 2.30
	2	-	-
hLF1-11_PLGA NPs	20	0.01	0.06 ± 0.01
	10	0.02	0.28 ± 0.01
	2	0.02	1.16 ± 0.17

As the theoretical peptide loading increased from 2% w/w to 20% w/w, the actual drug loading (DL %) for LL37_PLGA NPs varied. At the lowest theoretical drug loading (2% w/w), DL % was 0.44 ± 0.03 %, but it substantially increased to 1.50 ± 0.40% at 20%

w/w. The EE % also showed a specific trend. At 2% w/w of theoretical drug loading, EE % was 23.70 ± 1.66 %, while at 20 % w/w, EE % decreased to 7.38 ± 0.05 %. In the case of WLBU2_PLGA NPs, a similar pattern was observed. Specifically, lower theoretical loading concentrations resulted in higher EE %. The highest EE % was observed at 10 % w/w, reaching 19.75 ± 2.30 %. These findings aligned with those reported by Casciaro et al., about the encapsulation of the peptide esculetin in PLGA nanoparticles [113]. The authors demonstrated that with a maximum drug loading of 2 % w/w, effective drug encapsulation can be reached [91,113]. However, it is crucial to recognize that this consideration may not be universally applicable to all molecules. Understanding the drug's properties and its affinity for the polymer is imperative when considering encapsulation strategies [196]. Indeed, unlike the other two peptides, after the nanoparticle's purification, hLF1-11_PLGA NPs exhibited very low drug loading and encapsulation efficiency across all theoretical peptide loadings tested. The DL % and EE % remained consistently low, with only slight variations. At the highest theoretical loading of 20 % w/w, DL % was 0.01 %, and EE % was 0.06 ± 0.01 %. These results demonstrated that the choice of peptide and its initial concentration have a critical impact on the actual drug loading and encapsulation efficiency in PLGA nanoparticles. The variations observed can be attributed to the physicochemical properties of the peptides and their interactions with the PLGA matrix [196,208]. Indeed, for LL37_PLGA NPs and WLBU2_PLGA NPs, higher initial peptide amounts led to increased actual drug loading, likely due to more peptides being incorporated into the nanoparticles. However, the corresponding decrease in encapsulation efficiency at higher peptide concentrations suggests that a saturation point was reached, limiting the amount of drug encapsulated effectively [196,208]. In contrast to the other two peptides, hLF1-11 (GRRRSVQWCAV) possesses a cysteine residue in its sequence, which promotes the formation of alternating disulfide bonds when in an aqueous solution. Additionally, it exhibits a predominant hydrophilic balance compared to a hydrophobic one. Hydrophilic molecules face challenges when it comes to encapsulation within PLGA nanoparticles due to their relatively lower affinity for the inherently hydrophobic polymer [219].

4.2 Microfluidic-assisted PLGA nanoparticles manufacturing

4.2.1 Physical characterization

A preliminary screening was carried out to prepare PLGA nanoparticles loaded with LL37 and WLBU2 with desired chemical-physical properties by means of a microfluidic technique. Based on the findings obtained with the nanoprecipitation process in terms of EE % and DL %, the nanoparticle formulation of hLF1-11 was not further optimized and investigated with microfluidic approach as the polymeric system was found to be unsuitable for its proper delivery. The results are presented in Table 24.

Table 24. Particle size, polydispersity index, and zeta potential of LL37_PLGA NPs, WLBU2_PLGA NPs, and empty PLGA NPs.

	LL37 PLGA NPs		
FRR	**d_H (nm)**	**PDI**	**ζ potential (mV)**
1:8	251.63 ± 9.56	0.11 ± 0.03	-6.47 ±0.76
1:10	251.17 ± 1.55	0.14 ± 0.02	-4.45 ± 0.48
1:16	222.47 ± 7.13	0.11 ± 0.02	-6.30 ± 0.25
	WLBU2 PLGA NPs		
FRR	**d_H (nm)**	**PDI**	**ζ potential (mV)**
1:8	230.00 ± 5.87	0.08 ± 0.03	-1.86 ± 0.51
1:10	223.77 ± 7.78	0.09 ± 0.02	-2.75 ± 0.47
1:16	208.43 ± 5.71	0.07 ± 1.12	-1.59 ± 1.12
	Empty PLGA NPs		
FRR	**d_H (nm)**	**PDI**	**ζ potential (mV)**
1:8	153.00 ± 0.01	0.10 ± 0.01	-30.20 ± 0.1
1:10	196.27 ± 4.89	0.16 ± 0.03	-27.30 ± 0.30
1:16	189.37 ± 3.65	0.08 ± 0.02	-30.54 ± 1.64

Briefly, the influence of microfluidic process parameters such as the FRR and the TFR on particle size expressed by the d_H, the size distribution expressed by the PDI, and surface charge described by the ζ potential was assessed. During this preliminary phase, the composition of the nanoparticle system was kept equal to that developed in the batch-to-batch nanoprecipitation process, *i.e.* 5 mg/ml of PLGA and 0.1 mg/ml of peptide composing the organic phase and PVA 1.5 % w/v in aqueous solution as the external phase. The different FFR tested were 1:8, 1:10, 1:16 ml/min for the polymer phase versus the aqueous phase, thus exploring TFR from 1.8 ml/min to 3.4 ml/min.

The LL37_PLGA NPs had an average size of 250 nm, with PDI 0.1 and weakly negative ζ potential, while the WLBU2_PLGA NPs had a size of 230 nm with PDI < 0.1 and near-neutral ζ potential. An increase in size was observed between the blank and loaded particles with a significant change in the surface charge from intense negative to almost neutral, while the PDI remained unchanged. The former phenomenon may be associated with the effective encapsulation of the peptide, which led to an increase in size, while the latter may always be a consequence of the peptide being partially arranged along the nanoparticle surface [116]. The combination of the small size of the particles, their high surface area, and the cationic surface of the peptides allow them to cover the surface of the nanoparticles, masking the negative effect of the carboxyl groups of PLGA, leading to a reduction in the intensity of the ζ potential compared to empty nanoparticles [205].

Behnke et al. observed that by increasing the flow rate, the average particle size decreases while the PDI increases [208]. Indeed, the faster the flow, the faster the mixing and this leads to an increase in Reynold's number, whereby the friction force due to viscosity becomes minimal compared to the inertia force [208]. This finding agreed with the values obtained for LL37 and WLBU2 nanoparticles. The reduction in size with increasing velocity was also in agreement with Wang et al. and Lababidi et al., who stated that this phenomenon is due to the use of high volumes of aqueous solvent that causes a reduction in polymer concentration resulting in smaller particles [220,221].

The formulations here presented were produced by varying the FRR while keeping constant the flow rate of the organic phase and increasing the flow rate of the aqueous phase. As demonstrated by D'Addio et al., these two variables play a crucial role in

determining the size of nanoparticles. Specifically, high flow rate of the aqueous phase results in a reduction in the average diameter of the nanoparticles, as mentioned before. This reduction is attributed to the decrease in polymer concentration due to dilution in the aqueous phase, leading to smaller particle sizes. Additionally, this alteration in flow rates contributes to a decrease in the growth rate of the forming nanoparticles [221–224].

Furthermore, it has been reported that increasing the flow rate of the aqueous phase reduces the propensity of particles to aggregate, resulting in a PDI of ≤ 0.1 due to the presence of a higher volume of the aqueous phase, as observed by Lababidi [221]. These findings align partially with the results obtained, as statistical analysis through ANOVA tests revealed no significant differences in formulations with respect to the PDI for both peptides. This was true for the various FRRs employed. Similarly, ANOVA analysis only revealed a weak significant difference for LL37_PLGA NP in terms of size and ζ potential, as depicted in Figure 52.

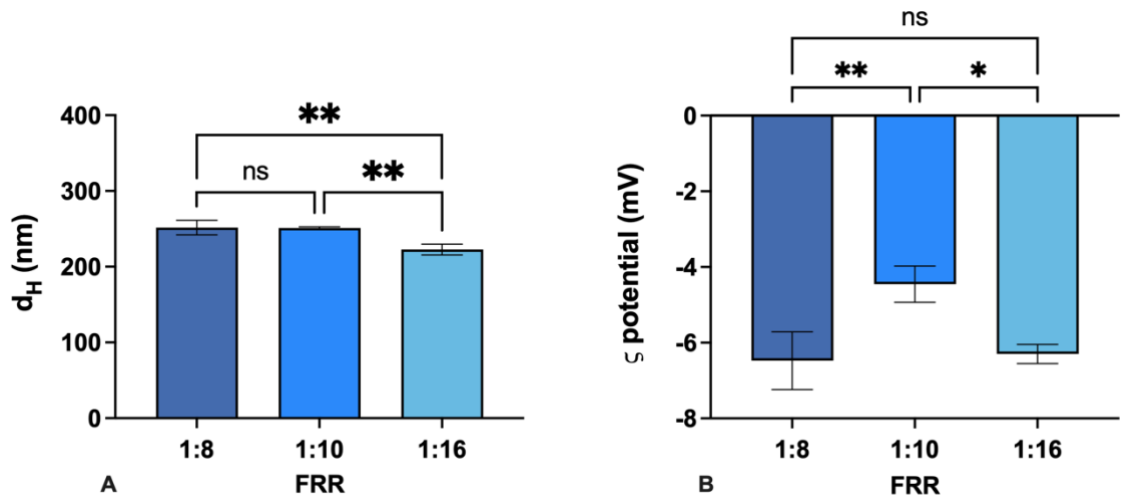

Figure 52. ANOVA analysis of formulation produced with different FRR investigating the influence on A) hydrodynamic diameter and B) ζ potential.

The preliminary study led to select formulations produced at FRR of 1:10, with FRop of 0.2 ml/min, FRwp of 2 ml/min and a TFR of 2.2 ml/min. Subsequently, the influence of PLGA, peptide, and stabilizer concentration on the nanoparticles' chemical-physical properties was evaluated. For this purpose, previously developed formulations consisting of 5 mg/ml PLGA, 0.1 mg/ml LL37 or WLBU2 and PVA 1.5 % w/v (5_PLGA NPs) were compared to formulations produced at half the concentration of PLGA (2.5 mg/ml), LL37 or WLBU2 0.1 mg/ml and PVA 0.55 % w/v (2.5_PLGA NPs). As will be

discussed in the following sections, optimization of the formulation was necessary to address the cytotoxicity observed with the 5_PLGA nanoparticles. C6 fluorescently labeled 2.5_PLGA NPs were also prepared by adding C6 to the organic solution for further investigation of nanoparticles' cellular uptake. Results comparing 2.5_PLGA NPs and 5_PLGA NPs in terms of their physical-chemical properties are shown in Figure 53.

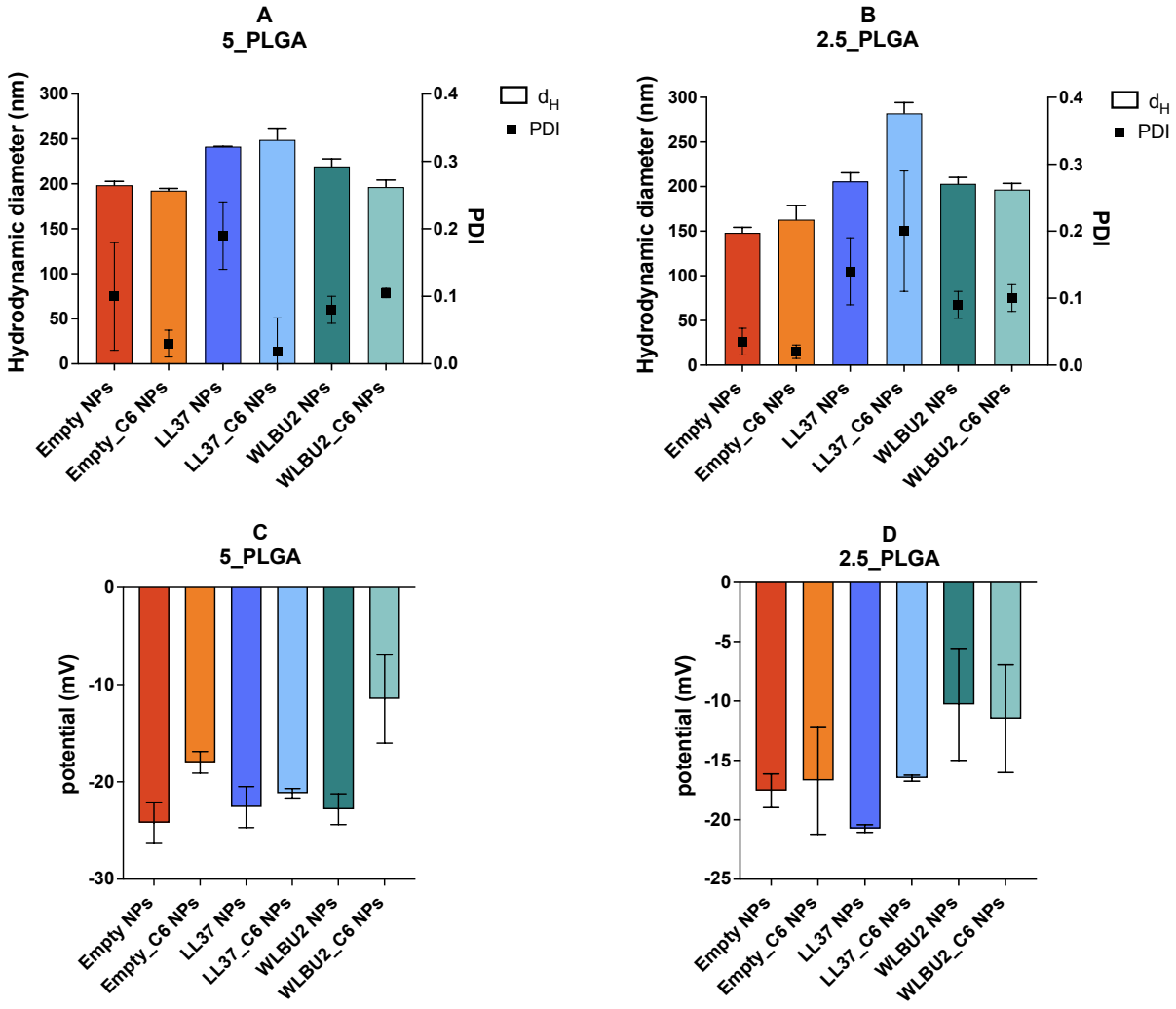

Figure 53. Physical-chemical characterization of PLGA nanoparticles formulation. A and C: hydrodynamic diameter and PDI average values for 5_PLGA nanoparticles; B and D: hydrodynamic diameter and PDI average values for 2.5_PLGA. Bars refer to d_H while points to the PDI.

Observing the bar graph referred to the hydrodynamic diameter In Figure 53 A and B, the reduction in polymer concentration was associated with smaller particle sizes

[203,208]. Indeed empty (or blank) 5_PLGA NPs presented an average size of 198 ± 4.27 nm, while at 2.5 mg/ml of PLGA the size decreased to 148 ± 6.08 nm. Similar trend can be described for WLBU2 nanoparticles where size changed from 219 ± 8.25 nm with 5 mg/ml PLGA to 203.16 ± 7.26 nm with half PLGA concentration. LL37 particles were found to be 241.6 ± 0.19 nm and 205.94 ± 9.54, for 5_PLGA NPs and 2.5_PLGA NPs, respectively. This was because of lower the PLGA concentration, the lower the viscosity of the feed solution so that the size is smaller [209]. The surface charge remained constant between the two formulations for both peptides, and no significant differences were observed when coumarin 6 was added to the organic phase.

The ζ potential (Figure 53 C and D) was negative with an average of -16 mV, an indication that peptides were not adsorbed on the particles surface and that carboxyl groups of PLGA were free [203,225,226]. It is possible to state that microfluidic in terms of size resulted in smaller particles than nanoprecipitation, in agreement with previous studies [203,224].

4.2.2 Encapsulation Efficiency and Drug Loading

During the preliminary study on 5_PLGA NPs, a maximum theoretical peptide loading of 2 % w/w was selected. The effect of different FRR applied by varying the flow of the aqueous phase was therefore evaluated concerning drug loading and encapsulation efficiency of the nanoparticles. The results obtained are presented in Table 25.

Regarding LL37, no significant differences were observed in terms of loading between the various FRRs applied (Figure 54 A), but relatively less loading was recorded when the ratio of the two flows was 1:16 with aqueous phase flow accelerated to 3.2 ml/min. Consequently, this resulted in an encapsulation efficiency of ~ 22 % compared to the ~ 33 % obtained with FRR 1:10 (Figure 54 B). For WLBU2, the differences between the formulations produced with different FRRs with respect to loading properties were also weakly significant (Figure 54 C and D) and the trend observed was like that described for LL37 with EE % values between ~ 42 % and ~ 47 % for FFR 1:10 and 1:8 respectively.

Table 25. Loading properties for LL37 PLGA nanoparticles and WLBU2 PLGA nanoparticles during the preliminary study for the assessment of the influence of FRR.

	LL37 NP	
FRR	**Drug Loading (%)**	**Encapsulation Efficiency (%)**
1:8	0.64 ± 0.76	24.86 ± 3.33
1:10	0.69 ± 0.04	33.13 ± 2.25
1:16	0.50 ± 0.04	22.62 ± 1.87
	WLBU2 NP	
FRR	**Drug Loading (%)**	**Encapsulation Efficiency (%)**
1:8	1.03 ± 0.12	47.96 ± 5.77
1:10	0.91 ± 0.05	42.97 ± 2.83
1:16	0.34 ± 0.06	15.91 ± 2.80

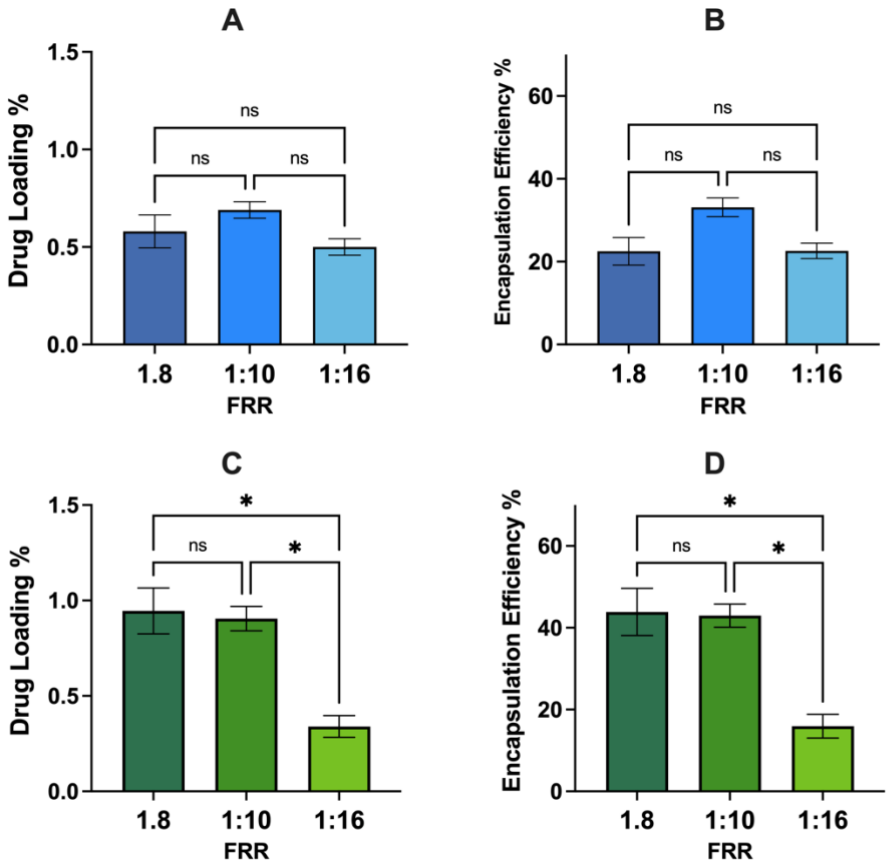

Figure 54. ANOVA Analysis of formulations produced during the preliminary study, *i.e.* 5_PLGA NP, investigating the influence of different FFR on drug loading % and encapsulation efficiency. A and B: LL37 nanoparticles; C and D: WLBU2 nanoparticles.

Li et al. conducted a more comprehensive examination of the impact of high FFR on encapsulation. In their research they utilized a mathematical model to illustrate that as FFR increases, it induces the formation of a central current within the channel, resulting in a slower mixing process. Consequently, with longer time intervals for mixing, the task of encapsulating molecules within PLGA nanoparticles becomes increasingly challenging [227].

Furthermore, an increase in size was observed for WLBU2_PLGA NPs in the presence of higher drug loading (FFR 1:8). This agreed with what observed by Govender et al. but could not be applied for LL37 [116].

The encapsulation efficiency exhibited variability between the two peptides, underlining the significance of the intrinsic properties of the molecules for which the delivery system is being developed.

PLGA is a highly hydrophobic polymer that tends to hydrolyze rapidly upon contact with water, depending on the ratio of glycolic to lactic acid. LL37 and WLBU2 on the other hand, are two amphipathic peptides whose structure makes them very different. WLBU2 has in its amino acid sequence the repetition of hydrophobic arginine and tryptophan [59,65]. From an antimicrobial activity point of view, these amino acids allow WLBU2 to structure itself into an amphipathic helix, enabling interaction with bacterial membranes; from the formulation point of view, they allow greater interaction with PLGA [31]. This implies increased encapsulation for WLBU2 compared to LL37 (37 aa) whose sequence is longer than WLBU2 (24 aa). LL37 is composed of several amino acids and the molecular weight is higher than the one of WLBU2 [65,114]. Specifically, the lower EE % for LL37 can be attributed to its greater hydrophilic character, compared to WLBU2, which allows the peptide to diffuse faster in the aqueous phase, reducing encapsulation in polymeric nanoparticles. Several examples in literature reported encapsulations of around 20 % for water-soluble compounds in PLGA nanoparticles [65,114,116]. In fact, encapsulating hydrophilic molecules in PLGA nanoparticles poses a challenge because of their weak affinity with the hydrophobic polymer. [219]. The different EE % and DL % with respect to the concentration of PLGA are graphically presented in Figure 55.

When the composition of the nanoparticle system was varied by halving the PLGA and PVA concentrations, keeping the peptide concentration constant at 0.1 mg/ml, an increase in drug loading was observed with an average of around 1 %, while the

encapsulation efficiency decreased from 30 % to 26 % for LL37 and from 47 % to 28-30 % for WLBU2 (Figure 55 B). This might be associated with the lower availability of PLGA and partly with the increase in theoretical peptide loading [208,221]. Indeed, Chiesa et al. noted that by increasing the polymer/drug ratio, drug loading notably changed. However, they observed EE % values greater than 25 % and around 37 - 45 %, in agreement with the results obtained in this study [224].

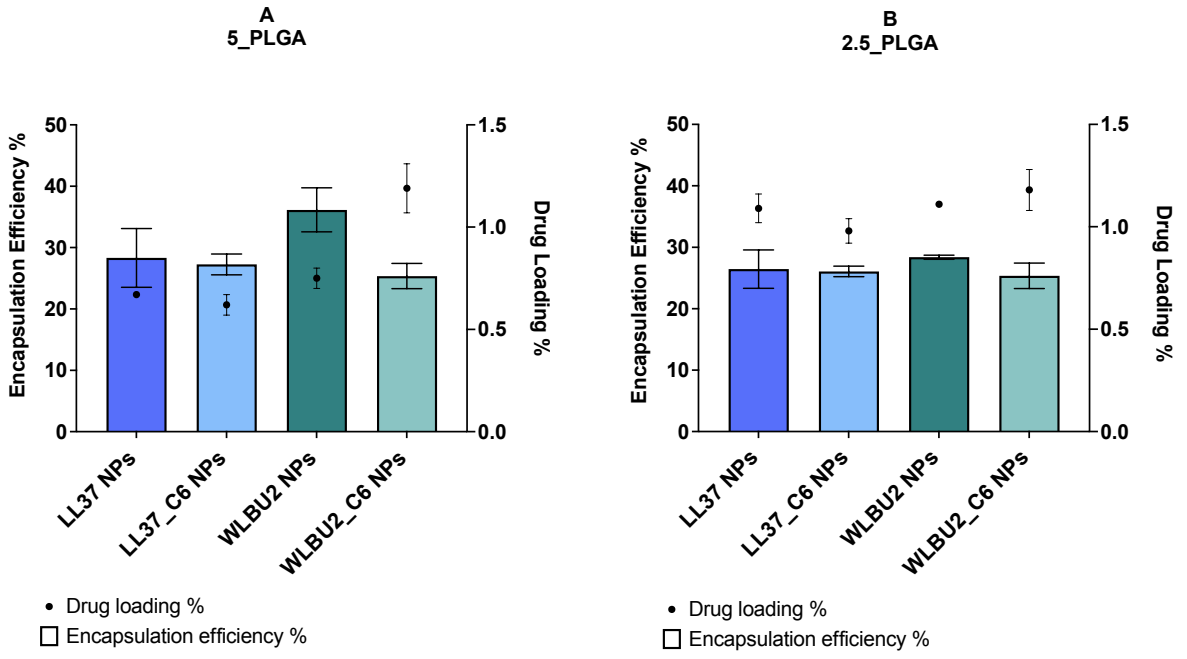

Figure 55. Encapsulation efficiency and drug loading for A. Formulation composed of 5 mg/ml PLGA, 0.1 mg/ml peptides, and 1.55 w/v PVA; B. Formulation composed of 2.5 mg/ml, 0.1 mg/ml peptides, and 0.55 w/v PVA. Bars refer to the EE %, while points to DL %.

Nanoprecipitation and microfluidics resulted in different encapsulations and drug loadings, whose values were certainly advantageous with the microfluidic procedure. Similarly, Vu H. et al. showed the superiority of microfluidics in the encapsulation of rutin in PLGA nanoparticles: this method was found to be suitable for the formation of small, homogeneous nanoparticles compared to those produced using the bulk technique, and above all an increase in encapsulation and loading was observed compared to the classical procedure [122].

4.2.3 Transmission Electron Microscopy

The morphology of the polymeric nanoparticles was observed by TEM using a FEI TITAN and images were acquired at 300 kV. The micrographs are presented in Figure 56. The nanoparticles were predominantly spherical, uniform in size and homogeneous, justifying the low PDI associated with the formulations. Their size was considerably smaller than 500 nm (around 200 nm), confirming what was observed in terms of Z-average. These results agree with previous studies presented by Streck et al. concerning the encapsulation of rutin in polymeric nanoparticles [54, 55] Again, the nanoparticles were spherical in shape without significant differences between loaded and unloaded nanoparticles, as was the case with WLBU2 and LL37 in this study.

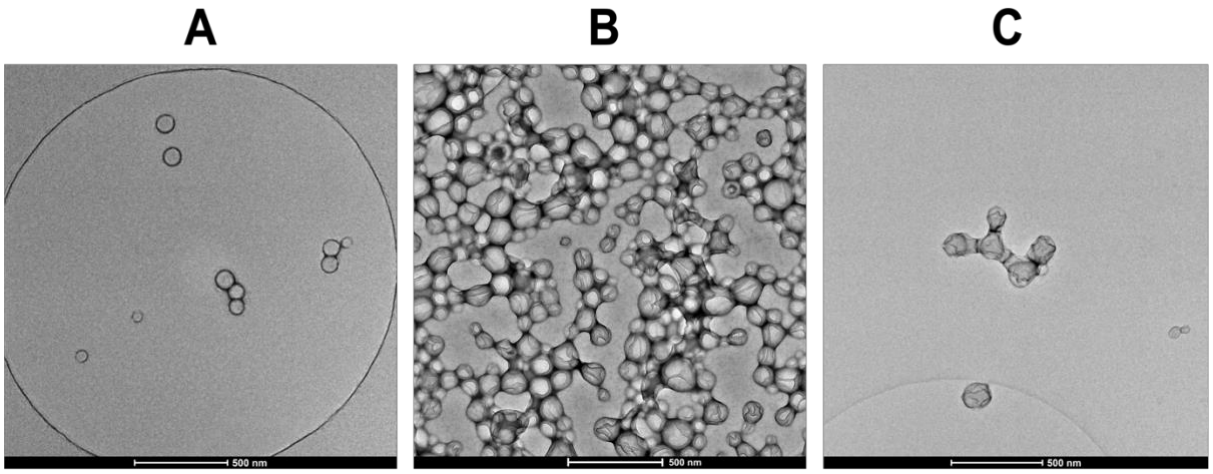

Figure 56. Spherical morphology of empty PLGA nanoparticles (A), WLBU2 nanoparticles (B) and LL37 nanoparticles (C) produced by microfluidic with a PLGA concentration of 5 mg/ml, 0.1 mg/ml peptide, and 0.55 % w/v PVA. FRR 1:10, FRop 0.2 ml/min, FRwp 2 ml/min.

4.2.4 MTT cytotoxicity assay

The cytotoxicity profiles of LL37, WLBU2, and their nanoparticulate formulations (5_PLGA and 2.5_PLGA) were determined by means of an MTT colorimetric assay on two cell lines, the human bronchial 16HBE14o- and the murine alveolar macrophage MHS. The 16HBE14o- cells are immortalized human bronchial epithelial cells that exhibit a slight differentiation capacity compared to BEAS 2B [83]. On the

other hand, murine alveolar macrophage MHS cell line is the model often used to evaluate the interaction between pathogens and macrophages, which represent a fundamental element for specific and non-specific immunity [228]. It is important that macrophages are healthy so that cytotoxicity and uptake of inhaled nanoparticles can be assessed [229]. The 3-(4,5-dimethylthiazol-2-yl)-2,5-diphenyl-2H-tetrazolium bromide (MTT) is a colorimetric assay developed by Mosmann et al. in 1983. It is based on the activity of certain enzymes expressed by viable cells, such as NAD(P)H-dependent cellular oxidoreductases, which can metabolize MTT into insoluble formazan crystals subsequently solubilized in DMSO. Dead cells no longer possess the capability to transform tetrazolium salts into colored formazan compounds. On the other hand, viable cells, which have an active metabolism, convert MTT into a purple formazan product with a peak absorbance at approximately 570 nm. Consequently, the intensity of this colored product directly correlates with the quantity of viable cells within the culture [230,231]. A schematic representation of MTT is shown in Figure 57.

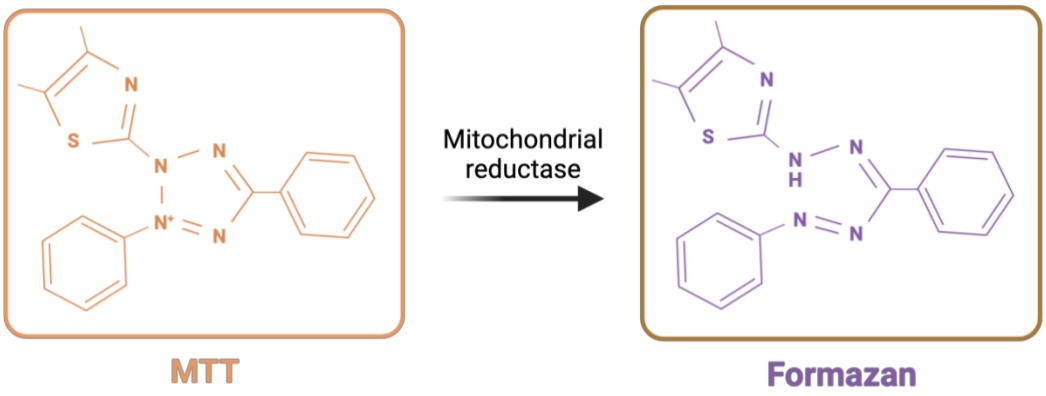

Figure 57. MTT assay was performed to investigate cell viability exposed to PLGA nanoparticle formulations (created with BioRender.com).

Peptides dissolved in medium were added to the wells according to the procedure described in Chapter IV, section 3.2.5. A range of concentrations from 1.5 μg/ml up to 75 μg/ml for LL37 and from 0.5 μg/ml to 32 μg/ml for WLBU2 was tested on both cell models. The results are presented in Figure 58 and Figure 59 as mean ± standard deviation of the percentage of live cells compared to the untreated control. Each experiment was performed at least in duplicate.

The cells were sensitive to treatment in different ways depending on the peptide and duration of treatment. LL37 did not induce significant cytotoxicity on 16HBE14o- bronchial cells 72 h after treatment, but inhibited cell growth by approximately 20 % from the lowest concentration tested (1.5 μg/ml) after 24 h of treatment. In spite of this, the concentration capable of inducing 50 % growth inhibition, *i.e.* IC_{50} was higher than the highest concentration tested, both at 24 h and at 72 h, and thus enabled the safety profile of this peptide to be affirmed (Figure 58 A). On the same cell line, WLBU2 showed some differences (Figure 59 A). After a 24-hour treatment, WLBU2 induced the inhibition of 16HBE14o- proliferation by approximately 50 % at 32 μg/ml, such that the IC_{50} obtained was approximately 28 μg/ml. Nevertheless, this IC_{50} was significantly higher than the EC_{50} required to inhibit the growth of *Pseudomonas* bacterial strains. After 72 h, the inhibition profile was not altered by the presence of the peptide, with IC_{50} > 100 μg/ml.

The MHS macrophage cell line was more sensitive to treatment with both peptides, especially after 24 h. For LL37 at 6 μg/ml the inhibitory effect was approximately 40 %, resulting in an IC_{50} of 6.5 μg/ml after 24 h and 30 μg/ml after 72 h (Figure 58 B). Similarly, the IC_{50} for WLBU2 towards MHS after 24 h IC_{50} was 12 μg/ml and 20 μg/ml after 72 h (Figure 59 B).

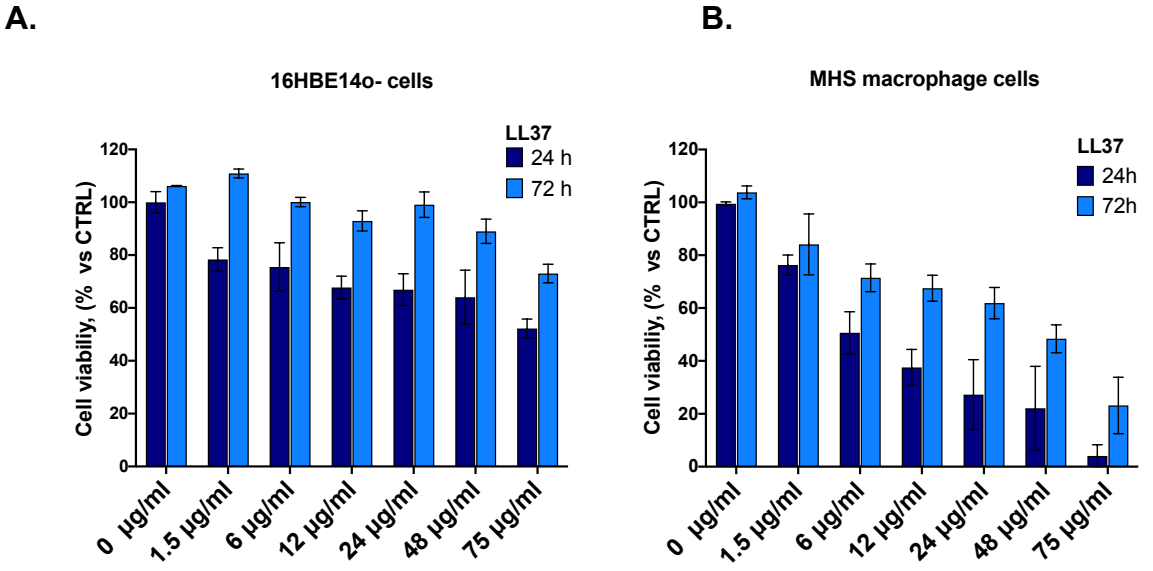

Figure 58. Viability (MTT) of 16HBE14O- (A) and MHS macrophages (B) cells after 24 h and 72 h exposed to LL37 peptide.

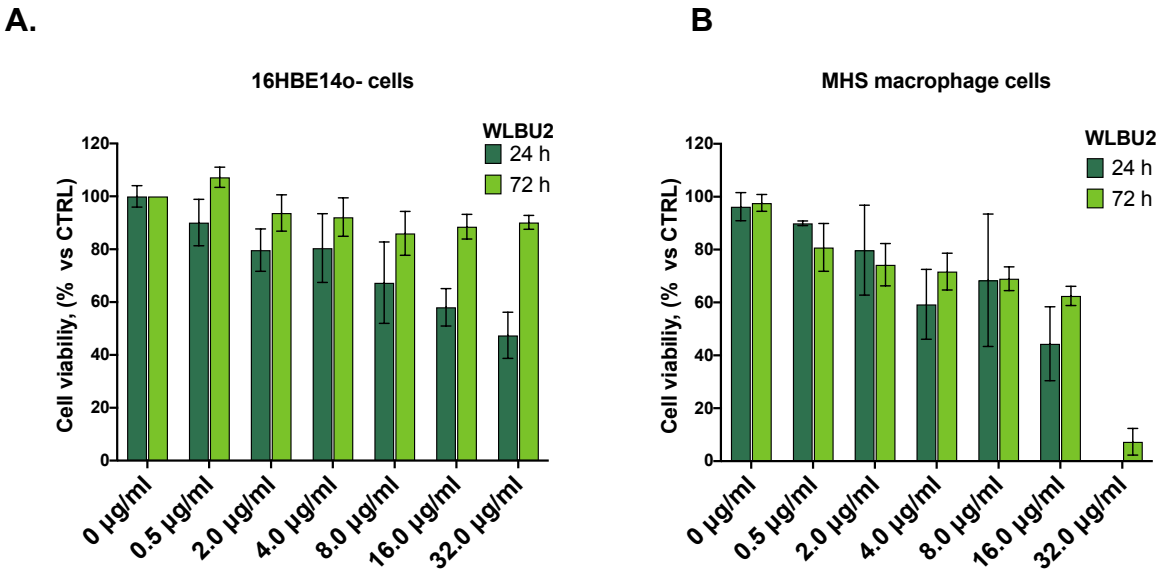

Figure 59. Viability (MTT) of 16HBE14O- (A) and MHS macrophages (B) cells after 24 h and 72 h exposed to WLBU2 peptide.

The cytotoxic effect of the nanoparticle systems unloaded and loaded with LL37 or WLBU2 was evaluated similarly to what was performed with raw material peptides. Initially, the formulations consisting of 5 mg/ml PLGA, 0.1 mg/ml peptide, and 1.5 % w/v PVA were tested. The results are shown in Figure 60, which clearly shows the significant sensitivity of the two cell lines when treated with LL37 and WLBU2 nanoparticles over time. Specifically, the inhibition profile was investigated following treatment for 24 h and 72 h. 16HBE14o^{-} cells were significantly sensitive and distressed following exposure to both systems after 24 h and 72 h of treatment. The reduction in cell viability was observed from the first tested concentration (0.16 μg/ml) of peptide within the system, with $IC_{50,24h\text{-}LL37NP}$ = 0.036 (0.022 – 0.196) μg/ml, $IC_{50,72h,LL37NP}$ = 0.139 (0.088 – 0.190) μg/ml, $IC_{50,\ 24h\text{-}WLBU2NP}$ = 0.03 μg/ml e $IC_{50,72h\text{-}WLBU2NP}$ = 0.016 μg/ml, for LL37 NPs and WLBU2 NPs, respectively (Figure 60 A and C). The administration of 0.16 μg/ml of encapsulated peptide corresponded to an unloaded system concentration of 15 μg/ml which is associated with zero inhibition of cell proliferation ($IC_{50,24h\text{-}emptyNP}$ = 61.35 μg/ml) and a pro-proliferative effect after 72 h of treatment from 54 μg/ml (Figure 60 E). The increase in viability observed can be explained by considering a non-specific response caused by a rapid and transient activation of cell metabolism [214]. However further investigations are required.

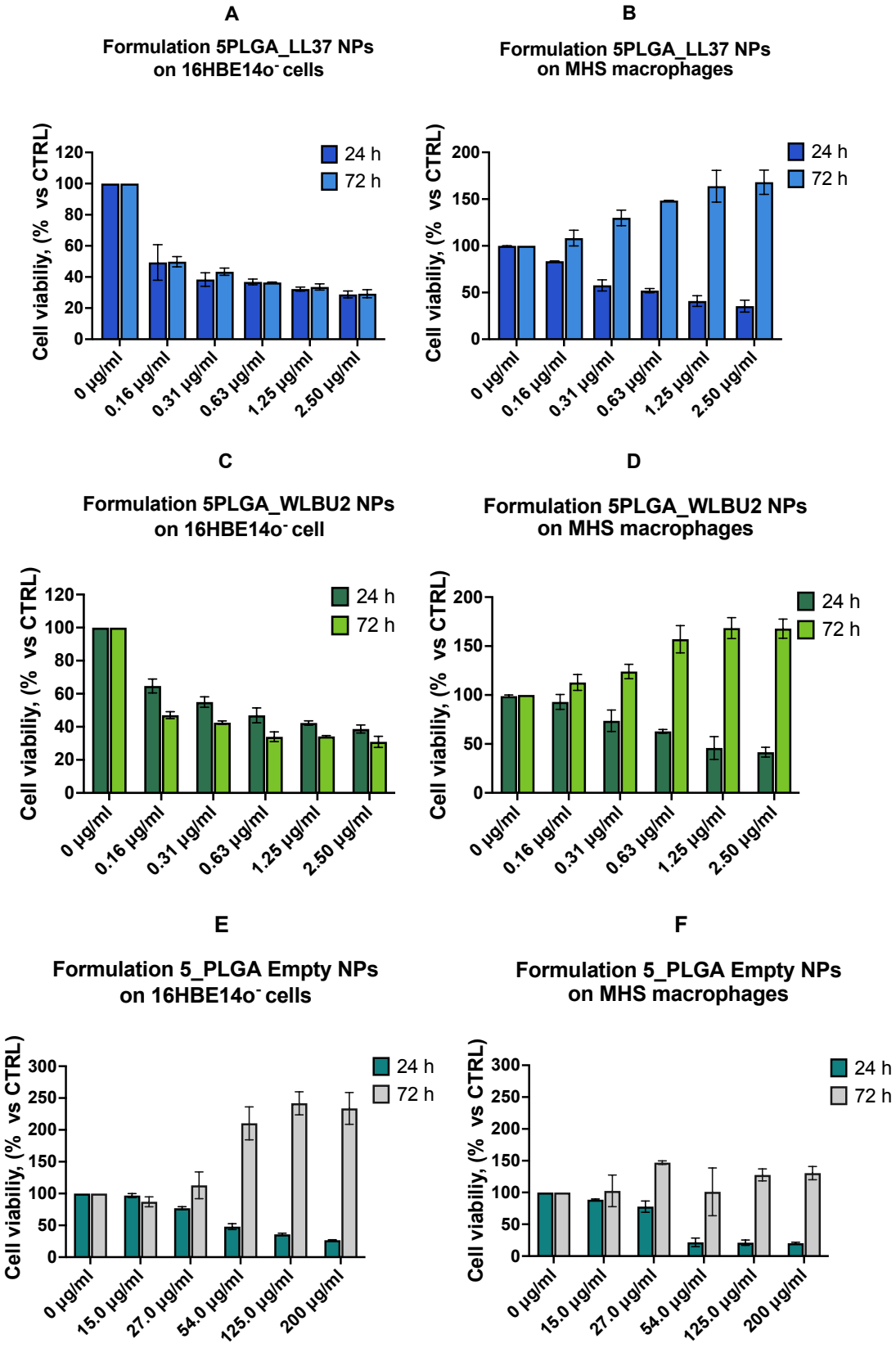

Figure 60. MTT results after 24 h and 72 h exposure of 16HBE14o- cells and MHS macrophages. A, B) LL37_PLGA NPs; C, D) WLBU2_PLGA NPs; E, F) empty or blank NPs. Data are expressed as the mean± standard deviation of at least two independent experiments.

The behavior was different regarding macrophages, which responded oppositely to treatments after 24 h and 72 h. Unloaded nanoparticles presented the same profile observed on 16HBE14o$^-$, with a pro-proliferative effect after 72 h of treatment ($IC_{50,24h\text{-}emptyNP}$ = 35μg/ml, $IC_{50,72h\text{-}emptyNP}$ > 250μg/ml). The cytotoxic effect of LL37 NP and WLBU2 NP systems was less intense for macrophages than for bronchial cells, contrary to what had been observed with pure peptides. For LL37 an $IC_{50,24h\text{-}LL37NP}$ = 0.20 μg/ml and $IC_{50,72h\text{-}LL37NP}$ > 0.32 μg/ml, while for WLBU2 $IC_{50,24h\text{-}WLBU2NP}$ = 0.39 μg/ml and $IC_{50,72h\text{-}WLBU2NP}$ > 0.34 μg/ml were observed (Figure 60 B and D).

The cytotoxicity of the nanoparticle systems observed posed the need to modify the formulation, halving the concentration of PLGA and PVA present in the particle system, while maintaining the peptide concentration at 0.1 mg/ml.

Cells exposed to a 24 h treatment were less sensitive, with differences between bronchial cells and macrophage cells. Specifically, unloaded nanoparticles guaranteed 80 % cell viability for macrophages, but again a 40 % inhibition of proliferation was observed from 12.5 μg/ml (0.5 μg/ml peptides) on bronchial cells (Figure 61 C). A similar scenario for the formulated peptides, where the change in system composition resulted in an unpromising inhibition profile on 16HBE14o- with 60 % inhibition of cell viability at 0.5 μg/ml. This effect was evident for LL37 PLGA NPs (Figure 61 A), a peptide that had shown an IC_{50} above 75 μg/ml when tested in its unprocessed form. In the case of WLBU2, an improved profile was evident; however, a notable 40% reduction in cell growth when exposed to a concentration of 0.8 μg/ml was observed (Figure 61 A). Macrophage cells showed greater resistance to treatment with 70 % cell viability at 0.8 μg/ml for both peptides (Figure 61 B).

Since bronchial cells represent the first filter and element encountered by any inhaled product, the result thus obtained must be carefully considered. The factors determined the results are various and may concern both the nanoparticle system and the type of assay applied. MTT-induced toxicity can not be ruled out. Indeed, the MTT reagent salt (3-(4,5-dimethylthiazol-2-yl)-2,5-diphenyl-2H-tetrazolium bromide) is reported to form formazan crystals that are extremely insoluble in water, and this represents a limitation as formazan often forms deposits that can damage cells, creating artifacts in the determination of cell viability [232,233]. This implies that a solvent must be used to dissolve these crystals before reading. Such a solvent is DMSO, which in turn can have a toxic effect on cells [234]

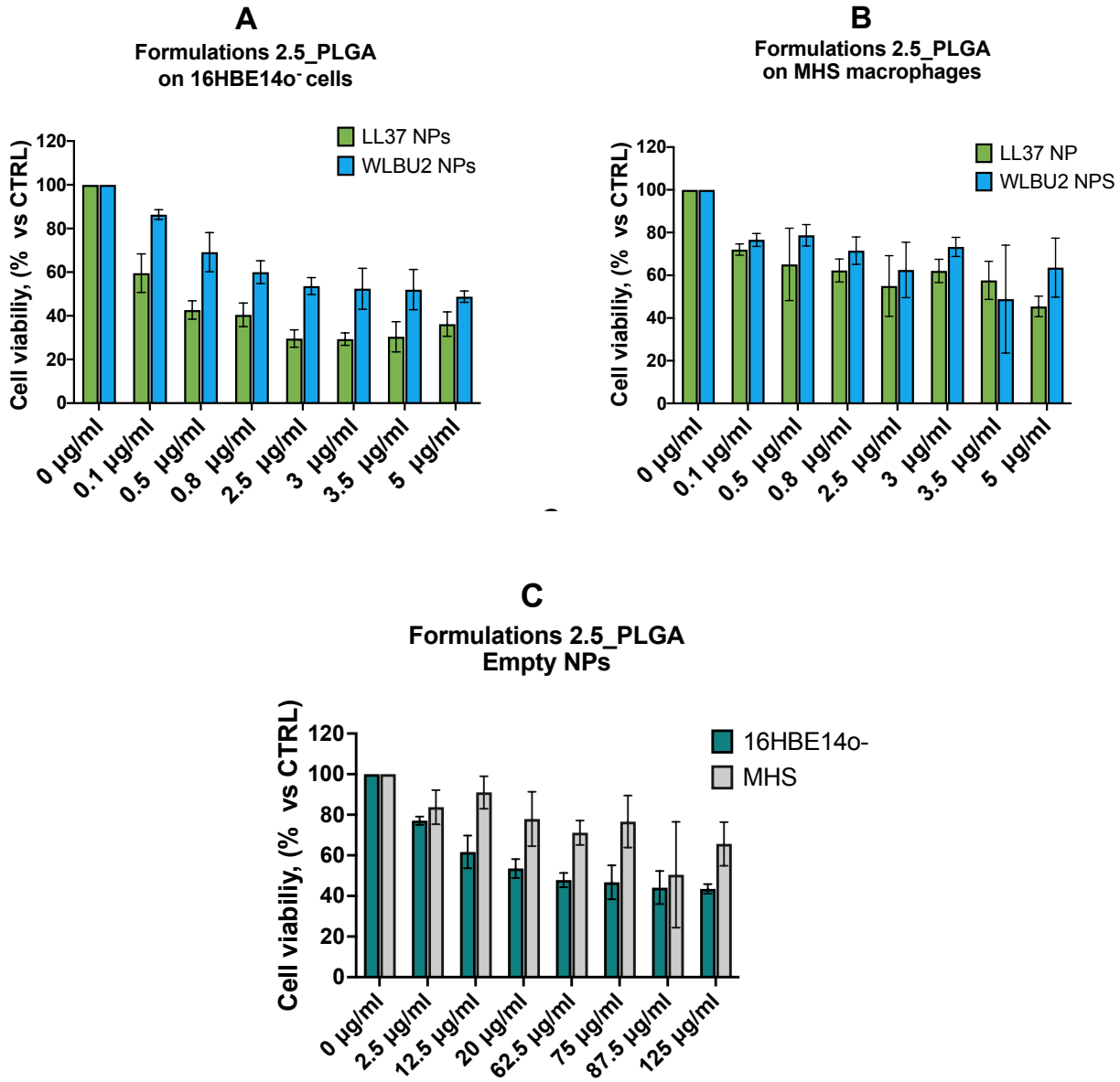

Figure 61. MTT assay results for formulations composed by 2.5 mg/ml PLGA, 0.1 mg/ml peptides, and 0.55 % w/v PVA. Data are presented as mean ± standard deviation of at least two independent experiments. A. Peptides formulations on 16HBE14o- cell line; B. Peptides formulation on MHS alveolar macrophage cell line.

4.2.5 CCK-8 cytotoxicity assay

Cell Counting Kit-8 (CCK-8) allows very convenient assays by utilizing highly water-soluble tetrazolium salt. WST-8 [2-(2-methoxy-4-nitrophenyl)-3-(4-nitrophenyl)-5-(2,4-disulfophenyl)-2H-tetrazolium, monosodium salt] produces a water-soluble formazan dye upon reduction in the presence of an electron mediator, as shown in Figure 62.

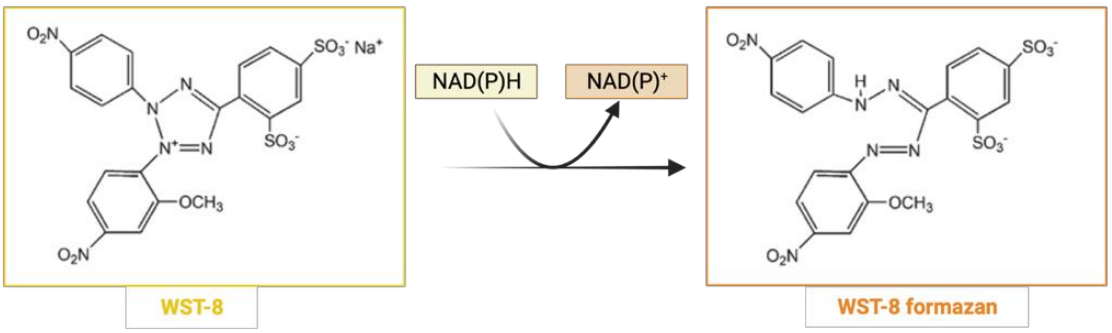

Figure 62. CCK-8 assay (created with BioRender.com).

The detection sensitivity using CCK-8 is higher than assays using other tetrazolium salts such as MTT [235]. The main advantage of the CCK-8 assay is a consequence of the formation of water-soluble formazan crystals, which do not accumulate inside the cells and do not require solubilization with aggressive solvents. As with MTT, the absorption at 460 nm is proportional to the number of live cells and the longer the incubation time, the greater the production of WST-8 formazan [232].

CCK-8 results are presented in Figure 63 and Figure 64. As can be seen, in contrast to what was observed for MTT, both peptides and formulations consisting of 2.5 mg/ml PLGA, 0.1 mg/ml peptides and 0.55 % w/v PVA were not cytotoxic for either cell models with over 99 % of viable cells.

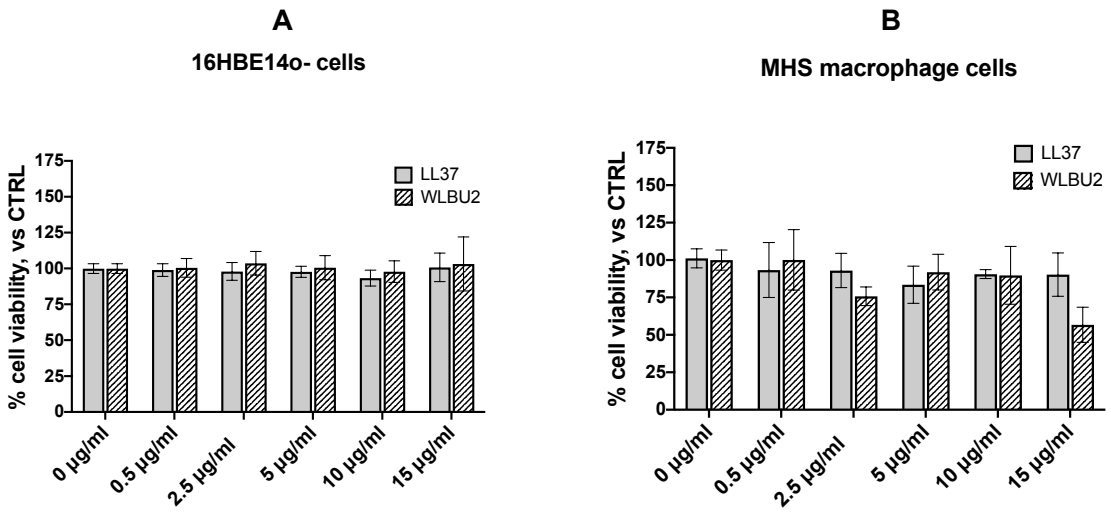

Figure 63. CCK – 8 assay results for LL37 and WLBU2 peptides on 16HBE14o- (A) and MHS macrophage (B) cell lines.

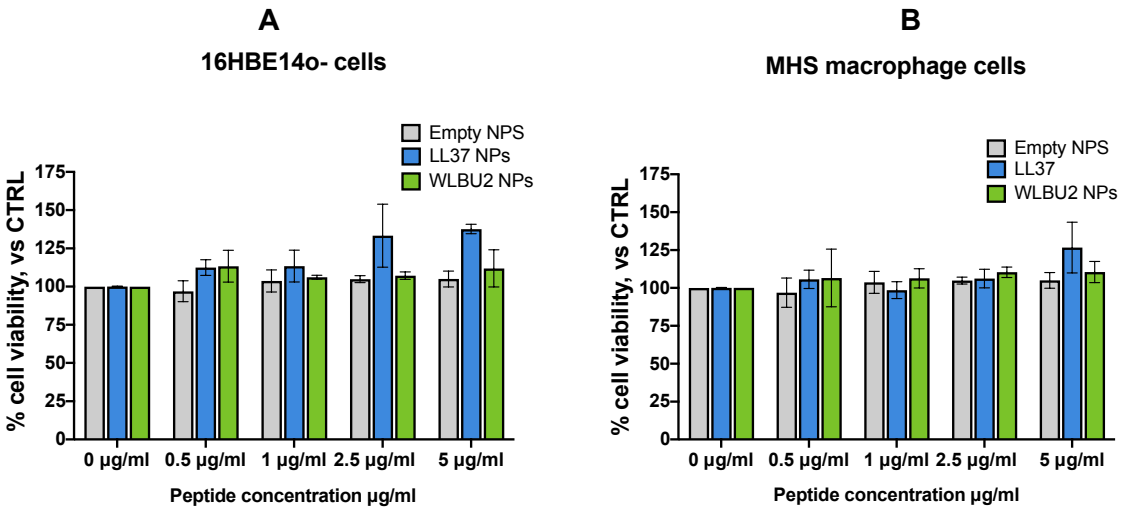

Figure 64. CCK – 8 assay results for peptide loaded and empty PLGA nanoparticles. Data are presented as mean ± standard deviation of at least two independent experiments.

The differential results observed between the MTT assay and the CCK-8 assay in evaluating the cytotoxicity of nanoparticles can be attributed to the specific mechanisms and sensitivities of each method.

The MTT (3-(4,5-dimethylthiazol-2-yl)-2,5-diphenyltetrazolium bromide) assay measures cytotoxicity by assessing the metabolic activity of cells. In this assay, MTT is converted into a purple formazan product by mitochondrial dehydrogenases in metabolically active cells. A decrease in formazan production indicates decreased cell viability [231,234]. The Cell Counting Kit-8 (CCK-8) assay also evaluates cell viability based on metabolic activity. It uses a water-soluble tetrazolium salt (WST-8) that is converted into a water-soluble formazan dye in the presence of cellular dehydrogenases. The absorbance of this dye is proportional to the number of viable cells [235]. The sensitivity of these two is quite different. Specifically, the CCK-8 assay is a more recent modification of the MTT assay, highly sensitive, designed to overcome some of the limitations of the MTT assay, such as solubility issues and the need for DMSO (dimethyl sulfoxide) to dissolve formazan crystals. CCK-8 offers the advantage of being a water-soluble reagent, making it more user-friendly [234,236].

The possible explanations for what happen when cells are treated with both nanoparticle peptide systems and MTT or CCK-8 are different and yet unresolved. The nanoparticles may interfere with the MTT assay reagent or alter mitochondrial function, leading to a decrease in the production of formazan products. This interference could

be specific to the MTT assay's chemical reaction [237]. Since the unprocessed peptides showed no antiproliferative effects, it is challenging to find an explanation for this phenomenon. One fact to consider could be the change in the pH of the medium following treatment with PLGA – peptides loaded nanoparticles towards values that are too acidic for the viability of the cells [238].

On the other side, the CCK-8 assay might be less susceptible to interference from the nanoparticles or more resilient to changes in cellular metabolism. It is possible that the nanoparticles have a minimal impact on the specific reaction involved in the CCK-8 assay.

Some nanoparticles or substances might affect one assay more than the other due to the differences in their chemical reactions and reagent requirements. As consequence, the observed difference in cytotoxicity results between the MTT and CCK-8 assays might be due to the specific sensitivities and mechanisms of these assays, as well as the potential interactions between the nanoparticles and the reagents [236]. This study is not the first to show an antiproliferative effect of polymeric nanoparticles following MTT. Chiu et al and Ibrahim et al. reported increased cytotoxicity when a ligand that increases cellular uptake is present and showed that PLGA nanoparticles can exhibit a time-dependent antiproliferative effect from 3 h up to a maximum of 240 h [236,237].

4.2.6 Cellular uptake by Flow Cytometry

Internalization by human bronchial 16HBE14o- cell line and murine alveolar macrophage MHS cells was studied quantitatively using flow cytometry. The nanoparticles were labeled with coumarin-6 dye and the cells were treated for 24 h with 0.2 μg/ml concentration of peptide in the nanoparticle suspension. The fluorescence-activated cell sorting (FACS) analysis shown in Figure 65 indicates the proportion of fluorescently labeled cells compared to the control, represented by untreated cells. This value, expressed as median fluorescence intensity, indicates the internalization of nanoparticle systems by the cells.

A positive association is denoted for both cell lines, *i.e.* the proposed formulations (2.5PLGA_LL37_C6, 2.5PLGA_WLBU2_C6, and 2.5PLGA_C6) were internalized

during a 24 h incubation with some differences among loaded and unloaded nanoparticles.

As can be seen from the fluorescence graph, for both cell models, the unloaded nanoparticles were partially internalized. This might be attributed to the absence of the peptide, which could have potentially arranged itself on the nanoparticle's surface, thereby enhancing cellular penetration [239]. This could only be a hypothesis since if this were the case, a variation of the zeta potential should also have been observed by virtue of the positive charges exposed by the peptides, whereas between loaded and unloaded the potential is similar, with an average of -18 ± 0.11 nm, -21.17 ± 0.49, and -11.48 ± 4 nm for 2.5PLGA_C6, 2.5PLGA_LL37_C6, 2.5PLGA_WLBU2_C6, respectively [214].

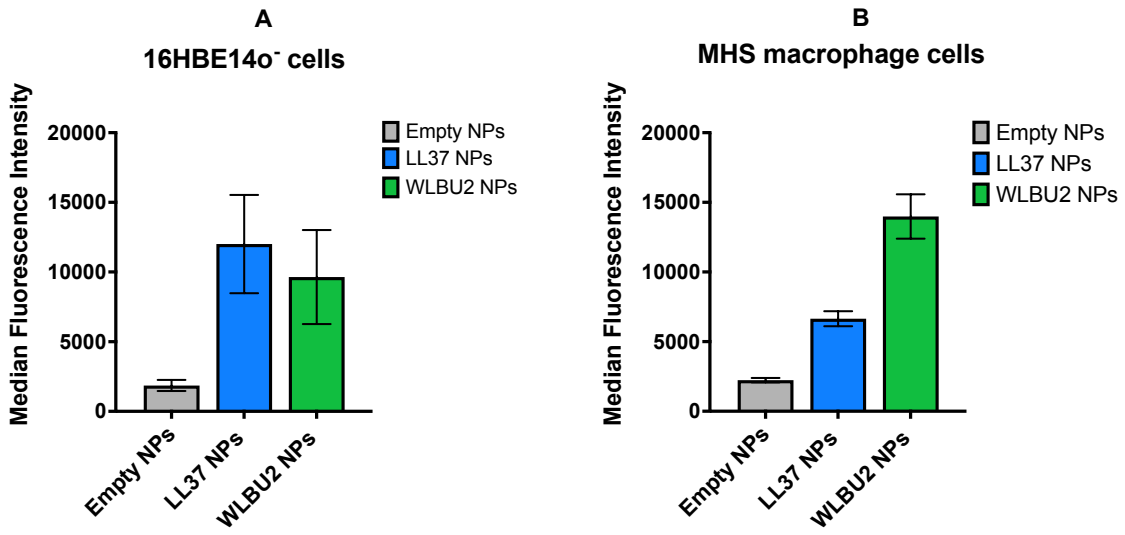

Figure 65. Cellular uptake of Empty PLGA NP, LL37 PLGA NPs, WLBU2 PLGA NPs composed by 2.5 mg/ml PLGA, 0.1 mg/ml peptides, 0.55 % w/v PVA and labeled with coumarin-6 dye (6 μg/ml) in A. 16HBE14o- cell line and B. MHS murine alveolar macrophage cell line. Data are presented as mean ± standard deviation of two independent experiments.

5 Conclusions

The encapsulation of pharmaceutical molecules within nanoparticle systems offers an innovative approach to address challenges associated with poorly soluble drugs, enzymatic degradation, and controlled drug delivery [240]. This chapter explores the preparation of polymeric nanoparticles through both bulk procedures and microfluidic techniques. One of the earliest and widely employed techniques for nanoparticle production is nanoprecipitation or solvent displacement, which involves the controlled mixing of a polymer solution with an anti-solvent [190]. Several key factors influence the characteristics of PLGA nanoparticles produced through nanoprecipitation, including the choice of solvent and non-solvent, mixing technique, and environmental conditions [120]. These variables collectively determine critical attributes such as nanoparticle size, shape, drug encapsulation efficiency, and release behavior. Managing these factors is essential for tailoring PLGA nanoparticle formulations to specific therapeutic needs. The polymer concentration used in the encapsulation process is an initial consideration, as it affects the organic phase's viscosity. Excessive viscosity can hinder proper polymer diffusion within the non-solvent, resulting in larger particle sizes [115]. Stabilizing materials have been employed to address this issue, with varying degrees of success. Among them, PVA is one of the most used stabilizers, but it can exhibit mucoadhesive properties that affect pulmonary drug delivery [197].
In this study, PLGA nanoparticles loaded with LL37, WLBU2, and hLF1-11 were prepared at different theoretical drug loading concentrations. The choice of peptide and its loading concentration exerted varying effects on nanoparticle size (200 nm), encapsulation efficiency (mid-low based on the theoretical loading), drug loading, and zeta potential. These findings emphasize the importance of tailoring encapsulation strategies to the specific properties of the drug and the intended therapeutic application.
Although batch to batch methods are versatile for preparing polymeric nanoparticles, they have limitations related to bulk variability and the need to increase polymer concentration to achieve suitable drug loading. In contrast, microfluidic techniques offer greater control over nanoparticle production, reduced mechanical stress on active molecules, and improved phase mixing efficiency, resulting in more consistent and desirable particle characteristics [122].

For the microfluidic-assisted nanoparticles preparation, parameters such as flow rate ratios, total flow rates, and nanoparticulate system composition, were investigated on size, size distribution, surface charge, drug loading, and encapsulation efficiency. The results demonstrated that these parameters play a crucial role in determining particle size and distribution. Additionally, the choice of peptide, such as LL37 or WLBU2, influenced loading and encapsulation efficiency due to differences in molecular properties.

Furthermore, the chapter discussed the cytotoxicity of both unprocessed peptides and their nanoparticulate formulations on two cell lines, human bronchial epithelial 16HBE14o- cells and murine alveolar macrophages MHS cells. The findings revealed varying sensitivities to the treatments, with some concentration-dependent effects. The differences observed between the MTT and CCK-8 assays in assessing cytotoxicity highlighted the importance of selecting the appropriate assay method for evaluating nanoparticle toxicity [233,234].

Finally, the study examined the internalization of labeled nanoparticles by the cell lines, demonstrating that both loaded and unloaded nanoparticles were internalized to some extent, suggesting the potential for cellular uptake of the nanoparticle systems.

Overall, this chapter contributes valuable insights into the preparation and characterization of polymer nanoparticles and provides data regarding their cytotoxicity and internalization, which are crucial factors in the development of effective drug delivery systems. Further research and optimization are needed to fully harness the potential of these nanoparticle formulations reducing the cytotoxicity effects observed.

Chapter V

Conclusions and future perspectives

1 Dry Powders for AMPs delivery to the lungs

The misuse and overuse of antibiotics exacerbate antimicrobial resistance (AMR), primarily affecting individuals with chronic diseases, leading to difficulties in treating conditions like cystic fibrosis and pneumonia [2]. In this context, bacteria develop resistance through mutations, horizontal gene transfer, and various biochemical mechanisms, which can be categorized into changes in the antimicrobial molecule, reduced access to the target, or alterations to target sites. Facing this emergency, antimicrobial peptides have emerged as promising candidates, offering a unique mechanism of disrupting bacterial cell membranes and reducing resistance development, exhibiting a broad spectrum of activity [241].

Our findings demonstrated the potency of WLBU2 and LL37 on *Pseudomonas aeruginosa* strains, with rapid bactericidal activity. WLBU2 exhibited over 99% inhibition in 2 minutes, while LL37 took 8 minutes. hLF1-11 displayed moderate bactericidal effects in just 2 minutes, although less potent.

However, because of susceptibility to *in vivo* proteolytic enzymes and the high manufacturing costs, only two AMPs have made it to the market. To advance more candidates through clinical trials, there is a persistent need for effective drug delivery systems [187]. Most antibiotics are administered systemically, leading to the exposure of the entire body to the drug, rather than solely targeting the infecting bacteria. Localized drug administration routes address some of these concerns. Among them, a valuable option is the pulmonary one [76]. This route provides an effective and efficient means of treating lung infections by directly targeting the site of the disease, reducing systemic exposure, and minimizing side effects and potential drug interactions. As reported in the literature, inhalation is the favorite route for administering AMPs when a direct antimicrobial response is needed [83].

A dry powder inhalation device was determined to be the optimal inhalation vehicle for these peptides in pursuit of this therapeutic goal. This choice was attributed to its ability to achieve enhanced antimicrobial, anti-biofilm, and mucolytic efficacy through the deposition of drug particles. This results from the high drug concentration achievable at the deposition site [76].

The initial phase of this PhD research project was mainly dedicated to fine-tuning the spray-drying process to produce microparticle powders containing WLBU2, LL37 and hLF1-11 peptides. To achieve this, a systematic DoE approach was firstly applied to identify the influence of spray drying process parameters on WLBU2 SD and then based on the DoE findings, LL37 SD and hLF1-11 SD were designed. Spray-dried formulations were composed of mannitol and leucine for WLBU2, while trehalose and leucine were selected for LL37 and hLF1-11. The DoE results revealed that feed concentration and inlet temperature exerted a significant influence on process yield, with feed concentration emerging as particularly impactful. The particle size distribution fell within the acceptable range for pulmonary delivery for all the formulations except for hLF1-11 SD where particles were > 6 μm in size. The *in vitro* aerodynamic assessment resulted in good aerosolization properties in terms of emitted fraction and respirable fraction for both WLBU2 SD and LL37 SD, while hLF1-11 SD was not further tested. The peptide recovery within the powders was around 90 % in most formulations, with only a few exceptions for LL37. The peptides and their respective formulations were tested *in vitro* for cytocompatibility by CV staining, on two cell models, *i.e.* A549 and BEAS2B. The results showed the absence of cytotoxicity for peptides, their formulations and for the excipient matrix alone, underlighting the safety of the presented formulation. Moreover, based on what was observed for peptides on *P.aeruginosa*, biological studies were also conducted to assess antibacterial activity for WLBU2 SD and LL37 SD.

WLBU2 was confirmed as the potent peptide among the others under investigation, with increased effect once formulated, while for LL37 SD a preliminary study showed that at 2 μg/ml of formulated peptide an inhibition of proliferation of 89 % was achieved. As *P. aeruginosa* grows and colonizes lung regions through biofilm formation, antibiofilm activity was also evaluated. Preliminary studies have therefore shown the ability to reduce biomass formation for both peptides, however as the structure and growth of bacteria in biofilms is extremely complex, further investigations are in

progress. In particular, the assessment of the effective concentration of the formulation needed to achieve a significant reduction in bacterial biomass is underway. This is also applied to hLF1-11/hLF1-11 SD.

Furthermore, by means of circular dichroism studies, the findings also demonstrated the strong interaction that took place between peptides and molecules that mimic the structure of bacterial membranes. This interaction was realized through a conformational change of the peptides from unstructured to alpha helix. However, this conformational change when the peptides were formulated was only demonstrated for WLBU2 for which an increase in interaction intensity was described. Indeed, future perspectives foresee the investigation of this interaction for LL37 SD and hLF1-11 SD.

In conclusion, the research includes conducting additional studies to further explore the potential of these processed AMPs. Key areas of focus should include dissolution studies to understand their behavior in physiological conditions, and a deeper antibiofilm activity investigation on *Pseudomonas* strains to assess their effectiveness in combating biofilm-associated infections. These studies will provide a more comprehensive understanding of the potential of spray-dried AMPs and facilitate their development into viable treatments for various bacterial infections, ultimately contributing to the global effort to combat AMR.

2 Polymeric (PLGA) nanoparticles for AMPs encapsulation

When the aim is to direct a drug towards *P. aeruginosa*, it is important to consider that in most cases an infection triggered by this bacterium is associated with a patient with cystic fibrosis [86]. The airways of a patient with CF present special characteristics in that the mutation in the CFTR gene leads to an overproduction of mucus, which is rich in salts, has an altered pH, and is highly sticky [85]. This can hinder the direct delivery of the peptide to the lung. Furthermore, with a microparticle system in which the matrix is composed of mannitol or trehalose, this in the upper tract dissolves releasing the peptide, which may not be able to cross the mucin network due to its large size and/or be easily degraded by the proteolytic action of enzymes [242]. For this reason, the use of nanoparticle systems can help overcome these issues.

In this study, LL37 and WLBU2 were encapsulated in polymeric nanoparticles of PLGA, resulting in a size of approximately 250 nm that would potentially be able to deliver these peptides through the mucus mucin network [113]. However, cytotoxicity studies showed a sensitivity of bronchial epithelial and macrophage cells to the nanoparticle system as investigated by MTT assays. Although a change in the type of assay used, *i.e*. CCK-8, did not show the same result, these findings have to be analyzed with caution, and further investigations and optimizations are necessary in order to demonstrate the applicability of this formulation system for LL37 and WLBU2. Furthermore, in addition to what has been emphasized above regarding the interaction with mucus, diffusion studies are ongoing to further investigate the applicability of these nanoparticle systems.

References

[1] O. Pacios, L. Blasco, I. Bleriot, L. Fernandez-Garcia, M.G. Bardanca, A. Ambroa, M. López, G. Bou, M. Tomás. Strategies to combat multidrug-resistant and persistent infectious diseases. Antibiotics 9 (2020) 1-20.

[2] P. Dadgostar. Antimicrobial resistance: implications and costs. Infect. Drug. Resist. 12 (2019) 3903-3910.

[3] G. Laverty, S.P. Gorman, B.F. Gilmore. The potential of antimicrobial peptides as biocides. Int. J. Mo.l Sci. 12 (2011) 6566-6596.

[4] S. Mukhopadhyay, A.S. Bharath Prasad, C.H. Mehta, U.Y. Nayak. Antimicrobial peptide polymers: no escape to ESKAPE pathogens—a review. World J. Microbiol. Biotechnol. 36 (2020) 1-14.

[5] P. Cardoso, H. Glossop, T.G. Meikle, A. Aburto-Medina, C.E. Conn, V. Sarojini, C. Valery. Molecular engineering of antimicrobial peptides: microbial targets, peptide motifs and translation opportunities. Biophys. Rev. 13 (2021) 35-69.

[6] B. Deslouches, J.D. Steckbeck, J.K. Craigo, Y. Doi, J.L. Burns, R.C. Montelaro. Engineered cationic antimicrobial peptides to overcome multidrug resistance by ESKAPE pathogens. Antimicrob. Agents Chemother. 59 (2015) 1329–1333.

[7] D.M.P. De Oliveira, B.M. Forde, T.J. Kidd, P.N.A. Harris, M.A. Schembri, S.A. Beatson, D.L. Paterson, M.J. Walker. Antimicrobial Resistance in ESKAPE pathogens. Clin. Microbiol. Rev. 33 (2020) e00181-19.

[8] M.K. Glynn, C. Bopp, W. Dewitt, P. Dabney, M. Mokhtar, F.J. Angulo. Emergence of multidrug-resistant Salmonella enterica serotype typhimurium DT104 infections in the United States. New Engl. J. Med. 338 (1998) 1333-1338.

[9] J.M. Munita, C.A. Arias. Mechanisms of Antibiotic Resistance. Microbiol. Spectr. 4 (2016) VMBF-0016-2015.

[10] C.C. Bell, O. Gilan. Principles and mechanisms of non-genetic resistance in cancer. Br. J. Cancer. 122 (2020) 465-472.

[11] G. Annunziato, G. Costantino. Antimicrobial peptides (AMPs): a patent review (2015–2020). Expert Opin. Ther. Pat. 30 (2020) 931-947.

[12] Y. Luo, Y. Song. Mechanism of antimicrobial peptides: antimicrobial, anti-inflammatory and antibiofilm activities. Int. J. Mol. Sci. 22 (2021) 11401.

[13] Y. Huang, J. Huang, Y. Chen. Alpha-helical cationic antimicrobial peptides: Relationships of structure and function. Protein Cell. 1 (2010) 143-152.

[14] J. Lei, L. Sun, S. Huang, C. Zhu, P. Li, J. He, V. Mackey, D.H. Coy, Q. He. The antimicrobial peptides and their potential clinical applications. Am. J. Transl. Res. 11 (2019) 3919-3931.

[15] H.X. Luong, T.T. Thanh, T.H. Tran. Antimicrobial peptides - Advances in development of therapeutic applications. Life Sci. 260 (2020) 118407.

[16] E.F. Haney, S.K. Straus, R.E.W. Hancock. Reassessing the host defense peptide landscape. Front Chem. 7 (2019) 2296-2646.

[17] J.M. Sierra, M. Viñas. Future prospects for Antimicrobial peptide development: peptidomimetics and antimicrobial combinations. Expert Opin. Drug. Discov. 16 (2021) 601-604.

[18] J.K. Boparai, P.K. Sharma. Mini review on antimicrobial peptides, sources, mechanism and recent applications. Protein Pept. Lett. 27 (2019) 4-16.

[19] M. Mahlapuu, J. Håkansson, L. Ringstad, C. Björn. Antimicrobial peptides: an emerging category of therapeutic agents, Front. Cell. Infect. Microbiol. 6 (2016) 1-12.

[20] Y. Zhu, M.U. Akhtar, B. Li, S. Chou, C. Shao, J. Li, A. Shan. The design of cell-selective tryptophan and arginine-rich antimicrobial peptides by introducing hydrophilic uncharged residues. Acta Biomater. 153 (2022) 557-572.

[21] C.H. Chen, T.K. Lu. Development and challenges of antimicrobial peptides for therapeutic applications. Antibiotics 9 (2020) 24.

[22] M. Dathe, T. Wieprecht. Structural features of helical antimicrobial peptides: their potential to modulate activity on model membranes and biological cells. Biochim. Biophys. Acta 1462 (1999) 71-87.

[23] M. Dathe, H. Nikolenko, J. Meyer, M. Beyermann, M. Bienert. Optimization of the antimicrobial activity of magainin peptides by modi¢cation of charge. FEBS Lett. 501 (2001) 146-150.

[24] I. Greco, N. Molchanova, E. Holmedal, H. Jenssen, B.D. Hummel, J.L. Watts, J. Håkansson, P.R. Hansen, J. Svenson. Correlation between hemolytic activity, cytotoxicity and systemic in vivo toxicity of synthetic antimicrobial peptides. Sci. Rep. 10 (2020) 13206.

[25] Z. Jiang, A.I. Vasil, J.D. Hale, R.E.W. Hancock, M.L. Vasil, R.S. Hodges. Effects of net charge and the number of positively charged residues on the biological activity of amphipathic α-helical cationic antimicrobial peptides. Biopolymers. 90 (2008) 369-383.

[26] C. Wang, T. Hong, P. Cui, J. Wang, J. Xia. Antimicrobial peptides towards clinical application: delivery and formulation. Adv. Drug Deliv. Rev. 175 (2021) 113818.

[27] M.M. Islam, F. Asif, S.U. Zaman, M.K.H. Arnab, M.M. Rahman, M. Hasan. Effect of charge on the antimicrobial activity of alpha-helical amphibian antimicrobial peptide. Curr. Res. Microb. Sci. 4 (2023) 100182.

[28] A. Tossi, L. Sandri, A. Giangaspero. Amphipathic, α-helical antimicrobial peptides. Biopolymers. 55 (2000) 4-30.

[29] S. Li, Y. Wang, Z. Xue, Y. Jia, R. Li, C. He, H. Chen. The structure-mechanism relationship and mode of actions of antimicrobial peptides: a review. Trends Food Sci. Technol. 109 (2021) 103-115.

[30] P. Kumar, J.N. Kizhakkedathu, S.K. Straus. Antimicrobial peptides: diversity, mechanism of action and strategies to improve the activity and biocompatibility in vivo. Biomolecules 8 (2018) 4.

[31] B. Deslouches, S.M. Phadke, V. Lazarevic, M. Cascio, K. Islam, R.C. Montelaro, T.A. Mietzner. De novo generation of cationic antimicrobial peptides: influence of length and tryptophan substitution on antimicrobial activity. Antimicrob. Agents Chemother. 49 (2005) 316-322.

[32] N. Papo, Y. Shai. Can we predict biological activity of antimicrobial peptides from their interactions with model phospholipid membranes?. Peptides 24 (2003) 1693-1703.

[33] J. Wu, X. Zhou, Q. Chen, Z. Chen, J. Zhang, L. Yang, Y. Sun, G. Wang, J. Dai, T. Feng. Defensins as a promising class of tick antimicrobial peptides: a scoping review. Infect. Dis. Poverty 71 (2022) 11.

[34] W. F. DeGrado, J. D. Lear. Induction of peptide conformation at apolar water surfaces. 1. A study with model peptides of defined hydrophobic periodicity. J. Am. Chem. Soc. 107 (1985), 7684-7689.

[35] M. Tajbakhsh, A. Karimi, F. Fallah, M.M. Akhavan. Overview of ribosomal and non-ribosomal antimicrobial peptides produced by Gram positive bacteria. Cell. Mol. Biol. 6 (2017) 20-32.

[36] K. Jiang, X. Chen, W. Zhang, Y. Guo, G. Liu. Nonribosomal antibacterial peptides isolated from Streptomyces agglomeratus 5-1-3 in the Qinghai-Tibet Plateau. Microb. Cell. Fact. 22 (2023) 5.

[37] S. Caboche, M. Pupin, V. Leclère, A. Fontaine, P. Jacques, G. Kucherov. NORINE: a database of nonribosomal peptides. Nucleic Acids Res. 36 (2008) D326-D331.

[38] K. Hilpert, T. Munshi, P.M. López-Pérez, J. Sequeira-Garcia, S. Hofmann, T.J. Bull. Discovery of antimicrobial peptides that can accelerate the diagnostics of slow-growing mycobacteria including mycobacterium tuberculosis by culture. Microorganisms 11 (2023) 2225.

[39] H.K. Kang, C. Kim, C.H. Seo, Y. Park. The therapeutic applications of antimicrobial peptides (AMPs): a patent review. J. Microbiol. 55 (2017) 1-12.

[40] E.M. Haisma, A. De Breij, H. Chan, J.T. Van Dissel, J.W. Drijfhout, P.S. Hiemstra, A. El Ghalbzouri, P.H. Nibbering. LL-37-derived peptides eradicate multidrug-resistant Staphylococcus aureus from thermally wounded human skin equivalents. Antimicrob. Agents Chemother. 58 (2014) 4411-4419.

[41] C. Chen, B. Deslouches, R.C. Montelaro, Y.P. Di. Enhanced efficacy of the engineered antimicrobial peptide WLBU2 via direct airway delivery in a murine model of Pseudomonas aeruginosa pneumonia. Clin. Microbiol. Infect. 24 (2018) 547.e1-547.e8.

[42] L. Zhang, J. Parente, S.M. Harris, D.E. Woods, R.E.W. Hancock, T.J. Falla. Antimicrobial peptide therapeutics for cystic fibrosis. Antimicrob. Agents Chemother. 49 (2005) 2921-2927.

[43] G. Rossetto, P. Bergese, P. Colombi, L.E. Depero, A. Giuliani, S.F. Nicoletto, G. Pirri. Atomic force microscopy evaluation of the effects of a novel antimicrobial multimeric peptide on Pseudomonas aeruginosa. Nanomedicine 3 (2007) 198-207.

[44] R. Geitani, C.A. Moubareck, Z. Xu, D. Karam Sarkis, L. Touqui. Expression and roles of antimicrobial peptides in innate defense of airway mucosa: potential implication in cystic fibrosis. Front. Immunol. 11 (2020) 1198.

[45] A. Parchebafi, F. Tamanaee, H. Ehteram, E. Ahmad, H. Nikzad, H. Haddad Kashani. The dual interaction of antimicrobial peptides on bacteria and cancer cells; mechanism of action and therapeutic strategies of nanostructures. Microb. Cell. Fact. 21 (2022) 118.

[46] B. Bechinger, K. Lohner. Detergent-like actions of linear amphipathic cationic antimicrobial peptides. Biochim. Biophys. Acta Biomembr. 1758 (2006) 1529-1539.

[47] H. Sato, J.B. Feix. Peptide-membrane interactions and mechanisms of membrane destruction by amphipathic α-helical antimicrobial peptides. Biochim. Biophys. Acta Biomembr. 1758 (2006) 1245-1256.

[48] A.D. Cirac, G. Moiset, J.T. Mika, A. Koçer, P. Salvador, B. Poolman, S.J. Marrink, D. Sengupta. The molecular basis for antimicrobial activity of pore-forming cyclic peptides. Biophys. J. 100 (2011) 2422-2431.

[49] R.M. van Harten, E. van Woudenbergh, A. van Dijk, H.P. Haagsman. Cathelicidins: immunomodulatory antimicrobials. Vaccines 6 (2018) 63.

[50] K.E. Ridyard, J. Overhage. The potential of human peptide LL-37 as an antimicrobial and anti-biofilm agent. Antibiotics 10 (2021) 650.

[51] K. Kuroda, K. Okumura, H. Isogai, E. Isogai. The human cathelicidin antimicrobial peptide LL-37 and mimics are potential anticancer drugs. Front. Oncol. 5 (2015) 144.

[52] U.H.N. Dürr, U.S. Sudheendra, A. Ramamoorthy. LL-37, the only human member of the cathelicidin family of antimicrobial peptides. Biochim. Biophys. Acta Biomembr. 1758 (2006) 1408-1425.

[53] M.G. Scott, D.J. Davidson, M.R. Gold, D. Bowdish, R.E.W. Hancock. The human antimicrobial peptide LL-37 is a multifunctional modulator of innate immune responses. J. Immunol. 169 (2002) 3883-3891.

[54] G. Wang, M. Elliott, A.L. Cogen, E.L. Ezell, R.L. Gallo, R.E.W. Hancock. Structure, dynamics, and antimicrobial and immune modulatory activities of human LL-23 and its single-residue variants mutated on the basis of homologous primate cathelicidins. Biochemistry 51 (2012) 653-664.

[55] M.F. Salamah, D. Ravishankar, X. Kodji, L.A. Moraes, H.F. Williams, T.M. Vallance, D.A. Albadawi, R. Vaiyapuri, K. Watson, J.M. Gibbins, S.D. Brain, M. Perretti, S. Vaiyapuri. The endogenous antimicrobial cathelicidin LL37 induces platelet activation and augments thrombus formation. Blood Adv. 2 (2018) 2973-2985.

[56] K. Felgentreff, C. Beisswenger, M. Griese, T. Gulder, G. Bringmann, R. Bals. The antimicrobial peptide cathelicidin interacts with airway mucus. Peptides 27 (2006) 3100-3106.

[57] S.M. Travis, P.K. Singh, M.J. Welsh. Antimicrobial peptides and proteins in the innate defense of the airway surface. Curr. Opin. Immunol. 13 (2001) 89-95.

[58] L. Elsalem, A. Khasawneh, S.A.L. Sheboul. WLBU2 antimicrobial peptide as a potential therapeutic for treatment of resistant bacterial infections. Turk. J. Pharm. Sci. 19 (2022) 110-115.

[59] B. Deslouches, K. Islam, J.K. Craigo, S.M. Paranjape, R.C. Montelaro, T.A. Mietzner. Activity of the de novo engineered antimicrobial peptide WLBU2 against Pseudomonas aeruginosa in human serum and whole blood: Implications for systemic applications. Antimicrob. Agents Chemother. 49 (2005) 3208-3216.

[60] J.K. Munk, C. Ritz, F.P. Fliedner, N. Frimodt-Moller, P.R. Hansen. Novel method to identify the optimal antimicrobial peptide in a combination matrix, using anoplin as an example. Antimicrob. Agents Chemother. 58 (2014) 1063-1070.

[61] F.J. Byfield, M. Kowalski, K. Cruz, K. Leszczyńska, A. Namiot, P.B. Savage, R. Bucki, P.A. Janmey. Cathelicidin LL-37 increases lung epithelial cell stiffness, decreases transepithelial permeability, and prevents epithelial invasion by pseudomonas aeruginosa. J. Immunol. 187 (2011) 6402-6409.

[62] J.B. Mandell, J. A. Koch, B. Deslouches, K.L. Urish. Direct antimicrobial activity of cationic amphipathic peptide WLBU2 against Staphylococcus aureus biofilms is enhanced in physiologic buffered saline. J. Orthop. Res. 38 (2020) 2657-2663.

[63] Q. Lin, B. Deslouches, R.C. Montelaro, Y.P. Di. Prevention of ESKAPE pathogen biofilm formation by antimicrobial peptides WLBU2 and LL37. Int. J. Antimicrob. Agents. 52 (2018) 667-672.

[64] J.A. Melvin, L.P. Lashua, M.R. Kiedrowski, G. Yang, B. Deslouches, R.C. Montelaro, J.M. Bomberger. Simultaneous antibiofilm and antiviral activities of an engineered antimicrobial peptide during virus-bacterium coinfection. mSphere 1 (2016) e00083-16.

[65] B. Deslouches, J.D. Steckbeck, J.K. Craigo, Y. Doi, T.A. Mietzner, R.C. Montelaro. Rational design of engineered cationic antimicrobial peptides consisting exclusively of arginine and tryptophan, and their activity against multidrug-resistant pathogens. Antimicrob. Agents Chemother. 57 (2013) 2511-2521.

[66] P. Morici, W. Florio, C. Rizzato, E. Ghelardi, A. Tavanti, G.M. Rossolini, A. Lupetti. Synergistic activity of synthetic N-terminal peptide of human lactoferrin in combination with various antibiotics against carbapenem-resistant Klebsiella pneumoniae strains. Eur. J. Clin. Microbiol. Infect. Dis. 36 (2017) 1739-1748.

[67] M. Dai, P. Pan, H. Li, S. Liu, L. Zhang, C. Song, Y. Li, Q. Li, Z. Mao, Y. Long, X. Su, C. Hu. The antimicrobial cathelicidin peptide hLF(1-11) attenuates alveolar macrophage pyroptosis induced by Acinetobacter baumannii in vivo. Exp. Cell. Res. 364 (2018) 95-103.

[68] J.P. Tam, C.-R. Wu, W. Liu, J.-W. Zhang. Disulfide bond formation in peptides by dimethyl sulfoxide. Scope and applications. J. Am. Chem. Soc. 113 (1991) 6657-6662.

[69] G. Bulaj. Formation of disulfide bonds in proteins and peptides. Biotechnol. Adv. 23 (2005) 87-92.

[70] M. Godoy-Gallardo, C. Mas-Moruno, M.C. Fernández-Calderón, C. Pérez-Giraldo, J.M. Manero, F. Albericio, F.J. Gil, D. Rodríguez. Covalent immobilization of hLf1-11 peptide on a titanium surface reduces bacterial adhesion and biofilm formation. Acta Biomater. 10 (2014) 3522-3534.

[71] A.M. Van Der Does, S.J.P. Bogaards, L. Jonk, M. Wulferink, M.P. Velders, P.H. Nibbering. The human lactoferrin-derived peptide hLF1-11 primes monocytes for an enhanced TLR-mediated immune response. BioMetals 23 (2010) 493-505.

[72] W.J.F.M. van der Velden, T.M.P. van Iersel, N.M.A. Blijlevens, J.P. Donnelly. Safety and tolerability of the antimicrobial peptide human lactoferrin 1-11 (hLF1-11). BMC Med. 7 (2009) 44.

[73] S.P. Newman. Drug delivery to the lungs: challenges and opportunities. Ther. Deliv. 8 (2017) 647-661.

[74] L. Santacroce, I.A. Charitos, A. Ballini, F. Inchingolo, P. Luperto, E. De Nitto, S. Topi. The human respiratory system and its microbiome at a glimpse. Biology 9 (2020) 1-16.

[75] N.A. ElKasabgy, I.M. Adel, M.F. Elmeligy. Respiratory tract: structure and attractions for drug delivery using dry powder inhalers. AAPS PharmSciTech. 21 (2020) 238.

[76] P.C. Lip Kwok, H.K. Chan. Pulmonary delivery of peptides and proteins. In *Peptide and Protein Delivery*, C. Van Der Walle Ed., Elsevier Academic Press, 23–46 (2011).

[77] M. Karimi, H. Kamali, M. Mohammadi, M. Tafaghodi. Evaluation of various techniques for production of inhalable dry powders for pulmonary delivery of peptide and protein. J. Drug. Deliv. Sci. Technol. 69 (2022) 1773-2247.

[78] D.K. Chellappan, P. Prasher, V. Saravanan, V.S. Vern Yee, W.C. Wen Chi, J.W. Wong, J.K. Wong, J.T. Wong, W. Wan, J. Chellian, N. Molugulu, S.L. Prabu, R. Ibrahim, T. Darmarajan, M. Candasamy, P.K. Singh, V. Mishra, M.D. Shastri, F.C.

Zacconi, A. Chakraborty, M. Mehta, P.K. Gupta, H. Dureja, M. Gulati, S.K. Singh, G. Gupta, N.K. Jha, B.G. George Oliver, K. Dua. Protein and peptide delivery to lungs by using advanced targeted drug delivery. Chem. Biol. Interact. 351 (2022) 109706.

[79] F. Cappiello, A. Di Grazia, L.A. Segev-Zarko, S. Scali, L. Ferrera, L. Galietta, A. Pini, Y. Shai, Y.P. Di, M.L. Mangoni. Esculentin-1a-derived peptides promote clearance of pseudomonas aeruginosa internalized in bronchial cells of cystic fibrosis patients and lung cell migration: Biochemical properties and a plausible mode of action. Antimicrob. Agents Chemother. 60 (2016) 7252-7262.

[80] R.Y.K. Chang, M.Y.T. Chow, D. Khanal, D. Chen, H.K. Chan. Dry powder pharmaceutical biologics for inhalation therapy. Adv. Drug. Deliv. Rev. 172 (2021) 64-79.

[81] B. Chaurasiya, Y.Y. Zhao. Dry powder for pulmonary delivery: a comprehensive review. Pharmaceutics 13 (2021) 1-28.

[82] D.M.K. Jensen, D. Cun, M.J. Maltesen, S. Frokjaer, H.M. Nielsen, C. Foged. Spray drying of siRNA-containing PLGA nanoparticles intended for inhalation. J. Control. Rel. 142 (2010) 138-145.

[83] P.S. Hiemstra, G.D. Amatngalim, A.M. Van Der Does, C. Taube. Antimicrobial peptides and innate lung defenses: role in infectious and noninfectious lung diseases and therapeutic applications. Chest 149 (2016) 545-551.

[84] P.C.L. Kwok, A. Grabarek, M.Y.T. Chow, Y. Lan, J.C.W. Li, L. Casettari, A.J. Mason, J.K.W. Lam. Inhalable spray-dried formulation of D-LAK antimicrobial peptides targeting tuberculosis. Int. J. Pharm. 491 (2015) 367-374.

[85] S.M. Kreda, C.W. Davis, M.C. Rose. CFTR, mucins, and mucus obstruction in cystic fibrosis. Cold Spring Harb. Perspect. Med. 2 (2012) a009589.

[86] M. Schobert, D. Jahn. Anaerobic physiology of Pseudomonas aeruginosa in the cystic fibrosis lung. Int. J. Med. Microbiol. 300 (2010) 549-556.

[87] F. Bittar, H. Richet, J.C. Dubus, M. Reynaud-Gaubert, N. Stremler, J. Sarles, D. Raoult, J.M. Rolain. Molecular detection of multiple emerging pathogens in sputa from cystic fibrosis patients. PLoS One 3 (2008) e2908.

[88] A.M. Sousa, M.O. Pereira. Pseudomonas Aeruginosa diversification during infection development in cystic fibrosis Lungs - a review. Pathogens 3 (2014) 680-703.

[89] U.S. Sajjan, L.T. Tran, N. Sole, C. Rovaldi, A. Akiyama, P.M. Friden, J.F. Forstner, D.M. Rothstein. P-113D, an antimicrobial peptide active against Pseudomonas

aeruginosa, retains activity in the presence of sputum from cystic fibrosis patients. Antimicrob. Agents Chemother. 45 (2001) 3437-3444.

[90] K.E. Ridyard, M. Elsawy, D. Mattrasingh, D. Klein, J. Strehmel, C. Beaulieu, A. Wong, J. Overhage. Synergy between human peptide LL-37 and polymyxin B against planktonic and biofilm cells of escherichia coli and Pseudomonas aeruginosa. Antibiotics 12 (2023) 389.

[91] I. d'Angelo, B. Casciaro, A. Miro, F. Quaglia, M.L. Mangoni, F. Ungaro. Overcoming barriers in Pseudomonas aeruginosa lung infections: engineered nanoparticles for local delivery of a cationic antimicrobial peptide. Colloids Surf. B. Biointerfaces 135 (2015) 717-725.

[92] F. Buttini, J. Hannon, K. Saavedra, I. Rossi, A.G. Balducci, H. Smyth, A. Clark, P. Colombo. Accessorized DPI: a shortcut towards flexibility and patient adaptability in dry powder inhalation. Pharm. Res. 33 (2016) 3012-3020.

[93] B. Constantin, H. Saarbrücken. Mucus and surfactant as barriers for the pulmonary delivery of anti-infectives: challenges, models and strategies for overcoming them. Doctoral dissertation, Universität des Saarlandes (2022).

[94] R. Vehring. Pharmaceutical particle engineering via spray drying. Pharm. Res. 25 (2008) 999-1022.

[95] B.B. Eedara, W. Alabsi, D. Encinas-Basurto, R. Polt, H.M. Mansour. Spray-dried inhalable powder formulations of therapeutic proteins and peptides. AAPS PharmSciTech. 22 (2021) 185.

[96] S.A. Shoyele, N. Sivadas, S.A. Cryan. The effects of excipients and particle engineering on the biophysical stability and aerosol performance of parathyroid hormone (1-34) prepared as a dry powder for inhalation. AAPS PharmSciTech. 12 (2011) 304-311.

[97] M. Ordoubadi, K.B. Shepard, H. Wang, Z. Wang, A.M. Pluntze, J.P. Churchman, R. Vehring. On the physical stability of leucine-containing spray-dried powders for respiratory drug delivery. Pharmaceutics 15 (2023) 435.

[98] A.L.R. Rattes, W.P. Oliveira. Spray drying conditions and encapsulating composition effects on formation and properties of sodium diclofenac microparticles. Powder Technol. 171 (2007) 7-14.

[99] J. Elversson, A. Millqvist-Fureby, G. Go¨, G. Alderborn, U. Elofsson. Droplet and particle size relationship and shell thickness of inhalable lactose particles during spray drying. J. Pharm. Sci. 92 (2010) 900-10.

[100] A. Sosnik, K.P. Seremeta. Advantages and challenges of the spray-drying technology for the production of pure drug particles and drug-loaded polymeric carriers. Adv. Colloid Interface Sci. 223 (2015) 40-54.

[101] W.S. Cheow, K. Hadinoto. Enhancing encapsulation efficiency of highly water-soluble antibiotic in poly(lactic-co-glycolic acid) nanoparticles: modifications of standard nanoparticle preparation methods, Colloids Surf. A Physicochem. Eng. Asp. 370 (2010) 79-86.

[102] J.T. Pinto, E. Faulhammer, J. Dieplinger, M. Dekner, C. Makert, M. Nieder, A. Paudel. Progress in spray-drying of protein pharmaceuticals: literature analysis of trends in formulation and process attributes. Dry. Technol. 39 (2021) 1415-1446.

[103] M.C. Teixeira, C. Carbone, M.C. Sousa, M. Espina, M.L. Garcia, E. Sanchez-Lopez, E.B. Souto. Nanomedicines for the delivery of antimicrobial peptides (Amps). Nanomaterials 10 (2020) 560.

[104] A. Shukla, K.E. Fleming, H.F. Chuang, T.M. Chau, C.R. Loose, G.N. Stephanopoulos, P.T. Hammond. Controlling the release of peptide antimicrobial agents from surfaces. Biomaterials 31 (2010) 2348-2357.

[105] A.O. Fadaka, N.R.S. Sibuyi, A.M. Madiehe, M. Meyer. Nanotechnology-based delivery systems for antimicrobial peptides. Pharmaceutics 13 (2021) 1795.

[106] Y. Herdiana, N. Wathoni, S. Shamsuddin, M. Muchtaridi. Scale-up polymeric-based nanoparticles drug delivery systems: development and challenges. OpenNano. 7 (2022) 100048.

[107] M.H. Xiong, Y. Bao, X.Z. Yang, Y.H. Zhu, J. Wang. Delivery of antibiotics with polymeric particles. Adv. Drug. Deliv. Rev. 78 (2014) 63-76.

[108] A. Gagliardi, E. Giuliano, E. Venkateswararao, M. Fresta, S. Bulotta, V. Awasthi, D. Cosco. Biodegradable polymeric nanoparticles for drug delivery to solid tumors. Front. Pharmacol. 12 (2021) 601626.

[109] A. C. Burman, R. Mukherjee, D. Khattar, S. Mullick, M. Jaggi, M. K. Singh, D. Prusthy, P. K. Gupta, R. Praveen, S. Singh. Biocompatible, non-biodegradable, non-toxic polymer useful for nanoparticle pharmaceutical compositions. US Patent 8,927,023 B2 (2015).

[110] P.C. Pires, F. Mascarenhas-Melo, K. Pedrosa, D. Lopes, J. Lopes, A. Macário-Soares, D. Peixoto, P.S. Giram, F. Veiga, A.C. Paiva-Santos. Polymer-based biomaterials for pharmaceutical and biomedical applications: a focus on topical drug administration. Eur. Polym. J. 187 (2023) 0014-3057.

[111] J. Zhou, Y. Zhai, J. Xu, T. Zhou, L. Cen. Microfluidic preparation of PLGA composite microspheres with mesoporous silica nanoparticles for finely manipulated drug release. Int. J. Pharm. 593 (2021) 120173.

[112] H.O. Alsaab, F.D. Alharbi, A.S. Alhibs, N.B. Alanazi, B.Y. Alshehri, M.A. Saleh, F.S. Alshehri, M.A. Algarni, T. Almugaiteeb, M.N. Uddin, R.M. Alzhrani. PLGA-based nanomedicine: history of advancement and development in clinical applications of multiple diseases. Pharmaceutics 14 (2022) 2728.

[113] B. Casciaro, I. D'Angelo, X. Zhang, M.R. Loffredo, G. Conte, F. Cappiello, F. Quaglia, Y.P.P. Di, F. Ungaro, M.L. Mangoni. Poly(lactide- co-glycolide) nanoparticles for prolonged therapeutic efficacy of esculentin-1a-derived antimicrobial peptides against Pseudomonas aeruginosa lung infection: in vitro and in vivo studies. Biomacromolecules 20 (2019) 1876-1888.

[114] K.K. Chereddy, C.H. Her, M. Comune, C. Moia, A. Lopes, P.E. Porporato, J. Vanacker, M.C. Lam, L. Steinstraesser, P. Sonveaux, H. Zhu, L.S. Ferreira, G. Vandermeulen, V. Préat. PLGA nanoparticles loaded with host defense peptide LL37 promote wound healing. J. Control. Rel. 194 (2014) 138-147.

[115] K. Miladi, S. Sfar, H. Fessi, A. Elaissari. Nanoprecipitation process: from particle preparation to in vivo applications. In *Polymer Nanoparticles for Nanomedicines*, Springer International Publishing (2016) 17-53.

[116] T. Govender, S. Stolnik, M.C. Garnett, L. Illum, S.S. Davis. PLGA nanoparticles prepared by nanoprecipitation: drug loading and release studies of a water soluble drug. J. Control. Rel. 57 (1999) 171-185.

[117] A. Zielinska, F. Carreiró, A.M. Oliveira, A. Neves, B. Pires, D. Nagasamy Venkatesh, A. Durazzo, M. Lucarini, P. Eder, A.M. Silva, A. Santini, E.B. Souto. Polymeric nanoparticles: production, characterization, toxicology and ecotoxicology. Molecules 25 (2020) 3731.

[118] X. Yan, J. Bernard, F. Ganachaud. Nanoprecipitation as a simple and straightforward process to create complex polymeric colloidal morphologies. Adv. Colloid. Interface Sci. 294 (2021) 102474.

[119] A. Simon, M.I. Amaro, L.M. Cabral, A.M. Healy, V.P. De Sousa. Development of a novel dry powder inhalation formulation for the delivery of rivastigmine hydrogen tartrate. Int. J. Pharm. 501 (2016) 124-138.

[120] K.Y. Hernández-Giottonini, R.J. Rodríguez-Córdova, C.A. Gutiérrez-Valenzuela, O. Peñuñuri-Miranda, P. Zavala-Rivera, P. Guerrero-Germán, A. Lucero-Acuña. PLGA nanoparticle preparations by emulsification and nanoprecipitation techniques: effects of formulation parameters. RSC Adv. 10 (2020) 4218-4231.

[121] X. Li, X. Jiang. Microfluidics for producing poly (lactic-co-glycolic acid)-based pharmaceutical nanoparticles, Adv. Drug. Deliv. Rev. 128 (2018) 101-114.

[122] H.T.H. Vu, S. Streck, S.M. Hook, A. McDowell. Utilization of microfluidics for the preparation of polymeric nanoparticles for the antioxidant rutin: a comparison with bulk production. Pharm. Nanotechnol. 7 (2019) 469-483.

[123] J. Ahn, J. Ko, S. Lee, J. Yu, Y.T. Kim, N.L. Jeon. Microfluidics in nanoparticle drug delivery; from synthesis to pre-clinical screening. Adv. Drug Deliv. Rev. 128 (2018) 29-53.

[124] G.M. Whitesides. The origins and the future of microfluidics. Nature. 442 (2006) 368-373.

[125] P. Shokoohinia, M. Hajialyani, K. Sadrjavadi, M. Akbari, M. Rahimi, S. Khaledian, A. Fattahi. Microfluidic-assisted preparation of PLGA nanoparticles for drug delivery purposes: experimental study and computational fluid dynamic simulation. Res. Pharm. Sci. 14 (2019) 459-470.

[126] X. Li, H.M. Mansour. Physicochemical characterization and water vapor sorption of organic solution advanced spray-dried inhalable trehalose microparticles and nanoparticles for targeted dry powder pulmonary inhalation delivery. AAPS PharmSciTech. 12 (2011) 1420-1430.

[127] E. Quarta, F. Sonvico, R. Bettini, C. De Luca, A. Dotti, D. Catalucci, M. Iafisco, L. Degli Esposti, G. Colombo, G. Trevisi, D. M. Rekkas, A. Rossi, T.W. Wong, F. Buttini, P. Colombo. Inhalable microparticles embedding calcium phosphate nanoparticles for heart targeting: The formulation experimental design. Pharmaceutics 13 (2021) 1825.

[128] V. A. Marple, D. Hochrainer, D. L. Roberts, F. J. Romay, N. C. Miller, K. G. Truman, M. Van Oort, B. Olsson, M. J. Holroyd, J.P. Mitchell. Next Generation Pharmaceutical Impactor (a new impactor for pharmaceutical inhaler testing). Part I: Design. J. Aerosol Med. 16 (2003) 283-299.

[129] A. Sharma, K. Vaghasiya, P. Gupta, A.K. Singh, U.D. Gupta, R.K. Verma. Dynamic mucus penetrating microspheres for efficient pulmonary delivery and enhanced efficacy of host defence peptide (HDP) in experimental tuberculosis. J. Control Rel. 324 (2020) 17-33.

[130] X. Wang, X. Zhang, L. Fan, H. He, X. Zhang, Y. Zhang, S. Mao. Influence of polymeric carrier on the disposition and retention of 20(R)-ginsenoside-rg3-loaded swellable microparticles in the lung. Drug Deliv. Transl. Res. 8 (2018) 252-265.

[131] N. E. Ceschan, V. Bucalá, M.V. Mateos, H.D.C. Smyth, M.V. Ramírez-Rigo. Carrier free indomethacin microparticles for dry powder inhalation. Int. J. Pharm. 549 (2018) 169-178.

[132] S. Dosler, E. Karaaslan. Inhibition and destruction of Pseudomonas aeruginosa biofilms by antibiotics and antimicrobial peptides. Peptides 62 (2014) 32-37.

[133] S. Kumar, R. Gokhale, D.J. Burgess. Quality by Design approach to spray drying processing of crystalline nanosuspensions. Int. J. Pharm. 464 (2014) 234-242.

[134] S. Focaroli, P.T. Mah, J.E. Hastedt, I. Gitlin, S. Oscarson, J.V. Fahy, A.M. Healy. A Design of Experiment (DoE) approach to optimise spray drying process conditions for the production of trehalose/leucine formulations with application in pulmonary delivery. Int. J. Pharm. 562 (2019) 228-240.

[135] N. Alhajj, N.J. O'Reilly, H. Cathcart. Designing enhanced spray dried particles for inhalation: a review of the impact of excipients and processing parameters on particle properties. Powder Technol. 384 (2021) 313-331.

[136] A. Singh, G. Van den Mooter. Spray drying formulation of amorphous solid dispersions. Adv. Drug Deliv. Rev. 100 (2016) 27-50.

[137] M. Mönckedieck, J. Kamplade, P. Fakner, N.A. Urbanetz, P. Walzel, H. Steckel, R. Scherließ. Dry powder inhaler performance of spray dried mannitol with tailored surface morphologies as carrier and salbutamol sulphate. Int. J. Pharm. 524 (2010) 351-363.

[138] L. Li, S. Sun, T. Parumasivam, J.A. Denman, T. Gengenbach, P. Tang, S. Mao, H. K. Chan. L-Leucine as an excipient against moisture on in vitro aerosolization performances of highly hygroscopic spray-dried powders. Eur. J. Pharm. Biopharm. 102 (2016) 132-141.

[139] S.M. Patil, D.S. Barji, S. Aziz, D.A. McChesney, S.Bagde, P. Muttil, N.K. Kunda. Pulmonary delivery of spray-dried nisin ZP antimicrobial peptide for non-small cell lung cancer (NSCLC) treatment. Int. J. Pharm. 634 (2023) 122641.

[140] J.K.W. Lam, Q. Zhou. Advances in pulmonary drug delivery systems and inhalation formulations. Pharm. Res. 40 (2023) 1013-1014.

[141] A. Ziaee, A.B. Albadarin, L. Padrela, T. Femmer, E. O'Reilly, G. Walker. Spray drying of pharmaceuticals and biopharmaceuticals: critical parameters and experimental process optimization approaches, Eur. J. Pharm. Sci. 127 (2019) 300-318.

[142] G. Soni, K.S. Yadav, M.K. Gupta. QbD based approach for formulation development of spray dried microparticles of erlotinib hydrochloride for sustained release. J. Drug. Deliv. Sci. Technol. 57 (2020) 101684.

[143] M. Razuc, J. Piña, M.V. Ramírez-Rigo. Optimization of ciprofloxacin hydrochloride spray-dried microparticles for pulmonary delivery using design of experiments. AAPS PharmSciTech. 19 (2019) 3085-3096.

[144] F. Cheng, X. Zhou, Y. Liu. Methods for improvement of the thermal efficiency during spray drying. E3S Web of Conferences, EDP Sciences 53 (2018).

[145] K.C. Lee, Y.S. Yoon, F.Z. Li, J.B. Eun. Effects of inlet air temperature and concentration of carrier agents on physicochemical properties, sensory evaluation of spray-dried mandarin (Citrus unshiu) beverage powder. Appl. Biol. Chem. 60 (2017) 33-40.

[146] N.R. Rabbani, P.C. Seville. The influence of formulation components on the aerosolisation properties of spray-dried powders. J. Control. Rel. 110 (2015) 130-140.

[147] H.I. Shahin, B.P. Vinjamuri, A.A. Mahmoud, R.N. Shamma, S.M. Mansour, H.O. Ammar, M.M. Ghorab, M.B. Chougule, L. Chablani. Design and evaluation of novel inhalable sildenafil citrate spray-dried microparticles for pulmonary arterial hypertension. J. Control. Rel. 302 (2019) 126-139.

[148] Y. B. Kwon, J.H. Kang, C.S. Han, D.W Kim, C.W. Park. The effect of particle size and surface roughness of spray-dried bosentan microparticles on aerodynamic performance for dry powder inhalation. Pharmaceutics 12 (2020) 1-15.

[149] B. Chaurasiya, Y.Y. Zhao. Dry powder for pulmonary delivery: a comprehensive review. Pharmaceutics 13 (2021) 31.

[150] K. Almansour, I.M. Alfagih, R. Ali, M.M.A. Elsayed. Inhalable microparticles containing terbinafine for management of pulmonary fungal infections: spray drying process

engineering using lactose vs. mannitol as excipients. J. Drug Deliv. Sci. Technol. 60 (2020) 101991.

[151] A. Lechanteur, B. Evrard. Influence of composition and spray-drying process parameters on carrier-free DPI properties and behaviors in the lung: a review. Pharmaceutics 12 (2020) 55.

[152] S. Belotti, A. Rossi, P. Colombo, R. Bettini, D. Rekkas, S. Politis, G. Colombo, A.G. Balducci, F. Buttini. Spray-dried amikacin sulphate powder for inhalation in cystic fibrosis patients: the role of ethanol in particle formation. Eur. J. Pharm. Biopharm. 93 (2015) 165-172.

[153] A. Borah, B. Deb, S. Chakraborty. A Crosstalk on Antimicrobial Peptides. Int. J. Pept. Res. Ther. 27 (2021) 229-244.

[154] W. Wang, C. Dufour, W. Zhou. Impacts of spray-drying conditions on the physicochemical properties of soy sauce powders using maltodextrin as auxiliary drying carrier. CYTA - J. Food 13 (2015) 548-555.

[155] M.J. Maltesen, S. Bjerregaard, L. Hovgaard, S. Havelund, M. van de Weert. Quality by design - spray drying of insulin intended for inhalation. Eur. J. Pharm. Biopharm. 70 (2008) 828-838.

[156] B. Vishwa, A. Moin, D.V. Gowda, S.M.D. Rizvi, W.A.H. Hegazy, A.S. Abu Lila, E.S. Khafagy, A.N. Allam. Pulmonary targeting of inhalable moxifloxacin microspheres for effective management of tuberculosis. Pharmaceutics 13 (2021) 1-17.

[157] N. Saadatkhah, A. Carillo Garcia, S. Ackermann, P. Leclerc, M. Latifi, S. Samih, G.S. Patience, J. Chaouki. Experimental methods in chemical engineering: thermogravimetric analysis-TGA. Can. J. Chem. Eng. 98 (2020) 34-43.

[158] M.I. Amaro, L. Tajber, O.I. Corrigan, A.M. Healy. Optimisation of spray drying process conditions for sugar nanoporous microparticles (NPMPs) intended for inhalation. Int. J. Pharm. 421 (2011) 99-109.

[159] B.P. Vinjamuri, R.V. Haware, W.C. Stagner. Inhalable ipratropium bromide particle engineering with multicriteria optimization. AAPS PharmSciTech. 18 (2017) 1925-1935.

[160] H. Adi, P.M. Young, H.K. Chan, H. Agus, D. Traini. Co-spray-dried mannitol-ciprofloxacin dry powder inhaler formulation for cystic fibrosis and chronic obstructive pulmonary disease. Eur. J. Pharm. Sci. 40 (2010) 239-247.

[161] W. Kaialy, T. Hussain, A. Alhalaweh, A. Nokhodchi. Towards a more desirable dry powder inhaler formulation: large spray-dried mannitol microspheres outperform small microspheres. Pharm. Res. 31 (2014) 60-76.

[162] Q. Zhang, Y. Li, L. Li, Y. Cheng, F. Yu, R. Li, S. Hou. Impact of solid-state properties on the aerosolization performance of spray-dried curcumin powders. AAPS PharmSciTech. 24 (2023) 1-12.

[163] F. Buttini, P. Colombo, A. Rossi, F. Sonvico, G. Colombo. Particles and powders: tools of innovation for non-invasive drug administration. J. Control. Rel. 16 (2012) 693-702.

[164] K.J. Paluch, L. Tajber, O.I. Corrigan, A.M. Healy. Impact of process variables on the micromeritic and physicochemical properties of spray-dried porous microparticles, part I: introduction of a new morphology classification system. J. Pharm. Pharmacol. 64 (2012) 1570-1582.

[165] D. Thiyagarajan, B. Huck, B. Nothdurft, M. Koch, D. Rudolph, M. Rutschmann, C. Feldmann, C. Hozsa, M. Furch, K.F.W. Besecke, R.K. Gieseler, B. Loretz, C.M. Lehr. Spray-dried lactose-leucine microparticles for pulmonary delivery of antimycobacterial nanopharmaceuticals. Drug Deliv. Transl. Res. 11 (2021) 1766-1778.

[166] M.A. Boraey, S. Hoe, H. Sharif, D.P. Miller, D. Lechuga-Ballesteros, R. Vehring. Improvement of the dispersibility of spray-dried budesonide powders using leucine in an ethanol-water cosolvent system. Powder Technol. 236 (2013) 171-178.

[167] I.Y. Saleem, F. Diez, B.E. Jones, N. Kayali, L. Polo. Investigation on the aerosol performance of dry powder inhalation hypromellose capsules with different lubricant levels. Int. J. Pharm. 492 (2015) 258-263.

[168] A. Sharma, D. Kumar, K. Dahiya, S. Hawthorne, S.K. Jha, N.K. Jha, P. Nand, S. Girgis, S. Raj, R. Srivastava, V.K. Goswami, Y. Gregoriou, S.A. El-Zahaby, S. Ojha, H. Dureja, G. Gupta, S. Singh, D.K. Chellappan, K. Dua. Advances in pulmonary drug delivery targeting microbial biofilms in respiratory diseases. Nanomedicine 16 (2021) 1905-1923.

[169] D.T. Osanlóo, J. Fransson, B. Bergenståhl, A. Millqvist-Fureby. Effects of drying methods on physical properties and morphology of trehalose/mannitol mixtures. Drying Technol. 41 (2023) 503-522.

[170] M.I. Amaro, L. Tajber, O.I. Corrigan, A.M. Healy. Co-spray dried carbohydrate microparticles: crystallisation delay/inhibition and improved aerosolization

characteristics through the incorporation of hydroxypropyl-β-cyclodextrin with amorphous raffinose or trehalose. Pharm. Res. 32 (2015) 180-195.

[171] R.Y.K. Chang, M.Y.T. Chow, D. Khanal, D. Chen, H.K. Chan. Dry powder pharmaceutical biologics for inhalation therapy. Adv. Drug Deliv. Rev. 172 (2021) 64-70.

[172] L. Yang, Y. Liu, N. Wang, H. Wang, K. Wang, X.L. Luo, R.X. Dai, R.J. Tao, H.J. Wang, J.W. Yang, G.Q. Tao, J.M. Qu, B.X. Ge, Y.Y. Li, J.F. Xu. Albumin-based LL37 peptide nanoparticles as a sustained release system against Pseudomonas aeruginosa lung infection. ACS Biomater. Sci. Eng. 7 (2021) 1817-1826.

[173] S. Thennarasu, A. Tan, R. Penumatchu, C.E. Shelburne, D.L. Heyl, A. Ramamoorthy. Antimicrobial and membrane disrupting activities of a peptide derived from the human cathelicidin antimicrobial peptide LL37. Biophys J. 98 (2010) 248-257.

[174] Y. Xu, L. Harinck, A.G. Lokras, P. Gerde, E. Selg, C.O. Sjöberg, H. Franzyk, A. Thakur, C. Foged. Leucine improves the aerosol performance of dry powder inhaler formulations of siRNA-loaded nanoparticles. Int. J. Pharm. 621 (2022) 121758.

175] M. Hara, T. Okazaki, N.V. Muravyev, N. Koga. Physico-geometrical kinetic aspects of the thermal dehydration of trehalose dihydrate. J. Phys. Chem. C. 126 (2022) 20423-20436.

[176] R. Surana, A. Pyne, R. Suryanarayanan. Effect of preparation method on physical properties of amorphous trehalose. Pharm. Res. 21 (2004) 1167-1176.

[177] X. Li, H.M. Mansour. Physicochemical characterization and water vapor sorption of organic solution advanced spray-dried inhalable trehalose microparticles and nanoparticles for targeted dry powder pulmonary inhalation delivery. AAPS PharmSciTech. 12 (2011) 1420-1430.

[178] R. Svoboda, J. Malek. Interpretation of crystallization kinetics results provided by DSC. Thermochimica Acta, 526 (2011) 237-251.

[179] O.G. Travkova, H. Moehwald, G. Brezesinski. The interaction of antimicrobial peptides with membranes. Adv. Colloid. Interface Sci. 247 (2017) 521-532.

[180] C. Avitabile, L.D. D'Andrea, A. Romanelli. Circular Dichroism studies on the interactions of antimicrobial peptides with bacterial cells. Sci Rep. 4 (2014) 4293.

[181] C. Garcia-Canton, E. Minet, A. Anadon, C. Meredith. Metabolic characterization of cell systems used in in vitro toxicology testing: lung cell system BEAS-2B as a working example. Toxicol. In Vitro 27 (2013) 1719-1727.

[182] M. Sharma, A.O. Stucki, S. Verstraelen, T.J. Stedeford, A. Jacobs, F. Maes, D. Poelmans, J. Van Laer, S. Remy, E. Frijns, D.G. Allen, A.J. Clippinger. Human cell-based in vitro systems to assess respiratory toxicity: a case study using silanes. Toxicol. Sci. 195 (2023) 213-230.

[183] S. Swedan, Z. Shubair, A. Almaaytah. Synergism of cationic antimicrobial peptide WLBU2 with antibacterial agents against biofilms of multi-drug resistant Acinetobacter baumannii and Klebsiella pneumoniae. Infect. Drug Resist. 12 (2019) 2019-2030.

[184] ISO 10993-1:2018 - Biological evaluation of medical devices.

[185] P.S. Hiemstra, G. Grootaers, A.M. van der Does, C.A.M. Krul, I.M. Kooter. Human lung epithelial cell cultures for analysis of inhaled toxicants: lessons learned and future directions. Toxicol. In Vitro 47 (2018) 137-146.

[186] C. Garcia-De-Alba. Repurposing A549 adenocarcinoma cells: new options for drug discovery. Am. J. Respir. Cell. Mol. Biol. 64 (2021) 405-406.

[187] A. León-Buitimea, C.R. Garza-Cárdenas, J.A. Garza-Cervantes, J.A. Lerma-Escalera, J.R. Morones-Ramírez. The demand for new antibiotics: antimicrobial peptides, nanoparticles, and combinatorial therapies as future strategies in antibacterial agent design. Front. Microbiol. 1 (2020) 1669.

[188] J.M. Lü, X. Wang, C. Marin-Muller, H. Wang, P.H. Lin, Q. Yao, C. Chen. Current advances in research and clinical applications of PLGA-based nanotechnology. Expert Rev. Mol. Diagn. 9 (2009) 325-341.

[189] O.I. Martínez-Muñoz, E.C. Mora-Huertas. Nanoprecipitation technology to prepare carrier systems of interest in pharmaceutics: an overview of patenting. Int. J. Pharm. 614 (2022) 121440.

[190] M. Andima, G. Costabile, L. Isert, A.J. Ndakala, S. Derese, O.M. Merkel. Evaluation of β-sitosterol loaded PLGA and PEG-PLA nanoparticles for effective treatment of breast cancer: preparation, physicochemical characterization, and antitumor activity. Pharmaceutics 10 (2018) 232.

[191] C.J. Martínez Rivas, M. Tarhini, W. Badri, K. Miladi, H. Greige-Gerges, Q.A. Nazari, S.A. Galindo Rodríguez, R.Á. Román, H. Fessi, A. Elaissari. Nanoprecipitation process: from encapsulation to drug delivery. Int. J. Pharm. 532 (2017) 66-81.

[192] M. Haim Zada, Y. Rottenberg, A.J. Domb. Peptide loaded polymeric nanoparticles by non-aqueous nanoprecipitation. J. Colloid Interface Sci. 622 (2022) 904-913.

[193] E. Lepeltier, C. Bourgaux, P. Couvreur. Nanoprecipitation and the “Ouzo effect”. Adv. Drug Deliv. Rev. 71 (2014) 86-97.

[194] M.C. Operti, A. Bernhardt, S. Grimm, A. Engel, C.G. Figdor, O. Tagit. PLGA-based nanomedicines manufacturing: technologies overview and challenges in industrial scale-up. Int. J. Pharma. 605 (2021) 120807.

[195] M. Alkholief, M.A. Kalam, M.K. Anwer, A. Alshamsan. Effect of solvents, stabilizers and the concentration of stabilizers on the physical properties of poly(D,L-lactide-co-glycolide) nanoparticles: encapsulation, in vitro release of indomethacin and cytotoxicity against HepG2-Cell. Pharmaceutics 14 (2022) 870.

[196] U. Bilati, E. Allémann, E. Doelker. Development of a nanoprecipitation method intended for the entrapment of hydrophilic drugs into nanoparticles. Eur. J. Pharm. Sci. 24 (2005) 67-75.

[197] A. Popov, E. Enlow, J. Bourassa, H. Chen. Mucus-penetrating nanoparticles made with “mucoadhesive” poly(vinyl alcohol). Nanomedicine 12 (2016) 1863-1871.

[198] J. Cheng, B.A. Teply, I. Sherifi, J. Sung, G. Luther, F.X. Gu, E. Levy-Nissenbaum, A.F. Radovic-Moreno, R. Langer, O.C. Farokhzad. Formulation of functionalized PLGA-PEG nanoparticles for in vivo targeted drug delivery. Biomaterials 28 (2007) 869-876.

[199] R. Bisht, L.D. Rupenthal. PLGA nanoparticles for intravitreal peptide delivery: statistical optimization, characterization and toxicity evaluation. Pharm. Dev. Technol. 23 (2018) 324-333.

[200] A. Budhian, S.J. Siegel, K.I. Winey. Haloperidol-loaded PLGA nanoparticles: systematic study of particle size and drug content. Int. J. Pharm. 336 (2007) 367-375.

[201] A. Budhian, S.J. Siegel, K.I. Winey. Production of haloperidol-loaded PLGA nanoparticles for extended controlled drug release of haloperidol. J. Microencapsul. 22 (2005) 773-785.

[202] K. Hadinoto, W.S. Cheow. Nano-antibiotics in chronic lung infection therapy against Pseudomonas aeruginosa. Colloids Surf. B. Biointerfaces 116 (2014) 772-785.

[203] Z. Jia, J. Li, L. Gao, D. Yang, A. Kanaev. Dynamic light scattering: a powerful tool for In Situ nanoparticle sizing. Colloids Interfaces 7 (2023) 15.

[204] P.M. Carvalho, M.R. Felício, N.C. Santos, S. Gonçalves, M.M. Domingues. Application of light scattering techniques to nanoparticle characterization and development. Front. Chem. 6 (2018) 237.

[205] J. Stetefeld, S.A. McKenna, T.R. Patel. Dynamic light scattering: a practical guide and applications in biomedical sciences. Biophys. Rev. 8 (2016) 409-427.

[206] Z. Huang, S.N. Kłodzińska, F. Wan, H.M. Nielsen. Nanoparticle-mediated pulmonary drug delivery: state of the art towards efficient treatment of recalcitrant respiratory tract bacterial infections. Drug Deliv. Transl. Res. 11 (2021) 1634-1654.

[207] R.L. Gibson, J.L. Burns, B.W. Ramsey. Pathophysiology and Management of Pulmonary Infections in Cystic Fibrosis. Am. J. Respir. Crit. Care Med. 168 (2003) 918-951.

[208] C.B. Morrison, M.R. Markovetz, C. Ehre. Mucus, mucins, and cystic fibrosis. Pediatr. Pulmonol. 54 (2019) S84-S96.

[209] T.L. Doane, C.H. Chuang, R.J. Hill, C. Burda. Nanoparticle ζ -potentials. Acc. Chem. Res. 45 (2012) 317-326.

[210] S. Mura, H. Hillaireau, J. Nicolas, B. Le Droumaguet, C. Gueutin, S. Zanna, N. Tsapis, E. Fattal. Influence of surface charge on the potential toxicity of PLGA nanoparticles towards Calu-3 cells. Int. J. Nanomedicine 6 (2011) 2591-2605.

[211] F. Ramazani, W. Chen, C.F. Van Nostrum, G. Storm, F. Kiessling, T. Lammers, W.E. Hennink, R.J. Kok. Strategies for encapsulation of small hydrophilic and amphiphilic drugs in PLGA microspheres: state-of-the-art and challenges. Int. J. Pharm. 499 (2016) 358-367.

[212] M. Behnke, A. Vollrath, L. Klepsch, B. Beringer-Siemers, S. Stumpf, J.A. Czaplewska, S. Hoeppener, O. Werz, U.S. Schubert. Optimized encapsulation of the FLAP/PGES-1 inhibitor BRP-187 in PVA-stabilized PLGA nanoparticles using microfluidics. Polymers 12 (2020) 1-6.

[213] J.M. Barichello, M. Morishita, K. Takayama, T. Nagai. Encapsulation of hydrophilic and lipophilic drugs in PLGA nanoparticles by the nanoprecipitation method. Drug Dev. Ind. Pharm. 25 (1999) 471-476.

[214] S. Streck, H. Neumann, H.M. Nielsen, T. Rades, A. McDowell. Comparison of bulk and microfluidics methods for the formulation of poly-lactic-co-glycolic acid (PLGA) nanoparticles modified with cell-penetrating peptides of different architectures. Int. J. Pharm. X 1 (2019) 100030.

[215] S. Streck, L. Hong, B.J. Boyd, A. McDowell. Microfluidics for the production of nanomedicines: considerations for polymer and lipid-based systems. Pharm. Nanotechnol. 7 (2019) 423-443.

[216] T. López-Royo, V. Sebastián, L. Moreno-Martínez, L. Uson, C. Yus, T. Alejo, P. Zaragoza, R. Osta, M. Arruebo, R. Manzano. Encapsulation of large-size plasmids in PLGA nanoparticles for gene editing: comparison of three different synthesis methods. Nanomaterials 11 (2021) 2723.

[217] J. Ahn, J. Ko, S. Lee, J. Yu, Y.T. Kim, N.L. Jeon. Microfluidics in nanoparticle drug delivery; from synthesis to pre-clinical screening. Adv. Drug Deliv. Rev. 128 (2018) 29-53.

[218] P.S. Nunes, P.D. Ohlsson, O. Ordeig, J.P. Kutter. Cyclic olefin polymers: emerging materials for lab-on-a-chip applications. Microfluid. Nanofluid. 9 (2010) 145-161.

[219] J. Jeevanandam, A. Barhoum, Y.S. Chan, A. Dufresne, M.K. Danquah. Review on nanoparticles and nanostructured materials: history, sources, toxicity and regulations. Beilstein. J. Nanotechnol. 9 (2018) 1050-1074.

[220] N. Lababidi, V. Sigal, A. Koenneke, K. Schwarzkopf, A. Manz, M. Schneider. Microfluidics as tool to prepare size-tunable PLGA nanoparticles with high curcumin encapsulation for efficient mucus penetration. Beilstein J. Nanotechnol. 10 (2019) 2280-2293.

[221] S.M. D'Addio, R.K. Prud'homme. Controlling drug nanoparticle formation by rapid precipitation. Adv. Drug Rev. 63 (2011) 417-426.

[222] J.M. Lim, N. Bertrand, P.M. Valencia, M. Rhee, R. Langer, S. Jon, O.C. Farokhzad, R. Karnik. Parallel microfluidic synthesis of size-tunable polymeric nanoparticles using 3D flow focusing towards in vivo study. Nanomedicine 10 (2014) 401-409.

[223] E. Chiesa, M. Bellotti, A. Caimi, B. Conti, R. Dorati, M. Conti, I.Genta, F. Auricchio. Development and optimization of microfluidic assisted manufacturing process to produce PLGA nanoparticles. Int J Pharm. 629 (2022) 122368.

[224] S.B. Sun, P. Liu, F.M. Shao, Q.L. Miao. Formulation and evaluation of PLGA nanoparticles loaded capecitabine for prostate cancer. Int. J. Clin. Exp. Med. 8 (2015) 19670-19681.

[225] H. Park, D.H. Ha, E.S. Ha, J.S. Kim, M.S. Kim, S.J. Hwang. Effect of stabilizers on encapsulation efficiency and release behavior of exenatide-loaded PLGA microsphere prepared by the W/O/W solvent evaporation method. Pharmaceutics 11 (2019) 627.

[226] W. Li, Q. Chen, T. Baby, S. Jin, Y. Liu, G. Yang, C.X. Zhao. Insight into drug encapsulation in polymeric nanoparticles using microfluidic nanoprecipitation. Chem. Eng. Sci. 235 (2021) 116468.

[227] K.P. Cruz, B.F.C. Patricio, V.C. Pires, M.F. Amorim, A.G.S.F Pinho, H.C. Quadros, D.A.S. Dantas, M.H.C. Chaves, F.R. Formiga, H.V.A. Rocha, P.S.T. Veras. Development and characterization of PLGA nanoparticles containing 17-DMAG, an Hsp90 inhibitor. Front. Chem. 9 (2021) 644827.

[228] M.D. Melo, R.W. Stokes. Interactioon of Mycobacterium tuberculosis with MH-S, an immortilized murine alveolar macrophage cell line: a comparison with primary murine macrophages. Tuber Lung Dis. 80 (2000) 35-46.

[229] M.S. Kang, G.H. Lee, I.H. Kwon, M.J. Yang, M.B. Heo, J.W. Choi, T.G. Lee, C.H. Yoon, B. Baek, M.C. Sung, D.W. Kim, E.J. Park. Uptake and toxicity of cerium dioxide nanoparticles with different aspect ratio. Toxicol. Lett. 373 (2023) 196-209.

[230] E.V. Sazonova, M.S. Chesnokov, B. Zhivotovsky, G.S. Kopeina. Drug toxicity assessment: cell proliferation versus cell death. Cell. Death Discov. 8 (2022) 417.

[231] S. Kamiloglu, G. Sari, T. Ozdal, E. Capanoglu. Guidelines for cell viability assays. Food Front. 1 (2020) 332-349.

[232] H. Tominaga, M. Ishiyama, F. Ohseto, K. Sasamoto, T. Hamamoto, K. Suzuki, M. Watanabe. A water-soluble tetrazolium salt useful for colorimetric cell viability assay. Anl. Commun. 36 (1999) 47-50.

[233] H.Y. Jo, Y. Kim, H.W. Park, H.E. Moon, S. Bae, J. Kim, D.G. Kim, S.H. Paek. The unreliability of MTT assay in the cytotoxic test of primary cultured glioblastoma cells. Exp. Neurobiol. 24 (2015) 235-245.

[234] M. Ghasemi, T. Turnbull, S. Sebastian, I. Kempson. The MTT assay: utility, limitations, pitfalls, and interpretation in bulk and single-cell analysis. Int. J. Mol. Sci. 22 (2021) 12827.

[235] C.H. Chen, Y.H. Liao, M. Muljadi, T.T. Lu, C.M. Cheng. Potential Application of the WST-8-mPMS assay for rapid viable microorganism detection. Pathogens 12 (2023) 343.

[236] H.I. Chiu, N.A. Samad, L. Fang, V. Lim. Cytotoxicity of targeted PLGA nanoparticles: a systematic review. RSC Adv. 16 (2021) 9433-9449.

[237] W.N. Ibrahim, L.M.B.M Rosli, A.A. Doolaanea. Formulation, cellular uptake and cytotoxicity of thymoquinone-loaded plga nanoparticles in malignant melanoma cancer cells. Int. J. Nanomedicine 15 (2020) 8059-8074.

[238] N. Guvenic, D. Dilek. An evaluation of the effects of medium pH on the viability of the HepG2 cell line. Etlik Vet. Mikrobiyol. Derg. 31 (2020) 107-114.

[239] S. Streck, A.J. Clulow, H.M. Nielsen, T. Rades, B.J. Boyd, A. McDowell. The distribution of cell-penetrating peptides on polymeric nanoparticles prepared using microfluidics and elucidated with small angle X-ray scattering. J. Colloid Interface Sci. 555 (2019) 438-448.

[240] S. Horikoshi, N. Serpone. Introduction to nanoparticles. In *Microwaves in Nanoparticle Synthesis: Fundamentals and application*. S. Horikoshi and N. Serpone Eds., Wiley (2013) chapter 1, 1-24.

[241] B.S. Fazly Bazzaz, S. Seyedi, N.H. Goki, B. Khameneh. Human antimicrobial peptides: spectrum, mode of action and resistance mechanisms. Int. J. Pep. Res. Ther. 27 (2021) 1-16.

[242] A. Torge, P. Grützmacher, F. Mücklich, M. Schneider. The influence of mannitol on morphology and disintegration of spray-dried nano-embedded microparticles. Eur. J. Pharm. Sci. 104 (2017) 171-179.